A STUDY OF MOLECULAR AND PHYSICAL PROCESSES IN COMETS

Thesis by

Claude Arpigny

In Partial Fulfillment of the Requirements

For the Degree of

Doctor of Philosophy

California Institute of Technology

Pasadena, California

1964

To my Mother and

to the Memory of my Father

ACKNOWLEDGEMENTS

I wish to express my most sincere gratitude to Professor Greenstein for giving me the opportunity to analyze his remarkable material on cometary spectra. It is a pleasure to thank Professor Greenstein and Professor Swings for some helpful comments. I am indebted to Professor Biermann for sending me a preprint of his paper in collaboration with Dr. Trefftz.

Financial support received from the following institutions

Belgian American Educational Foundation

California Institute of Technology

North Atlantic Treatise Organization

Patrimoine de l'Universite de Liege

is thankfully acknowledged.

I am also indebted to the California Institute of Technology and to the Mount Wilson and Palomar Observatories for their very kind hospitality.

My studies at Caltech have been a tremendous enrichment, my stay in the United States a very great and unforgettable experience. I am very happy to say how deeply grateful I am to Professor Greenstein and to Professor Swings who have offered me this wonderful opportunity.

ABSTRACT

The rotational structure of the violet CN (0, 0) band in cometary spectra is investigated from a new point of view. The usual assumption of a Boltzmann distribution of populations of the rotational levels in the ground state is abandoned. These populations are determined by solving the system of steady-state equations which describes the resonance-fluorescence of the CN band. As expected, it is possible in this way to reproduce the observed profile more satisfactorily than in the case when a Boltzmann distribution is used. Furthermore, it is shown that the Swings effect (presence of absorption lines in the solar exciting light) has to be taken into account from the beginning in the resolution of the system of the steady-state equations, to achieve complete agreement between observed and computed profiles.

The Greenstein effect (differences in relative intensities of rotational lines in different regions of the comet) has been studied in high-resolution spectrograms of Comet Seki-Lines (1962c). The observations can be interpreted partly by means of either of two simple models for the comet's head (uniform, isotropic expansion, or "fountain model"). In addition there are random motions of the order of a few km/sec.

A detailed analysis of spectra of Comet Humason (1961c) has furnished the following results:

a) The CO^+ comet-tail bands are excited by the same resonance-fluorescence mechanism known to be responsible for the emissions of the neutral molecules observed in the head.

b) The continuum is of the pure reflection type: there is no detectable selective scattering.

c) Molecular abundances are estimated (at 10^4 km from the nucleus)

$$N(CO^+) = 10^{13}\ cm^{-2}$$
$$N(N_2^+) = 10^{11}\ cm^{-2}$$
$$N(CN) = 5 \times 10^{10}\ cm^{-2}$$

The probable error on these estimates corresponds to a factor of 2 or 3.

d) The infra-red surface brightness produced by the CO^+ ions in pure vibration transitions $v'' = 1 \rightarrow v'' = 0$ ($\lambda \approx 4.6\ \mu$) is found to be rather large: ≈ 0.001 erg cm^{-2} sec^{-1}.

e) The radial distributions of the various molecules are discussed. While CN follows the usual $1/\rho$ law (ρ being the projected distance from the nucleus), it is suggested that the remarkable flatness of the ion distributions might be explained in terms of a "magnetic model."

A critical discussion of some physical and chemical characteristics of comets is presented in the last chapter. In particular, the results of a number of abundance determinations are tabulated.

(Photographic material on page 46 will not reproduce clearly on Xerox copies).

TABLE OF CONTENTS

Part One

ON THE RESONANCE FLUORESCENCE EXCITATION OF MOLECULAR EMISSIONS IN THE SPECTRA OF THREE RECENT COMETS

INTRODUCTION

The suggestion that the luminosity of a comet is mainly due to a process of absorption of sunlight followed by re-emission of light of the same or different wavelengths dates back to 1911. It was first introduced by Schwarzschild and Kron to explain the observed brightness in the tail of Halley's comet (Schwarzschild and Kron, 1911). Around 1928 Zanstra successfully applied Schwarzschild and Kron's suggestion in a quantitative study of the luminosities of eight comet heads (Zanstra, 1928). Later Wurm based his determination of the density of C_2 molecules in the head of Halley's comet on the same hypothesis, which he also used to interpret the sharpness exhibited by the (0, 0) band of the CN violet system in cometary spectra (Wurm, 1932 and 1934). However, it was not until 1941 that this so-called resonance-fluorescence excitation mechanism (also referred to as "Swings mechanism") was put forward for the first time in a systematic study of spectroscopic details in the cometary light by Swings who succeeded in fully explaining the peculiar profiles of the CN violet bands (Swings, 1941). The basic feature of the Swings mechanism lies in the fact that absorption lines present in the solar radiation will lead to underpopulation of some rotational levels whenever they coincide in wavelengths with molecular transitions. When studying the population of a given rotational level in the excited electronic state of a molecular system, one has to ascertain that all the transitions leading to this level have been considered, each with its respective probability. Furthermore, account must be taken of the shift of the Fraunhofer lines produced by the Doppler effect due to the relative radial velocity

between sun and comet. With these ideas in mind different authors, especially McKellar and Hunaerts*, have been able to show that the resonance-fluorescence mechanism accounts for all the details of the odd intensity distributions of several molecular bands (of OH, NH, CH, CN, C_2) observed in the heads of various comets. Hunaerts (1953) has developed an elaborate method which consists essentially in evaluating the populations of the rotational levels after each one of a number of fluorescence cycles, starting with all molecules in the lowest level (or levels, according to the particular selection rules involved), and leaving off when the derived theoretical intensities agree with the observations. Such a dissection into separate processes undergone by all the molecules treated together is not rigorously correct, however, as Carrington has pointed out recently. Rather, one should regard each individual molecule as accomplishing its own "random walk" among the possible states, and thus treat the fluorescence as a Markov process continuous in time (Carrington, 1962). On practical grounds this simply means that the correct procedure is to solve the relevant set of steady-state equations to obtain the relative distribution of populations of the rotational levels. The large number of such equations often to be considered is no longer prohibitive thanks to the electronic computers now at our disposal.

The principal aim of my work has been to present a detailed investigation of the resonance-fluorescence mechanism based on studies of spectra of three recent comets: Comet Mrkos (1957d), Comet Seki-

*Numerous references can be found in a review article on the spectra of comets by P. Swings (1956).

Lines (1962c), and Comet Humason (1961e), which will be considered in chapters I, II, and III, respectively. Besides the CN radical and the C_2 molecule, for which previous investigations have already established that the fluorescence excitation process does account for the observations, the NH_2 radical and the CO^+ tail ion, which have not yet been studied from this point of view, will be envisaged. Examples of anomalous intensity ratios of NH_2 lines that can be explained by a fluorescent mechanism will be given, and it will be shown that the measured intensities of the CO^+ comet-tail bands can be reproduced theoretically if we assume a fluorescent excitation again.

The fluorescence of the violet CN (0, 0) band, which, at the relatively high dispersion (18 Å/mm) used for Comet Seki-Lines, is completely resolved into its rotational lines, will be treated in a rigorous manner. We shall solve the system of the steady-state equations in order to derive the true distribution of populations of the rotational levels in the ground state of CN instead of arbitrarily adopting a Boltzmann distribution, as has always been done in previous similar studies. Then, a method will be suggested for analyzing the effect of internal motions of the molecules upon the relative intensities of the rotational lines in different regions of a comet (Greenstein effect). As a by-product of our work on Comet Humason, in which the fluorescence of the CO^+ emissions will be studied on the basis of lower dispersion spectra (180 Å/mm), we shall obtain estimates for the densities of CO^+, N_2^+, and CN, which will be compared with results derived from studies of other comets in chapter IV.

The order in which the report will be presented coincides with the chronological order of the observations; the necessary theoretical developments will appear wherever the need for them arises.

A review of the present state of our knowledge concerning some important characteristics of comet heads and tails (forms, particle distributions, brightness, abundances) will be given in chapter IV.

Chapter I

COMET MRKOS (1957d)

1. C_2 Emissions

The visual region of the spectrum of this comet (dispersion 18 Å/mm and 27 Å/mm) has been identified by Dr. Greenstein and myself and the wavelength measurements and identifications have been published recently (Greenstein and Arpigny, 1962). The case of the fluorescence of the C_2 molecule in a comet has been treated only recently. Stawikowski and Swings (1960) have studied the (1, 0) and (2, 1) bands of the Swan system in the spectrum of Comet Mrkos (1957d) itself and have shown that some distortions of the intensity distributions in these bands from smooth curves can be attributed to the presence of absorption features in the exciting solar radiation. An extension of this study to the $\Delta v = 0$, -1 and -2 sequences of the Swan system was required for the work of identification of the visual region of the spectrum of Comet Mrkos (1957d). A few typical examples of correlations between weakened rotational lines in the comet spectrum and minima in the spectrum of the sun will be given below. Of course, as Stawikowski and Swings have already remarked, we do not expect the fluorescence to produce spectacular effects in the case of the C_2 molecule as it does in the case of the CN violet system, simply because the Fraunhofer lines are less numerous and less strong in the spectral region of the Swan bands than in the violet and also because the number of transitions that populate a given rotational level is larger in the case of the $A\ ^3\Pi_g - X\ ^3\Pi_u$ system of C_2. A complete quantitative treatment of the fluorescence of the carbon molecule in comets would

have to include an exceptionally large number of vibrational and rotational levels, owing to the homonuclear character of C_2, and would thus not be feasible in a reasonably short amount of time. Moreover, a comet with a purely gaseous head would be more suitably adapted to such a study than Comet Mrkos (1957d) which had a strong continuous scattered spectrum. We shall, therefore, have to content ourselves with qualitative considerations. Quantitative examples will be presented later on when we come to the better suited CN and CO^+ band systems. The method here is:

a. to list, for a given cometary line, all the transitions that give access to the upper level in which this line originates;

b. to determine, for each of these transitions, the wavelength at which they were excited, according to the formula

$$\lambda_{exc} = \lambda_{lab} \left(1 - \left(\frac{dr}{dt}\right) \times \frac{1}{c}\right), \qquad (1)$$

where λ_{lab} is the laboratory wavelength of the transition and $\frac{dr}{dt}$ is the radial velocity of the comet with respect to the sun, with its usual sign (positive for recession);

c. to read the corresponding residual intensities $r_{\lambda_{exc}}$ in the solar spectrum from intensity tracings such as those of the Utrecht Solar Atlas.

A parallelism should then appear between the observed intensities of the rotational lines in the cometary spectrum on the one hand, and the occurrence or nonoccurrence of coincidences of certain or of all the relevant transitions with Fraunhofer lines on the other hand. The transitions mentioned under a are to be determined as follows, in the case of the

Swan system. To each $R_i(J)$ (respectively $P_i(J)$) line is associated a $P_i(J+2)$ (respectively $R_i(J-2)$) line and these pairs of lines have to be taken in as many vibrational bands (with the same upper vibrational quantum number v' as the band to which the line considered belongs) as indicated by the vibrational transition probabilities and by the relative populations of the vibrational levels of the lower electronic state. For the latter it is sufficient, in a rough analysis, to adopt a Boltzmann distribution at some temperature ($\approx 3000\,^{\circ}K$) suggested by the observations, although there is rigorously no a priori reason for such a distribution to be achieved in the actual situation.

The number of clear-cut examples is not large in the case of C_2, for the reasons already mentioned, and also because of the frequent occurrence of blends. Some of the best examples are listed in tables 1 and 2. The relative importance of the various vibrational transitions leading to the same upper level v' can be evaluated by:

$$N_{v''}C_{v'v''} \propto p_{v'v''} \cdot (\lambda^2 F_\lambda)_{v'v''} \cdot e^{-\frac{G_o(v'')hc}{kT}} , \qquad (2)$$

where $C_{v'v''}$ represents the upward transition rate, $p_{v'v''}$ is the relative vibrational transition probability (Nicholls, 1956), $(\lambda^2 F_\lambda)_{v'v''}$ is proportional to the energy available, per unit frequency interval, in the solar radiation at the wavelength of the transition (Allen, 1963), and finally, the last factor is based on the assumption of a Boltzmann distribution among the lower vibrational levels as stated previously ($T = 3000\,^{\circ}K$). In the case when $v' = 0$, (0, 0) plays by far the most important role, (the transition rates for (0,1) and (0, 2) are about 10% and 1%,

Table 1. Fluorescence of lines in the $v' = 0$ progression of the Swan system

	λ_{lab}	(v', v'')	Main exciting lines λ_{exc}	r_λ
a. Unweakened Lines				
$R_1(28)$, $R_2(27)$	5109.16	(0, 0)	5108.57	0.98
$P_1(30)$, $P_2(29)$	57.64		57.06	0.97
$R_1(28)$, $R_2(27)$	5565.78	(0, 1)		
$P_1(30)$, $P_2(29)$	5622.77			
$R_1(50)$	5037.71	(0, 0)	5037.13	0.99
$R_2(49)$	37.80		37.22	0.96
$P_1(52)$	5120.66		5120.08	0.97
$P_2(51)$	20.73		20.15	0.98
$R_1(50)$, $R_2(49)$	5472.65	(0, 1)		
$P_1(52)$, $P_2(51)$	5569.33			
b. Weakened Lines				
$R_1(17)$	5134.30	(0, 0)	5133.72	0.28
$R_2(16)$	34.47		33.89	0.80
$R_3(15)$	34.65		34.07	0.92
$P_1(19)$	5164.46		5163.88	0.91
$P_2(18)$	64.53		63.95	0.91
$P_3(17)$	64.64		64.06	0.91
$R_1(17)$	5598.22	(0, 1)		
$R_2(16)$	98.41			
$R_3(15)$	98.63			

Table 1 (Continued)

	λ_{lab}	(v', v")	Main exciting lines λ_{exc}	r_λ
$R_1(39)$, $R_2(38)$	5076.64	(0, 0)	5076.06	0.95
$R_3(37)$,	76.79		76.21	0.75
$P_1(41)$, $P_2(40)$	5142.87		5142.29	0.92
$P_3(39)$	42.97		42.39	0.80
$R_1(39)$, $R_2(38)$	5523.57	(0, 1)		
$R_3(37)$	23.84			
$P_1(41)$, $P_2(40)$	5601.19			
$P_3(39)$	01.34			

c. Missing Lines

$R_1(14)$	5139.97	(0, 0)	5139.38	0.44
$R_2(13)$	40.17		39.58	0.58
$R_3(12)$	40.41		39.82	0.90
$P_1(16)$, $P_2(15)$	5165.12		5164.53	0.59
$P_3(14)$	65.29		64.70	0.81
$R_1(49)$, $R_2(48)$	5041.41	(0, 0)	5040.84	0.33
$P_1(51)$, $P_2(50)$	5122.86		5122.28	0.95
$R_1(49)$, $R_2(48)$	5477.56	(0, 1)		
$P_1(51)$, $P_2(50)$	5572.81			

Table 2. Fluorescence of lines in the $v' = 1$ progression of the Swan system

			Main exciting lines	
	λ_{lab}	(v', v'')	λ_{exc}	r_λ
		a. Unweakened Lines		
$R_1(35)$	4677.75	(1, 0)	4677.22	1.00
$P_1(37)$	4728.32		4727.79	0.95
$R_1(35)$	5055.75	(1, 1)	5055.17	1.00
$P_1(37)$	5114.25		5113.67	1.00
$R_1(35)$	5493.26	(1, 2)	5492.63	1.00
$P_1(37)$	5561.73		5560.99	1.00
		b. Missing Lines		
$R_3(29)$	4686.87	(1, 0)	4686.34	0.50
$P_3(31)$	4731.89		4731.36	0.40
$R_3(29)$	5067.63	(1, 1)	5067.06	0.43
$P_3(31)$	5119.41		5118.83	0.79
$R_3(29)$	5508.10	(1, 2)	5507.48	1.00
$P_3(31)$	5569.16		5568.53	1.00

respectively, of that for (0, 0)), so that we consider exciting transitions only in this band in table 1, where we are concerned with lines of (0, 0) and (0, 1). On the other hand, $v' = 1$ can be populated by transitions whose rates are approximately in the ratios:

$$N''_o C_{10} : N''_1 C_{11} : N''_2 C_{12} : N''_3 C_{13} = 1.00 : 0.76 : 0.32 : 0.05 . \qquad (3)$$

As a result, when considering lines with $v' = 1$, as in table 2, we have to include exciting transitions in (1, 0), (1, 1) and (1, 2). It is seen that, while the exciting lines in tables 1a and 2a do not coincide with Fraunhofer absorptions, those in tables 1b, 1c and 2b are definitely affected by such absorptions. These examples are convincing, but it must be said that there is a number of unexplained situations in which, for instance, lines $R_i(J)$ and $P_i(J+2)$, or the same lines $R_i(J)$ in different bands of a v'-progression, do not seem to have similar behaviors. In general, however, these cases concern relatively weak lines and this merely suggests that it would be desirable to repeat a study similar to the one described here, or even, possibly, of a more quantitative nature, but based on high-resolution spectra of a comet that would be free of dust. At any rate, apart from the few exceptions just mentioned, it can be concluded that the spectrum of Comet Mrkos (1957d) tends to support the view that the Swan system of C_2 was excited by fluorescence in this comet.

2. NH_2 Emissions

A similar conclusion can be drawn about the NH_2 radical, as we shall see presently. It would be even more difficult to treat the case of this triatomic radical quantitatively than that of C_2, not only because of the more complicated structure, our lack of knowledge of the transition probabilities involved, and even the nonexistence of a complete analysis of the emisssion spectrum of NH_2, but also because of the combined effect of the concentration of the NH_2 emissions toward the nucleus and of the presence of a strong continuum in the spectrum of Comet Mrkos (1957d), which is to mask the weaker lines of this radical. The procedure that is followed, then, is to look for irregularities in the relative intensities of NH_2 emissions and to show that such irregularities are correlated with the unevenness of the spectral distribution of the exciting light that produced these emissions. Table 3 contains some examples of NH_2 emissions issued from a given upper level and weakened by fluorescence in the spectrum of Comet Mrkos (1957d).

Table 3. Weakened NH_2 Emissions (Upper Levels)

(v_1', v_2', v_3')	$N'_{K_a', K_c'}$
(0, 8, 0)	2_{11}
(0, 9, 0)	3_{21}, 4_{41}
(0, 10, 0)	3_{30}
(0, 11, 0)	3_{21}
(0, 12, 0)	3_{12}
(0, 13, 0)	3_{21}, 7_{07}, 5_{05}, 0_{00}

Only the notations of the upper level in question are listed. For instance, in (0, 8, 0), the red component of $^2_{11}$- $^2_{21}$, which is absent from the comet spectrum, coincides, after due correction for the Doppler shift, with the line Fe λ6318.04 in the solar spectrum; the same component of $^2_{11}$- $^3_{21}$ and of $^2_{11}$- $^1_{01}$, which have the same upper level as the line just referred to, are also absent. Similarly, in (0, 9, 0), the absence of the violet components of the doublets $^3_{21}$- $^2_{11}$, $^3_{21}$- $^3_{13}$, $^3_{21}$- $^3_{31}$ and $^3_{21}$- $^4_{31}$ can be assigned to the coincidence of $^3_{21}$- $^2_{11}$ (violet component) with the solar line Mn λ6016.65 and, less importantly, to the depletion in radiation capable of exciting the violet component of $^3_{21}$- $^4_{31}$ produced by the presence of Ni λ6108.13 in the sun spectrum.

It is also interesting to compare the behaviors of various rotational NH_2 lines in different vibrational transitions, as this also can provide some clues to the excitation mechanism. The rotational line strengths being independent of the vibrational quantum numbers, the relative intensities of the lines of a given sub-branch will be the same in all bands if these are excited by a nonfluorescent process. If, on the contrary, the emissions are produced by fluorescence, the relative intensity distributions in sub-branches will, in general, bear the impress of this fluorescence because they will be influenced by chance coincidences with Fraunhofer lines and because they are likely to be affected differently in different bands. A series of sub-branches have been examined systematically from this point of view in all the bands in which they appear and some of the most significant cases have been collected in table 4.

Table 4. Observed Relative Intensities of NH_2 Lines In Various Vibrational Bands

Bands / Lines	(1, 7, 0)	(0, 13, 0)	(0, 11, 0)	(0, 9, 0)	(0, 7, 0)
0_{00} - 1_{10}	abs (⊙)	abs (⊙)	abs (⊙)	1	1N
1_{01} - 2_{11}	2n	1N	1	5(bl)	3
2_{02} - 3_{12}	1N	1d	0	2(bl)	0N(bl)
3_{03} - 4_{13}	2(bl)	1n(bl)	abs	4(bl)	2n
4_{04} - 5_{14}	abs	abs	abs	abs	abs
2_{20} - 1_{10}	abs	abs	abs	4(bl)	abs
3_{21} - 2_{11}	abs(⊙)	abs(⊙)	abs (⊙)	1(bl)	0N(bl)
4_{22} - 3_{12}	abs	abs	abs	abs	abs
5_{23} - 4_{13}	abs	2(bl)	abs	2(bl)	abs

	(0, 12, 0)	(0, 10, 0)	(0, 8, 0)
1_{10} - 2_{20}	0n(bl)	3n(bl)	abs (⊙)
2_{11} - 3_{21}	1(bl)	2(bl)	2N(bl)
3_{12} - 4_{22}	abs (⊙)	1	3
4_{13} - 5_{23}	abs	abs	abs
3_{30} - 4_{40}	on	abs (⊙)	1n
4_{31} - 5_{41}	abs	2(bl)	abs
5_{32} - 6_{42}	abs	(2d)*	abs

*The line 5_{32} - 6_{42} illustrates the fact that such an analysis may be helpful for the identifications. This line is absent from (0, 12, 0) and from (0, 8, 0) while there is no coincidence with any Fraunhofer absorption. Thus this indicates that the emission feature measured at λ5939 in the comet spectrum cannot be assigned to 5_{32} - 6_{42}.

Although the situation is sometimes rather complex, mainly because of the presence of numerous blends (bl), there seems, in a first approximation, to be a general tendency for the sub-branches to show parallel behaviors in the various vibrational bands. Of course, no conclusion can be inferred from the absence from the comet spectra of lines like 4_{04}- 5_{14}, 4_{22}- 3_{12} and 4_{13}- 5_{23} which have small strengths. However, it is noteworthy to find cases in which lines are present in some of the bands while absent from others, and it is then remarkable to see that, when the lines are absent, they just happen to coincide with solar absorptions, account being taken of the radial velocity shift. (This is indicated by "abs (⊙)" in table 4.) This represents a strong argument in favor of the resonance-fluorescence excitation mechanism, since we do not know of any other process that might produce such selective effects in a comet head. Thus, the spectrum of Comet Mrkos (1957d) has been the first to give good indications that the NH_2 emissions are excited by this mechanism in the same manner as the other head emissions, for which this was already known. But here again it is recommendable that more detailed discussions be undertaken when high-resolution spectra of a bright comet with a weak continuum are available and we are better informed about the physical characteristics of the NH_2 radical.

Chapter II

COMET SEKI-LINES (1962c)

High-resolution spectra of Comet Seki-Lines (1962c) were secured by Greenstein in April 1962 when this comet was about 0.8 A.U. distant from the sun. Relevant data concerning these observations are given in table 5.

Table 5. Comet Seki-Lines (1962c). Description of the observational material.

Plate	Pd 6545	Pd 6552	Pd 6558
Emulsion	IIaO Bkd	103aD + Yellow Filter	IIaO Bkd
Dispersion	18 Å/mm	27 Å/mm	18 Å/mm
Date (U.T.) (Apr 1962)	22.180	23.163	24.150
Heliocentric distance, r(A.U.)	0.79	0.82	0.85
Heliocentric radial velocity, $\frac{dr}{dt}$ (km/sec)	46.3	45.6	44.9
Geocentric radial velocity, $\frac{d\Delta}{dt}$ (km/sec)			
computed*	44.6	45.3	46.1
observed**	43.4 ± 2.7	44.6 ± 3.6	45.1 ± 2.2
Band system studied	CN violet	C_2 Swan, NH_2	CN violet

*From the orbit by Candy (IAU Circ. 1795). It is unnecessary to calculate very accurate radial velocities, since the errors from readings in the Utrecht Solar Atlas cannot be much smaller than 0.01 Å, which e.g. corresponds to 0.8 km/sec at λ3883.

**No systematic difference is found between the values derived from C_2 lines and those from NH_2 lines.

1. The CN (0, 0) Violet Band

The mean of the wavelength measurements in the wavelength range λλ3858-3884 of Pd 6545 and Pd 6558, corrected for the Doppler shift due to the geocentric radial velocity of the comet, appears in table 6, together with visual intensity estimates and assignments. The resonance-fluorescence of the (0, 0) band of the CN violet system has been studied in detail (Greenstein, 1958; Hunaerts, 1959a). Actually, as Swings and his collaborators have already pointed out on several occasions, a complete, precise study would require solar spectrophotometric tracings of greater accuracy and greater resolution than those of the Utrecht Solar Atlas which have been used in previous works. Since such very accurate tracings are not yet available, we shall content ourselves with using the Utrecht Solar Atlas, which will prove sufficient for our purposes.

a. The Radial Velocity Effect

As mentioned in the Introduction, the interpretation of the odd structure of the CN violet band observed in cometary spectra became clear when Swings realized the essential role played by the absorption lines present in the exciting solar radiation. Swings also stressed the importance of changes in the radial velocity "which could bring the cometary absorption lines inside or outside strong Fraunhofer lines" and thus modify the CN structure appreciably. Three spectra corresponding to different heliocentric distances and radial velocities will be compared here. It will be shown that the differences in r and principally in $\frac{dr}{dt}$ are sufficient to explain the main differences observed

Table 6. The Violet CN (0, 0) Band in Comet Seki-Lines (1962c)

λ	I	Identifications
3857.68	0?	57.69 R(21)
58.71	0	58.69 R(20)
59.71	1	59.67 R(19)
60.60	0	60.60 R(18)
61.59	1	61.57 R(17)
62.52	6	62.48 R(16)
63.39	8	63.40 R(15)
64.29	4	64.30 R(14)
65.16	7	65.16 R(13)
66.03	6	65.99 R(12)
66.84	7	66.82 R(11)
67.61	8	67.62 R(10)
68.41	8	68.41 R(9)
69.18	10	69.18 R(8)
69.90	8	69.92 R(7)
70.66	1	70.65 R(6)
71.37	3	71.37 R(5)
72.06	4	72.05 R(4)
72.69	3	72.74 R(3)
73.37	4	73.37 R(2)
73.99	4	74.00 R(1)
74.60	1	74.61 R(0)
75.78	2	75.77 P(1)
76.32	2	76.32 P(2)
76.85	5	76.84 P(3)
77.36	3	77.35 P(4)
77.80	2	77.84 P(5)
78.33	2	78.30 P(6)
79.90	20	} Head of P-branch
83.05	20	

among the three spectra. For this purpose we shall compute the theoretical intensity profiles of the violet (0, 0) band for the particular values of the heliocentric distances and radial velocities involved. These values are as follows:

Comet Mrkos (1957d), $r = 0.60$ A. U., $\frac{dr}{dt} = 34.7$ km/sec

Comet Seki-Lines (1962c), $r = 0.55$ A. U., $\frac{dr}{dt} = 50.0$ km/sec

Comet Seki-Lines (1962c), $r = 0.85$ A. U., $\frac{dr}{dt} = 44.9$ km/sec

Figure 1, which we shall make use of in the proposed comparison, has been composed by joining the crests of the rotational lines of the (0, 0) band in density tracings of the three spectra. The vertical scale has been adjusted in such a way that the highest points of the three curves more or less agree with each other. (This is sufficient for our purpose, for we shall refer only to the presence or absence of maxima or minima at some places in the curves.) For Comet Seki-Lines (1962c) I the curve has been obtained from a visual inspection of a reproduction of the spectrum taken by Swings and Fehrenbach (1962). We notice at once that, for each of these curves, the behavior of the first lines of the P-branch ($2 \leq K'' \leq 6$) is very similar to that of the first lines of the R-branch ($0 \leq K'' \leq 4$), as it should. The crowding of the P-lines for larger values of K'' prevents such a similarity to show up in the case of these lines. Another obvious remark is that the first few lines (up to $K' = 5$) are relatively stronger in Comet Seki-Lines than in Comet Mrkos: this results from the fact that the 10 to 20 km/sec extra positive radial velocity of the former comet shifts the exciting radiation for these lines slightly more off the strong solar absorption at $\lambda 3878.03$. Before proceeding to a closer

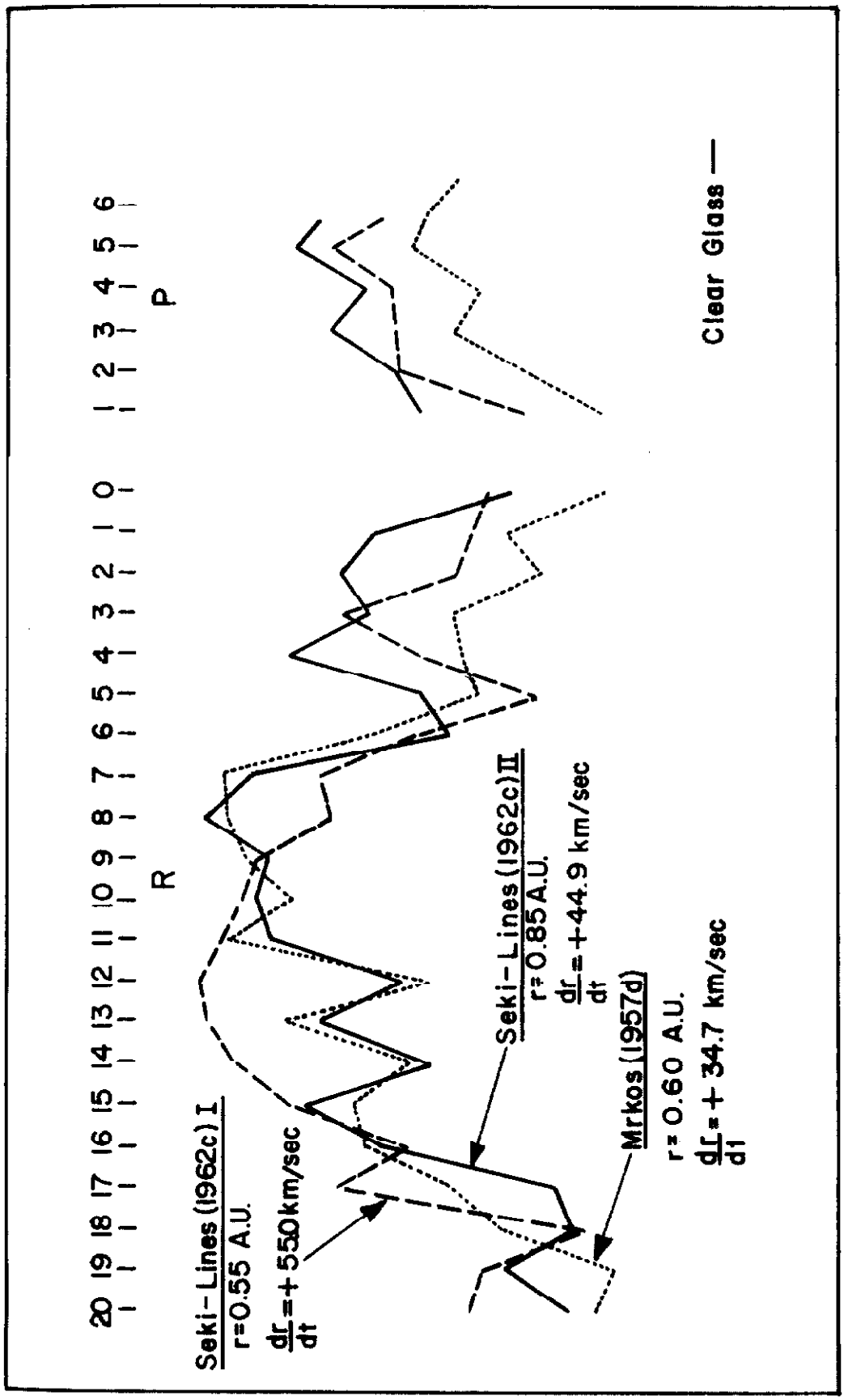

Fig. 1. Schematic representation of the profiles of the CN violet (0,0) band observed in three cometary spectra (density tracings).

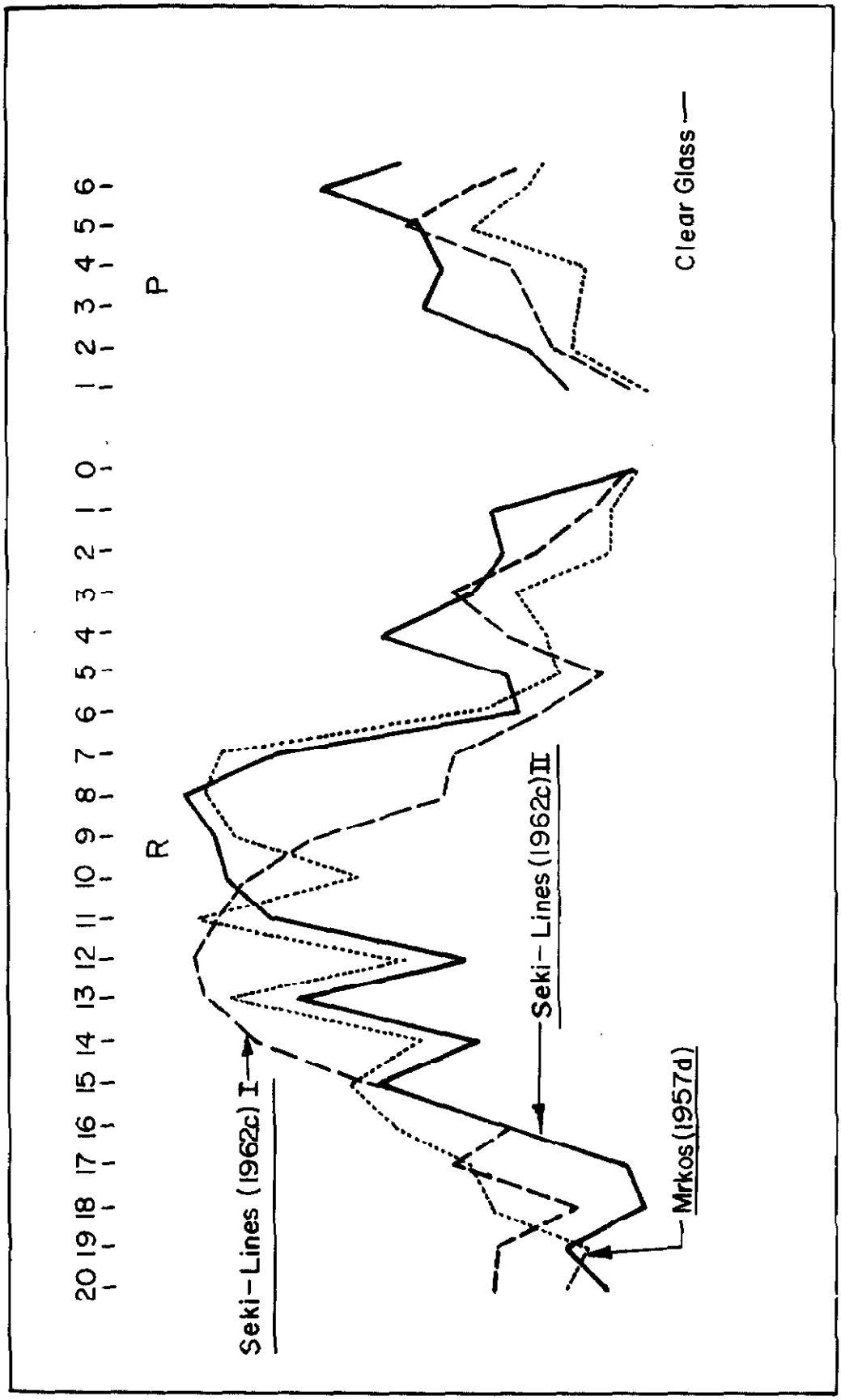

Fig. 1A. Theoretical profiles of the CN (0, 0) band to be compared with the observed profiles shown in Fig. 1. The computed intensities (see text) have been transformed into densities by using a characteristic curve typical for a IIaO plate at λ 3880 under usual conditions, in order to allow a more direct comparison with Fig. 1.

examination of figure 1, we have to lay down a few formulae which will be useful in the ensuing discussion.

Theoretical Treatment of the Fluorescence

The computation of a theoretical profile is carried out in two steps. First, one has to determine the relative populations of the rotational levels in the ground electronic state. Then, combining these populations with the rotational line strengths of the transitions involved and with the relevant values of the residual intensities in the solar spectrum, one derives the relative intensities of the individual lines. Explicit formulae will be given below.

It has been customary, in previous investigations concerning the resonance-fluorescence mechanism in comets, to make the convenient assumption that the distribution of populations of the rotational levels in the ground state of a molecule follows the Boltzmann law at some appropriately chosen temperature. As recognized by the authors of these investigations themselves, there is, of course, no justification for such a hypothesis. Not only will the Fraunhofer lines bring about various irregularities in the relative populations of the rotational levels, but the agent that would tend to produce a Boltzmann distribution is even lacking, since collisions are so infrequent in a cometary atmosphere. All that can be asserted safely is that, if a state of equilibrium is established, the populations of the energy levels will be constant, which is expressed by the following steady-state equations valid for the case of a $^2\Sigma - {}^2\Sigma$ transition, like that of the CN violet system, when we neglect the very small spin splitting in both the upper and lower levels.

$$N_{v',K'} \cdot \sum_{v''} A_{v'v''} = \sum_{v''} \left[N_{v'',K''=K'-1} \cdot \left(r_\lambda \frac{S^R}{g} \right)^{v''}_{K''=K'-1} + N_{v'',K''=K'+1} \cdot \left(r_\lambda \frac{S^P}{g} \right)^{v''}_{K''=K'+1} \right] \cdot C_{v'v''} \qquad (4)$$

$$N_{v'',K''} \cdot \left[\sum_{v'} \left(\left(r_\lambda \frac{S^R}{g} \right) + \left(r_\lambda \frac{S^P}{g} \right) \right)^{v'}_{K''} \cdot C_{v'v''} + A^{rot}_{K''} \right]$$

$$= \sum_{v'} \left[N_{v',K'=K''+1} \cdot \left(\frac{S^R}{g} \right)^{v'}_{K'=K''+1} + N_{v',K'=K''-1} \cdot \left(\frac{S^P}{g} \right)^{v'}_{K'=K''-1} \right] \cdot A_{v'v''} + N_{v'',K''+1} \cdot A^{rot}_{K''+1} \qquad (5)$$

The first of these relations expresses the equality between the number of transitions leaving a given level (v', K') in the upper electronic state to the number of transitions entering that level, while the second does the same for a level (v'', K'') in the lower electronic state. $A_{v'v''}$, the transition rate for the vibrational downward transition (v', v'') (or Einstein coefficient of spontaneous emission), is given by:

$$A_{v'v''} = \frac{64\pi^4}{3hc^3} \frac{g_\ell}{g_u} \nu^3_{v'v''} \cdot |R_{v'v''}|^2 \quad (\sec^{-1}) \qquad (6)$$

or

$$A_{v'v''} = \frac{8\pi^2 e^2}{mc} \frac{g_\ell}{g_u} \frac{p_{v'v''}}{\lambda^3_{v'v''}} f\lambda_{oo} \ , \qquad (7)$$

where $\nu_{v'v''}$ is the frequency of the transition, $R_{v'v''}$ the transition moment, $p_{v'v''}$ the relative transition probability (for which numerical values have been tabulated by Nicholls (1956)), and where f is the f-value of the electronic transition referred to the wavelength λ_{oo} of the (0, 0) band of the system.* g_ℓ and g_u are the statistical weights of the lower and upper electronic states respectively. The other symbols are obvious. Similarly, the transition rate for upward transitions is

$$C_{v'v''} = B_{v'v''} u_{v'v''} \qquad (\sec^{-1}) \tag{8}$$

or

$$C_{v'v''} = \frac{4\pi^2 e^2}{mhc^3} p_{v'v''} f\lambda_{oo} (\lambda^2 F_\lambda)_{v'v''} W \tag{9}$$

where $B_{v'v''}$ is the Einstein coefficient of absorption, $u_{v'v''}$ is the energy density of exciting light, per unit frequency interval, at the wavelength of the transition at the distance r from the sun, F_λ the mean intensity of the solar disk in the continuum, per unit wavelength interval, at the same wavelength (the effect of absorption lines is taken care of by the residual intensity factor r_λ** in equations 4 and 5, and

*The relation between the line strength (equivalent to $|R_{v'v''}|^2$ here) and the oscillator strength involving a factor λ, a particular wavelength has to be specified before an f-value can be defined in the case of a molecular band system. The most natural choice is, of course, to take λ_{oo}, the wavelength of the (0, 0) band -- although another wavelength may be more appropriate in some cases (cf. Appendix C, b, where the definition of f is also given).

**The residual intensity as determined from the Utrecht Photometric Atlas has to be corrected in order to allow for the difference between "apparent" continuum (ordinate 100 in the Utrecht Atlas) and true continuum, as indicated by Michard (1950).

W is the dilution factor:

$$W = \frac{1}{2}\left(1 - \sqrt{1 - \frac{R_\odot^2}{r^2}}\right) \approx \frac{R_\odot^2}{4r^2} \tag{10}$$

S^R and S^P denote the rotational line strength for an R- and a P-line respectively, g_K the statistical weight of level K and A_K^{rot} the transition rate for pure rotational transition from level K to K-1 (for simplicity we shall write K for K"), which can be expressed as:

$$A_K^{rot} = \frac{64\pi^4}{3hc^3}\,\nu_K^3 e^2 \sigma^2 \frac{S_K}{g_K} \tag{11}$$

or

$$A_K^{rot} = \frac{256\pi^4 \mu^2 B^3}{3h}\,\frac{K^4}{K + \frac{1}{2}} \tag{12}$$

where ν_K is the frequency of the pure rotation transition $K \rightarrow K-1$,* $\mu = e\sigma$ is the electric dipole moment of the molecule, S_K the pure rotation line strength, and B the rotational constant in the vibrational level $v'' = 0$ of the $X\,^2\Sigma^+$ state.

If we recall that of the four possible arrangements of absorptions and subsequent emissions (absorption in either of R- or P-branch followed by emission in either of these branches) the process of absorption in the R-branch followed by emission in the P-branch, the net result of

---

*We note incidentally that $\nu_K = 2BKc$ is expressed in terms of K, not J as Hunaerts has written (Hunaerts, 1959b). Indeed the rotational term values are given in terms of the quantum number K:

$$F(K) = BK(K+1).$$

We can neglect the term in $K^2(K+1)^2$ because the corresponding term in K^3 in ν_K would be important only for $K \gtrsim 50$, since $D/B \approx 3 \times 10^{-6}$. The numerical values given in table 1 of the above-mentioned paper should be revised accordingly, especially for the lower K-values (cf. Appendix A).

which is a passage from K to K + 2 in the ground state, has the largest probability,* it will become clear that, as Wurm first showed in 1937, the distribution of populations in the lower state of the cometary molecule will be governed by two competitive processes: (1) absorptions of solar light followed by emissions, which tend to increase the populations of the higher levels, and (2) pure rotation transitions in the ground state, which have the effect of bringing molecules back to lower K-levels.

As a rule we possess only poor data on the permanent dipoles of molecules -- when we have any knowledge at all -- so that it would be hard to solve systems of equations like equations 4 and 5 in a satisfactory manner. However, Hunaerts has found recently a nice way out of this difficult situation. Hunaerts makes use of the cometary observations themselves: he assumes that the last line seen in a band corresponds to a lower level K" such that for the next higher rotational level the lifetime against pure rotation transition, τ_{rot}, is equal to the lifetime against absorption, τ_{abs}. Since we know τ_{abs}, it is then easy to derive the rotational transition rates A_K^{rot}.

In the case of the CN radical, the vibrational transition probabilities are such that we can consider only the two levels $v' = 0$ and $v'' = 0$. This greatly simplifies the equations. Combining equations 4 and 5 and numbering the rotational levels in the ground state with K instead of K", we obtain after some simple manipulations:

---

*The products of the line strengths of the lines involved in the various arrangements are as follows:

RP ($K \rightarrow K + 2$) : $4(K + 1)(K + 2)$
RR (no change in K) : $4(K + 1)^2$
PP (no change in K) : $4K^2$
PR ($K \rightarrow K - 2$) : $4K(K - 1)$

$$x_K\left(1 + \frac{A_K^{rot}}{C_{oo}}\right) = x_K\left(\frac{S_K^R}{g_{K+1}} \cdot \frac{S_K^R}{g_K} + \frac{S_K^P}{g_{K-1}} \cdot \frac{S_K^P}{g_K}\right) + x_{K-2}\frac{S_K^P}{g_{K-1}} \cdot \frac{S_{K-2}^R}{g_{K-2}}$$

$$+ x_{K+2}\frac{S_K^R}{g_{K+1}} \cdot \frac{S_{K+2}^P}{g_{K+2}} + x_{K+1}\frac{A_{K+1}^{rot}}{C_{oo}} \qquad (13)$$

where x_K is the relative population of level K in the ground electronic state. We disregard the influence of the Fraunhofer lines for the time being, so that the residual intensity factor r_λ has been set everywhere equal to unity. Carrington (1962) has proposed a slightly different optics which lumps absorption and emission together and thus deals only with levels in the lower electronic state from the very beginning. Equation 13 can be rewritten:

$$p_{K-2}x_{K-2} - (p_K + q_K + m_K)x_K + m_{K+1}x_{K+1} + q_{K+2}x_{K+2} = 0 \qquad (14)$$

where

$$p_K = \frac{(K+1)(K+2)}{(2K+1)(2K+3)}, \quad q_K = \frac{K(K-1)}{(2K-1)(2K+1)}, \quad m_K = \frac{K^4}{K + \frac{1}{2}} \cdot R, \qquad (15)$$

R being a dimensionless parameter which measures the relative importance of the pure rotation transitions as compared with the fluorescence processes:

$$R = \left(\frac{256\,\pi^2 mc^3 r_1^2}{3e^2 R_\odot^2}\right) \cdot \frac{\mu^2 B^3}{p_{oo} f\lambda_{oo} (\lambda^2 F_\lambda)_{oo}} \cdot r^2 \qquad (16)$$

(r_1 is one A. U. expressed in cm, so that r is the heliocentric distance

of the comet in A. U.). The second factor in equation 16 contains the dependence of R on the molecule itself. λ is taken to be constant and it is assumed that F_λ does not vary over the wavelength range of the CN (0, 0) band. A more useful expression for R is:

$$R = \frac{\tau_{abs}(r)}{\tau_{rot}(K)} \times \frac{K + \frac{1}{2}}{K^4} \quad , \tag{17}$$

which shows that, if $(K_\ell - 1)$ is the quantum number of the lower level corresponding to the last line observed in the comet spectrum, the value of R for the particular molecule involved and for the particular heliocentric distance at which the spectrum was taken, is given by:

$$R = \frac{K_\ell + \frac{1}{2}}{K_\ell^4} \quad , \tag{18}$$

provided that we make the reasonable assumption that $\tau_{abs}(r) = \tau_{rot}(K_\ell)$.

Our purpose is to determine the distributions of x_K to be used in the analysis of the CN (0, 0) band in the three spectra mentioned earlier. However, it has been found instructive to make this study somewhat more general and to endeavor to remove the arbitrariness attached to the method which uses a Boltzmann distribution at a temperature adjusted so as to give a more or less satisfactory fit with the observations. Accordingly, a computer program has been written in order to treat some 20 cases corresponding to values of r ranging from 0.2 to 4.0 A. U. and including 30 rotational levels. The computations have also been carried out for a larger number of rotational

levels (36); in the range of heliocentric distances of interest their results are essentially identical to those obtained when 30 levels are considered. The complete sets of results are given in tabular form in Appendix B. Some of the distributions have been plotted in figure 2 which shows their dependence on the heliocentric distance. Each curve has been normalized in such a way that

$$\sum_{K=0}^{29} x_K = 1 \qquad (19)$$

The competition between fluorescence and pure rotation transitions is clearly illustrated: the maximum of the distribution curve is displaced toward lower K-values as the comet recedes from the sun, i.e., as the illumination decreases and the rotation transitions become more and more predominant.

We have already seen how a numerical value of the parameter R can be obtained. For CN reference has been made to Hunaerts' work on Comet 1942g (Hunaerts, 1959b). The last line of the CN (0, 0) band seen in the spectrum of this comet, which was observed at r = 1.4 A.U., corresponds to K = 15. Thus we should write:

$$\tau_{rot}\,(16) = \tau_{abs}\,(r = 1.4)\ ,$$

from which we should derive the value of R corresponding to unit distance: $R_1 = 1.25 \times 10^{-4}$. Calculations based on this value, however, lead to a distribution of x_K at r = 0.6 A.U. which fails to reproduce the details of the intensity distribution observed in the spectrum of Comet Mrkos (1957d) in the sense that it predicts too small intensities for K values greater than about 19 when the Fraunhofer

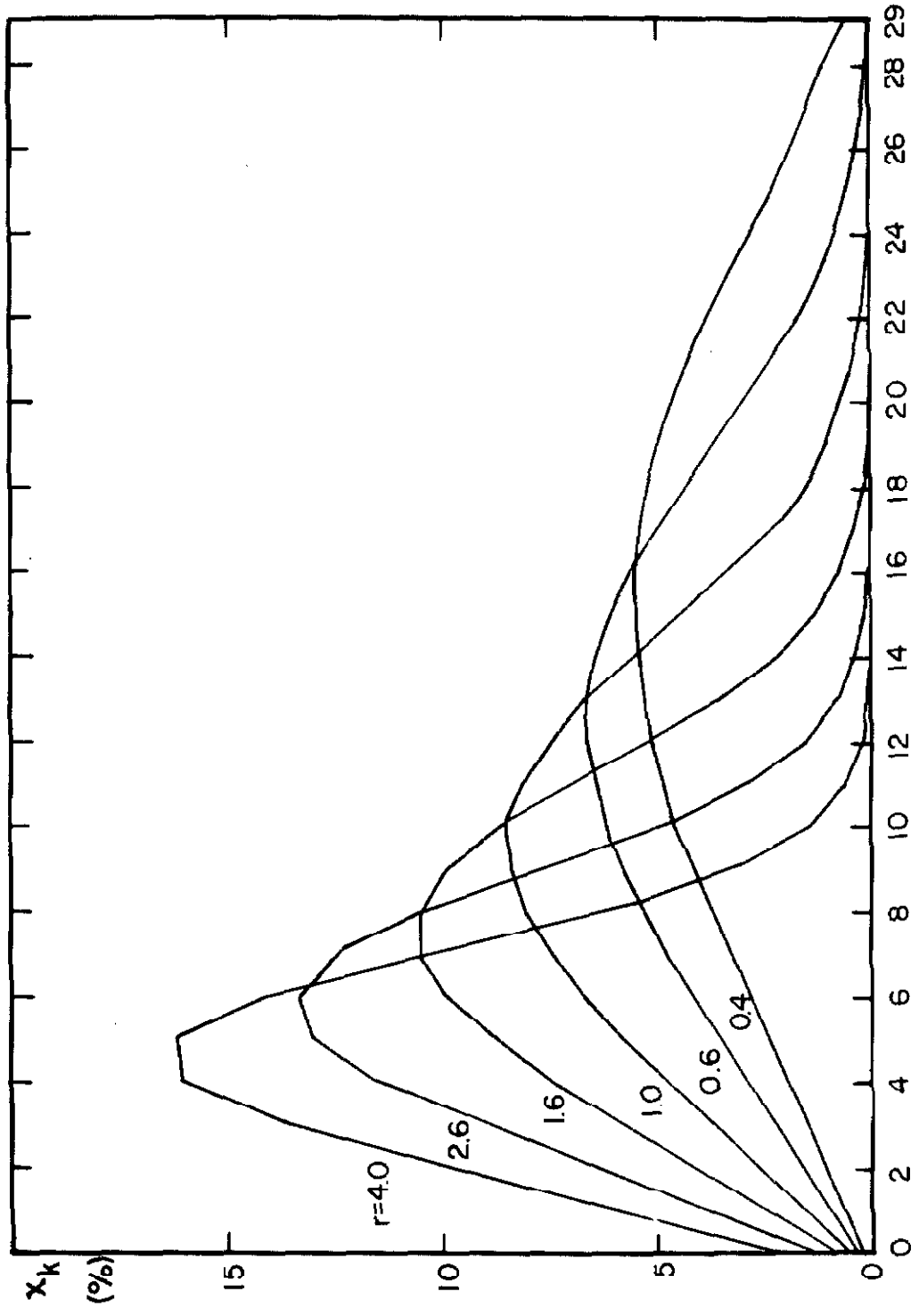

Fig. 2. Relative populations of rotational levels of the ground state of CN in comets for various heliocentric distances (r in A.U.).

lines are taken into account.* The discrepancy can be partly removed when the presence of the (1,1) band is taken into account, but this is insufficient to explain it completely. Improvement could not be achieved by merely relaxing the condition that $\tau_{rot}(K_\ell)$ is exactly equal to $\tau_{abs}(r)$: one might, indeed, expect the rotational lifetime of the lower level corresponding to the first unobserved line to be only a fraction of the lifetime against absorption of sunlight depending on the exposure time, but this would only make the situation worse, as the corresponding value of R_1 would be larger and the x_K-distribution would, accordingly, extend still less toward high K's. However, another more important modification of Hunaerts' condition ought to be made. For a given cometary molecule the lifetime against absorption, $\tau_{abs}(r)$, has been regarded so far as depending only on the heliocentric distance of the comet, while, in fact, it will also show up a dependence on K through the effect of the Fraunhofer lines again, and hence on heliocentric radial velocity. If we examine the case of Comet 1942g more closely we find that for the few lines just following the last line observed, from K = 17 to 20, the values of r_λ are very small -- taking account that $\frac{dr}{dt}$ = + 6 to 8 km/sec (McKellar, 1944) -- which suggests that some of these lines may be absent not because $\tau_{rot}(K)$ is already so small, but rather because $\tau_{abs}(r)$ is so long owing to the weakness of the exciting light at the appropriate wavelengths for these lines. Thus the value of K at which $\tau_{rot}(K)$ becomes equal to that part of $\tau_{abs}(r)$ which does not depend on K -- or to a fraction of it -- is probably

*Hunaerts has treated this case recently (Hunaerts, 1959a). I must say that I do not understand completely his results, especially the numbers in the column headed "$I_\odot$" of his table 5: this $I_\odot$ should be equal to what is called here r_λ but Hunaerts' values seem, in general, too high.

larger than 16. In order to determine the best value for R_1 the steady-state equations were solved at $r = 0.6$ A. U. assuming successively the values $K_\ell = 16, 17, 18, 19, 20$, for Comet 1942g and the corresponding theoretical intensities in the R-branch were compared with the intensities observed in the spectrum of Comet 1957d. The final result was:

$$R_1 = 1.0 \times 10^{-4} .$$

It should be emphasized that in order to reach complete agreement between theory and observation the solar absorptions have to be included at the very beginning, i.e. in the determination of x_K. This result is not surprising at all. As a matter of fact, the computations which neglect the Fraunhofer lines in the first step (determination of x_K) and take them into account in the second phase (evaluation of the intensities) obviously involve an inconsistency. The distribution marked "c" in figure 3 results from the solution of a system of equations equivalent to system 13 but in which allowance is made for the effect of the Fraunhofer lines, while "a" is a steady-state distribution which does not include the solar absorption lines and the "b" curves are Boltzmann distributions. To go over to the intensity profiles we have to make use of the following formulae:

$$y_{K'} = x_{K=K'-1} \cdot \left(r_\lambda \frac{S^R}{g}\right)_{K=K'-1} + x_{K=K'+1} \cdot \left(r_\lambda \frac{S^P}{g}\right)_{K=K'+1} , \quad (20)$$

which gives the relative population in the excited level K', and

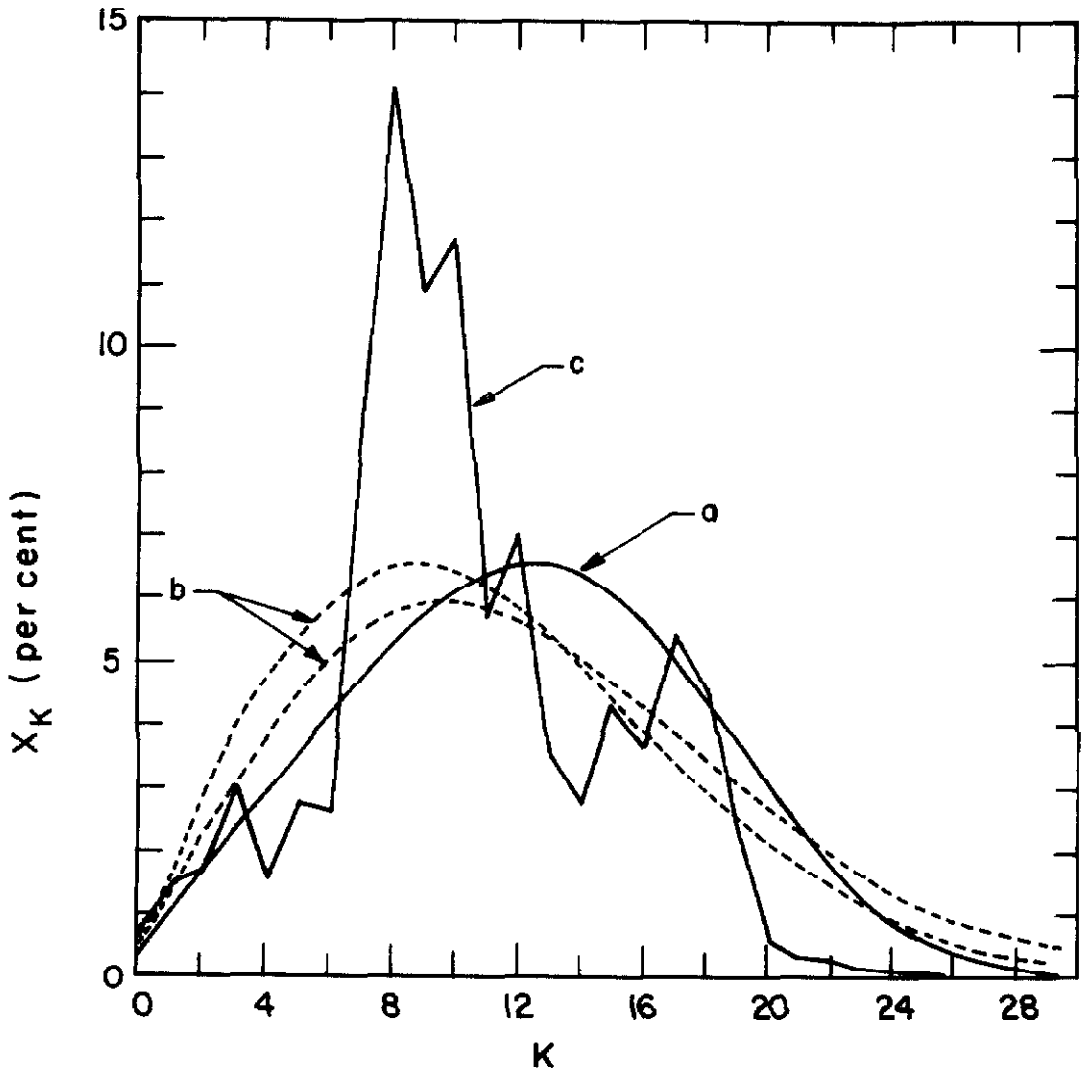

Fig. 3. Comparison of distribution of relative populations of rotational levels of CN at r = 0.6 A.U.:

a. from steady-state equations neglecting Fraunhofer lines
b. Boltzmann distributions (450 and 550 °K)
c. from steady-state equations taking account of Fraunhofer lines (dr/dt = + 34.7 km/sec).

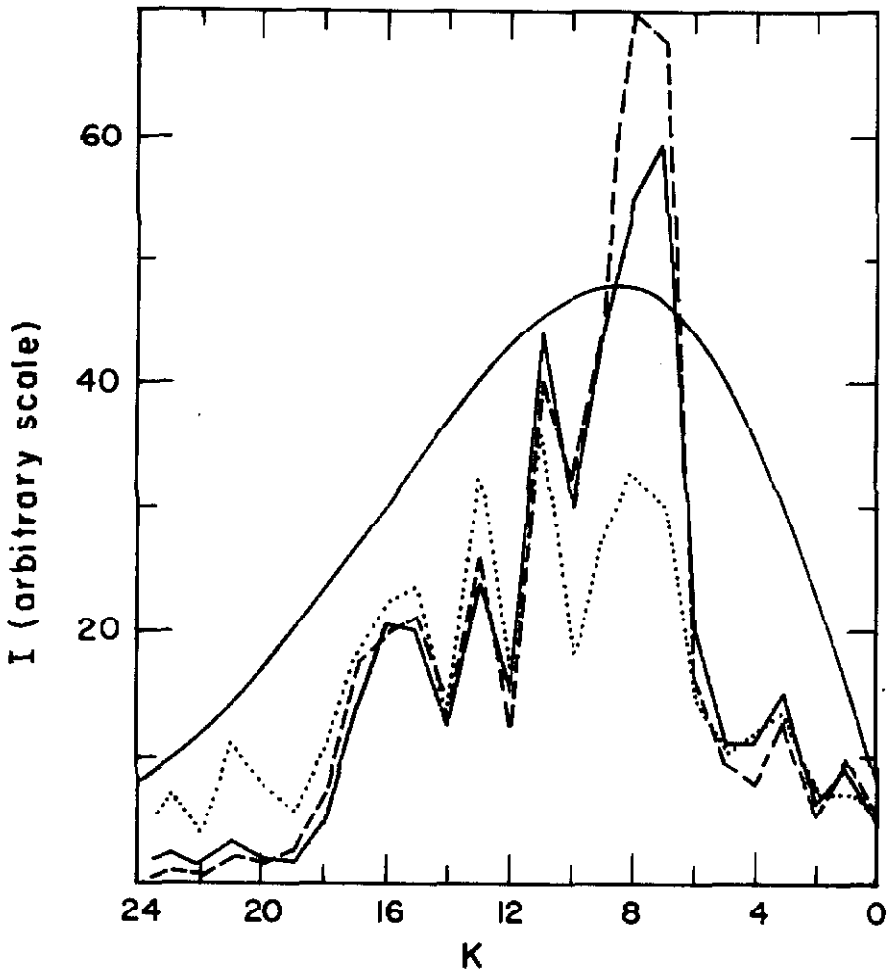

Fig. 3A. Intensity distribution in the R-branch of the CN violet (0, 0) band in the spectrum of Comet Mrkos (1957d).
Solid curve: observed distribution
Dotted curve: theoretical curve based on x_K-distribution neglecting Fraunhofer lines
Dashed curve: theoretical curve corresponding to steady-state distribution taking Fraunhofer lines into consideration.
The smooth curve represents the thermal equilibrium intensity distribution ($T = 500\,^{\circ}K$).

$$i_K^R = \left(y_{K'} \frac{S_{K'}^R}{g_{K'}}\right)_{K'=K+1} = y_{K'=K+1} \cdot \frac{K+1}{2K+3}, \qquad (21)$$

$$i_K^P = \left(y_{K'} \frac{S_{K'}^P}{g_{K'}}\right)_{K'=K-1} = y_{K'=K-1} \cdot \frac{K}{2K-1}, \qquad (22)$$

which express the intensities of the rotational lines in the R- and P-branch respectively (an unimportant factor involving the wavelength has been omitted). Figure 3A shows the intensity distributions predicted on the basis of x_K-distributions ignoring the effect of Fraunhofer lines (dotted curve) or including this effect (dashed line): it is clear that the latter accounts better than the former for the observed intensity distribution in the R-branch of the (0, 0) band. Distribution "a" and distributions "b" give nearly the same result; only one intensity distribution has been plotted for these two cases in figure 3A. It is seen that these x_K-distributions are definitely unable to reproduce the high intensity jump from R(6) to R(7) and that, on the contrary, they predict too high intensities for the last lines (the observed intensity profile has been corrected for the presence of the (1,1) band assuming a ratio (1,1)/(0, 0) = 0.10). The fact that the maximum in curve "c" of figure 3 is more pronounced and shifted to the left with respect to what it is in curve "a" can be understood roughly from the circumstance that the weakening due to the solar absorption lines has, on the whole, an effect similar to that of an increase in the heliocentric distance, which is precisely to push the distribution curve toward lower K-values, as we have already seen in figure 2.

A final remark concerning the general treatment of the

fluorescence problem of CN in comets is necessary. It has been tacitly assumed in the foregoing considerations, as has always been in previous studies of this problem, that the fluorescence of the CN violet system ($B\ ^2\Sigma^+ - X\ ^2\Sigma^+$) can be dealt with independently of any other electronic transition in which the ground state $X\ ^2\Sigma^+$ might be involved. Actually, however, the ground state $X\ ^2\Sigma^+$ of CN is connected not only with $B\ ^2\Sigma^+$ but also with $A\ ^2\Pi$, the corresponding transition being the CN red system. Now the red system has long been known to occur in cometary spectra and there is indeed some definite evidence that the overall strength of the red system is probably comparable to that of the violet system in comets (Dufay and Swings, 1958). Thus in order to be completely rigorous it would be required to consider both transitions at the same time. This would make the treatment of the fluorescence appreciably more complicated, especially since it would be necessary to include several vibrational bands in the $A\ ^2\Pi - X\ ^2\Sigma^+$ transition and since each of these bands contains as many as 12 different branches, but on the other hand it would presumably tend to remove some slight discrepancies that still exist between observed and computed intensities (figure 3A). In particular, since the effect of the Fraunhofer lines is not likely to be important in the red system, we may expect that the x_K-distribution would be somewhat smoother than in the case when the violet system is studied alone. This might reduce the maximum observed in curve "c" of figure 3 and thus also the peak occurring at R(7) and R(8) in figure 3A. On the other hand we notice that including the $A\ ^2\Pi - X\ ^2\Sigma^+$ transition would not affect the value of the parameter R_1, which is

determined by K_ℓ, but that it would modify the value of τ_{abs} and consequently, also that of $\tau_{rot}(K)$. (See Appendix A.)

No one of the steady-state distributions can be fitted satisfactorily by a Boltzmann distribution. Nevertheless, if one insists on representing the curves by a parametric formula of the form of the Boltzmann law, one can find such a rough representation. This is shown in figure 3 for the case $r = 0.6$ A.U. (curves "a" and "b"); the Boltzmann curves drawn (450 and 550 ^{o}K) indicate that it is not possible to find an equilibrium distribution that exactly imitates the steady-state curve at both low and high values of K. The Boltzmann curve at 500 ^{o}K used by Hunaerts (1959a) gives about the "best" fit to the steady-state distribution. If this is done for a series of values of r it is found that the parameter T to be used in the Boltzmann formula varies according to the law

$$T = \frac{300}{r} \quad {}^{o}K \tag{23}$$

to be compared with:

$$T = \frac{375}{\sqrt{r}} \quad {}^{o}K, \tag{24}$$

as used recently by Hunaerts (1959a). If one realizes that the difference between curve "a" and curves "b" of figure 3 is not very important,* one can understand roughly, from formula 23 and from the present results concerning the distributions of x_K, why Hunaerts had to switch from:

*This is due to the fact that, as long as one uses x_K's that do not include the effect of the solar absorption lines, the essential factors in formula 20 are the r_λ's rather than the x_K's.

$$T = \frac{300}{\sqrt{r}} \quad {}^{o}K , \tag{25}$$

which he used for OH (Hunaerts, 1953) at r = 1.0 A.U., to formula 24, which he applied to CN at r = 0.6 A.U. Indeed formula 23 gives T = 300 °K at r = 1.0 as formula 24 does, while it gives T = 500 °K at r = 0.6 as formula 25 does. Although the lower electronic state of the relevant transition in OH is a $^2\Pi$ state, the case of OH can be compared, in first approximation, to that of CN since the band systems of these two radicals that we are concerned with have very similar relative vibrational transition probabilities; moreover, the difference between R(OH) and R(CN) -- the former being about 200 times larger than the latter at a given heliocentric distance -- is compensated by the difference between the rotational constants B of the ground states of OH and CN which occur in the Boltzmann formula.

Carrington (1962) has carried out computations similar to the ones presented here, but he has included only 18 rotational levels and he has made an unnecessary approximation which unfortunately invalidates his numerical results. This author has taken a mean value for the factor ν_K^3 in equation 11, which is approximately equivalent to assuming a constant value for K^3 which actually varies from 1 to about 5000 when K varies from 1 to 17. In this way the pure rotation transition rates for the higher levels are underestimated and the resultant distributions are too broad, as they extend too far toward high K-values. Furthermore, the distribution changes too rapidly with the parameter $\frac{m}{\mathcal{F}}$ (equivalent to our parameter R), i.e. with r, as illustrated in figure 4, where

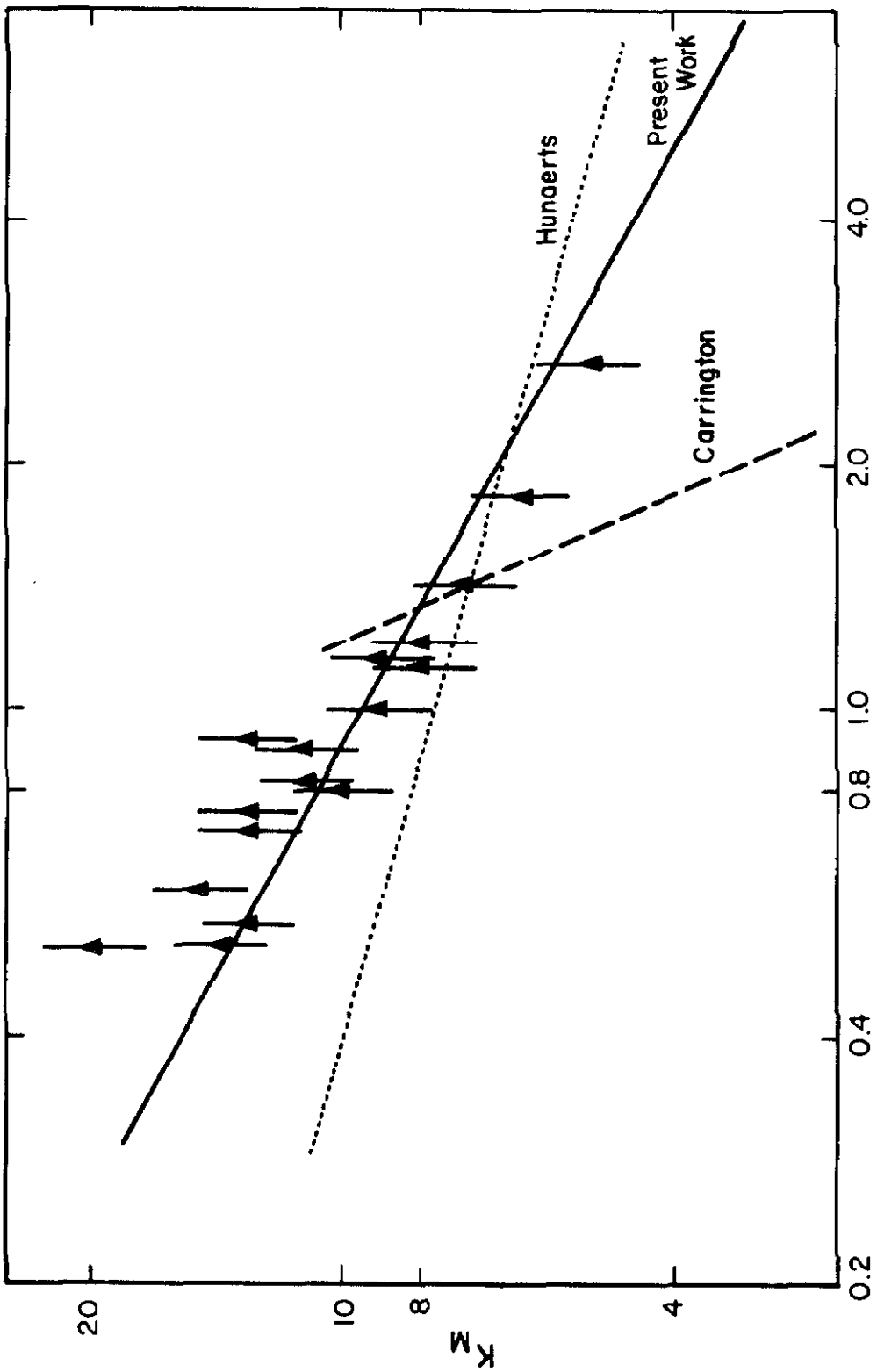

Fig. 4. Relation between K_M and r (logarithmic scales). The triangles represent observational points for which a uniform relative error on K_M has been assumed in spite of the variety of their origins (Dufay, 1938; McKellar, 1942; Dossin et al., 1961; Comet Humason: Pd 6741).

K_M, the value of K at which the maximum of the curve occurs, is plotted against r. Also shown on this plot are a number of observational points taken from various sources. This diagram should be interpreted with great care, the apparent good agreement between the observations and the solid line being only indicative. Indeed, no complete agreement is to be expected, since the observational values for K_M are affected not only, in some cases, by the difficulty of accurately estimating the position of the maximum from the visual inspection of a spectrum, but also, in general, by the effect of the Fraunhofer absorptions, which is not included in the theoretical curve.

We can now turn to the comparison of the three spectra represented schematically in figure 1 (p. 21). Using the appropriate x_K-distributions determined by the respective heliocentric distance and reading r_λ at λ_{exc} indicated by the radial velocities $\frac{dr}{dt}$, we can show by means of formula 20 that there does exist a correlation between minima or maxima appearing in figure 1 on the one hand, and low or large values of the populations of the upper levels corresponding to the lines involved on the other hand. This appears clearly on figure 1A (p. 22) where the quantities i_K^R and i_K^P given by equations 21 and 22 have been plotted after a slight transformation which brings them on to a density scale. Although here again one cannot hope that the theoretical computations will reproduce the observations in all their details, a quick comparison of figures 1 and 1A suffices to disclose a striking similarity between these two diagrams. In particular, the following points are especially evident:

(a) R(18) : weak in Seki-Lines I (S-L I) and Seki-Lines II (S-L II)

(b) R(12), R(14) : valleys in Mrkos (M) and S-L II,

(c) R(10) : dip in M,

(d) R(7), R(8) : stronger in M and S-L II,

(e) R(5) : valley in S-L I,

(f) R(4) : peak in S-L II,

(g) R(3) : peak in S-L I,

(h) The first lines of both the R- and P-branches are stronger in S-L I and S-L II than in M.

No doubt it is significant that we are able to explain such variations in terms of differences in heliocentric radial velocities and heliocentric distances, even in the same comet, on the basis of the resonance-fluorescence excitation mechanism alone. The simplicity of this explanation is certainly not the least of its merits. Beside these convincing examples, a few minor discrepancies between figures 1 and 1A could be pointed out, but there are good reasons for such differences to arise: (1) the effect of Fraunhofer lines has not been taken into consideration in deriving the distribution of relative populations of the rotational levels in the ground state; (2) the accuracy of the solar tracings used is not sufficient; (3) the effective radial velocity, which includes both the orbital radial velocity and a component representing the motion of the molecules within the comet itself, is not known.

b. The Effect of Internal Motions

The latter point leads us into the question of internal motions of the cometary gas. The effect of these motions, first noticed by Greenstein (1958), is to create differences in the relative intensities of certain rotational lines at different places in the comet. These lines are the ones that are most sensitive to small changes in radial velocity, i.e., the ones for which λ_{exc} falls on or near a steep portion of the solar spectrum. The "Greenstein effect" manifests itself in Comet Seki-Lines though less conspicuously than in Comet Mrkos, as we can see from figures 5, 6, and 7. In each of the first two of these figures three "envelopes" corresponding to different positions along the lines, as indicated in figure 7, have been drawn. Noticeable differences exist between these curves, as, for example, on PD 6545:

(a) R(12)/R(11) : ≈ 1 in the central region, while appreciably < 1 elsewhere.

(b) R(11)/R(10) : < 1 except on the sunward side where it is $\gtrsim 1$.

(c) R(3)/R(2) : ≈ 1 at the center and on the tailward side, but < 1 on the sunward side.

(d) In the P-branch the intensity decreases from P(3) to P(6) in the central and tailward regions, with a marked peak at P(3) especially near the center, whereas it is really more constant on the sunward part.

All these differences in relative intensities can be detected visually in figure 7. Figure 6, which corresponds to Pd 6558, shows a more uniform pattern, although examples of intensity ratios that are not the same on the three curves can still be found.

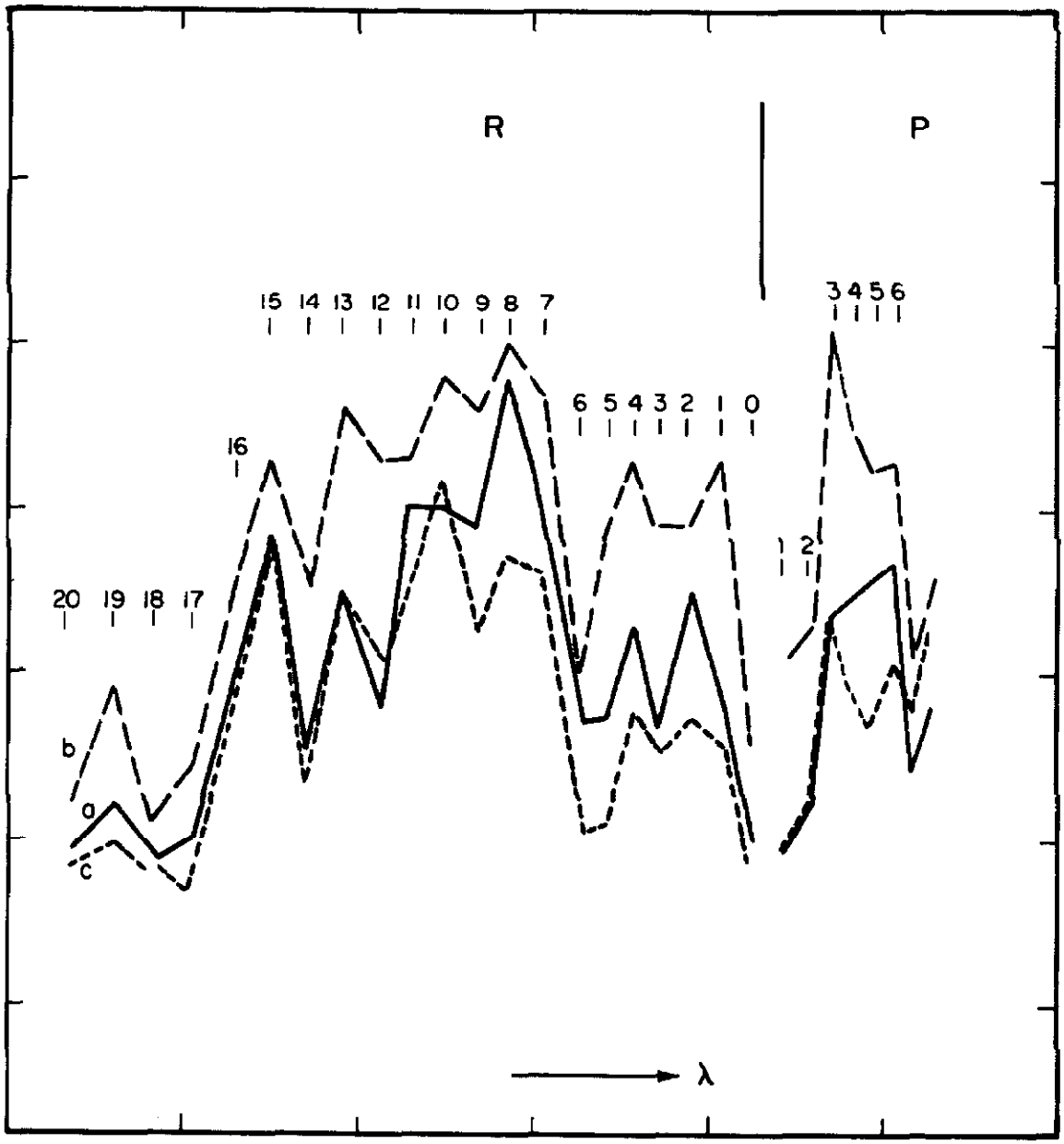

Fig. 5. The Greenstein effect - Pd 6545. The letters (a, b, c) refer to the positions indicated in fig. 7.

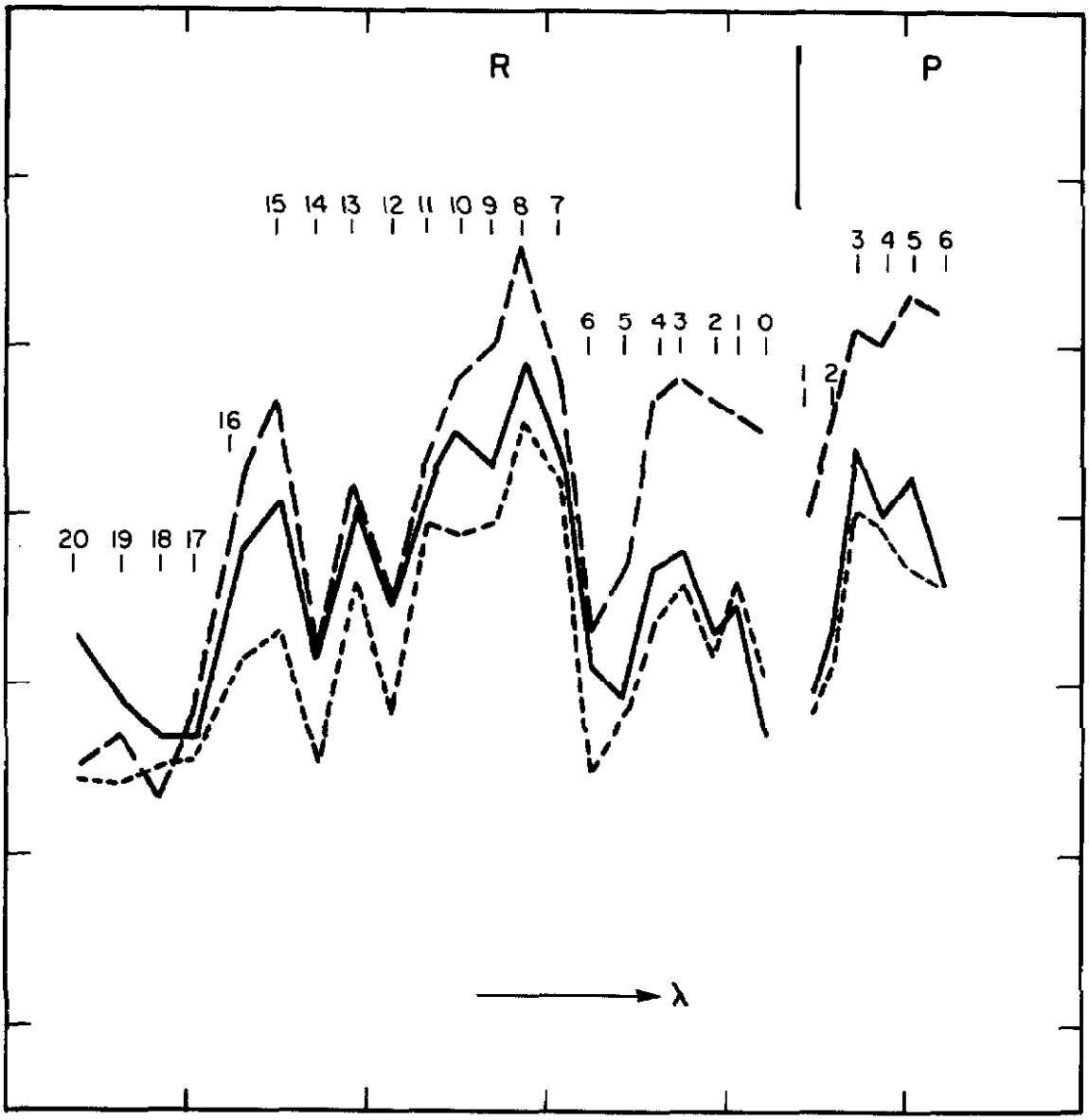

Fig. 6. The Greenstein effect - Pd 6558.

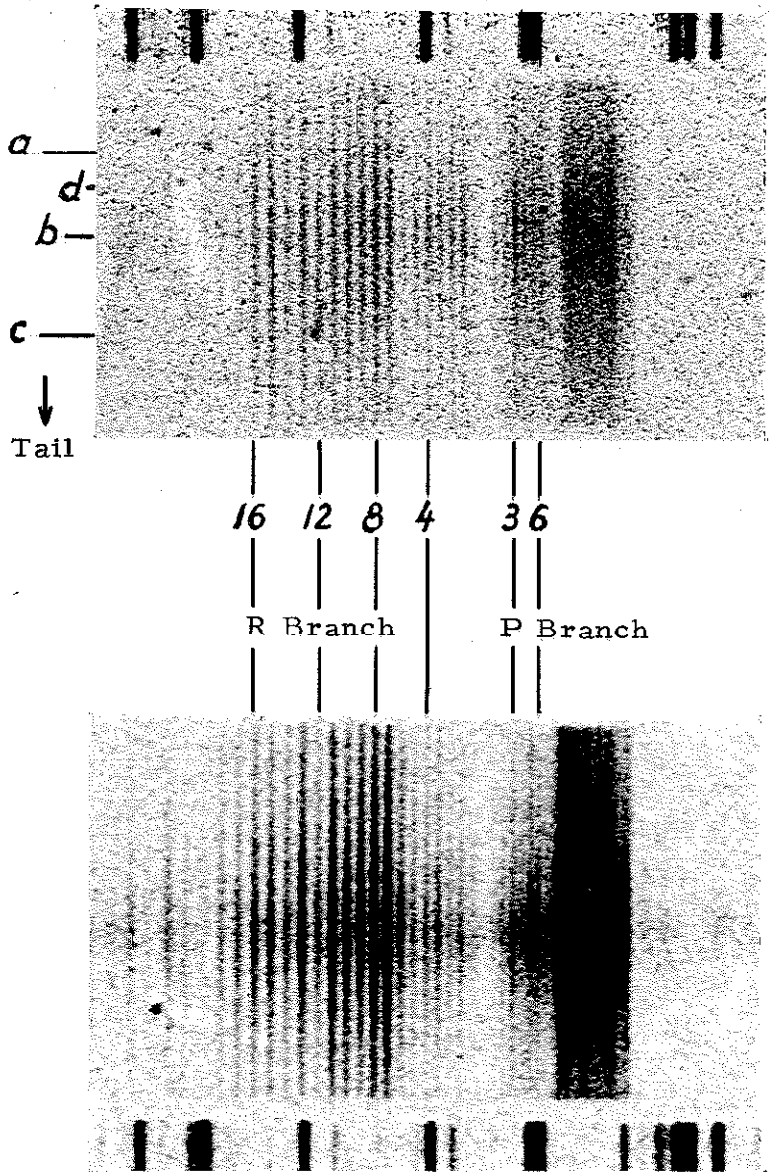

SEKI-LINES
(1962c)

r = 0.79 A.U.

$\frac{dr}{dt}$ = + 46.3 km/sec

MRKOS
(1957d)

r = 0.60 A.U.

$\frac{dr}{dt}$ = + 34.7 km/sec

Fig. 7. The violet CN (0, 0) band in Comet Seki-Lines (1962c) and in Comet Mrkos (1957d)

In a study of the spectrum of Comet Mrkos (1957d) Hunaerts (1959a) proposed to explain the variation of the profile of the violet (0, 0) band with the distance from the center of the nucleus by a possible rotation of the cometary nucleus. This assumption cannot be confirmed in the case of Comet Seki-Lines (1962c) any more than it could be by the spectroscopic observations of Comet Burnham (1959k) (Dossin et al., 1961). Fixing our attention to Pd 6545, for instance, and knowing that the slit of the spectrograph was oriented along the tail of the comet when this plate was taken, we can look for another possible explanation. Whatever the cause of the formation of a comet tail may be, we know at least that some cometary particles are susceptible to undergo the influence of such a cause and are consequently accelerated in a general direction away from the sun. Thus according as the CN radicals are indeed affected by a "wind" of some nature or not we can think of the comet, as far as these radicals are concerned, in terms of either one of the two classical models sketched in figure 8. Model I represents the simplest comet head model that can be imagined: the particles are ejected isotropically with velocity v_o from the nucleus and move radially, undisturbed. Model II is Eddington's "fountain model" in which the particles after ejection (assumed to be isotropic) are submitted to a constant acceleration g directed away from the sun and thus describe parabolic orbits. Let us first consider the possible effects of these motions alone. Since the cometary atmosphere is very tenuous, an observer looking through the comet at a projected distance ρ from the nucleus will see molecules with varying radial velocity components

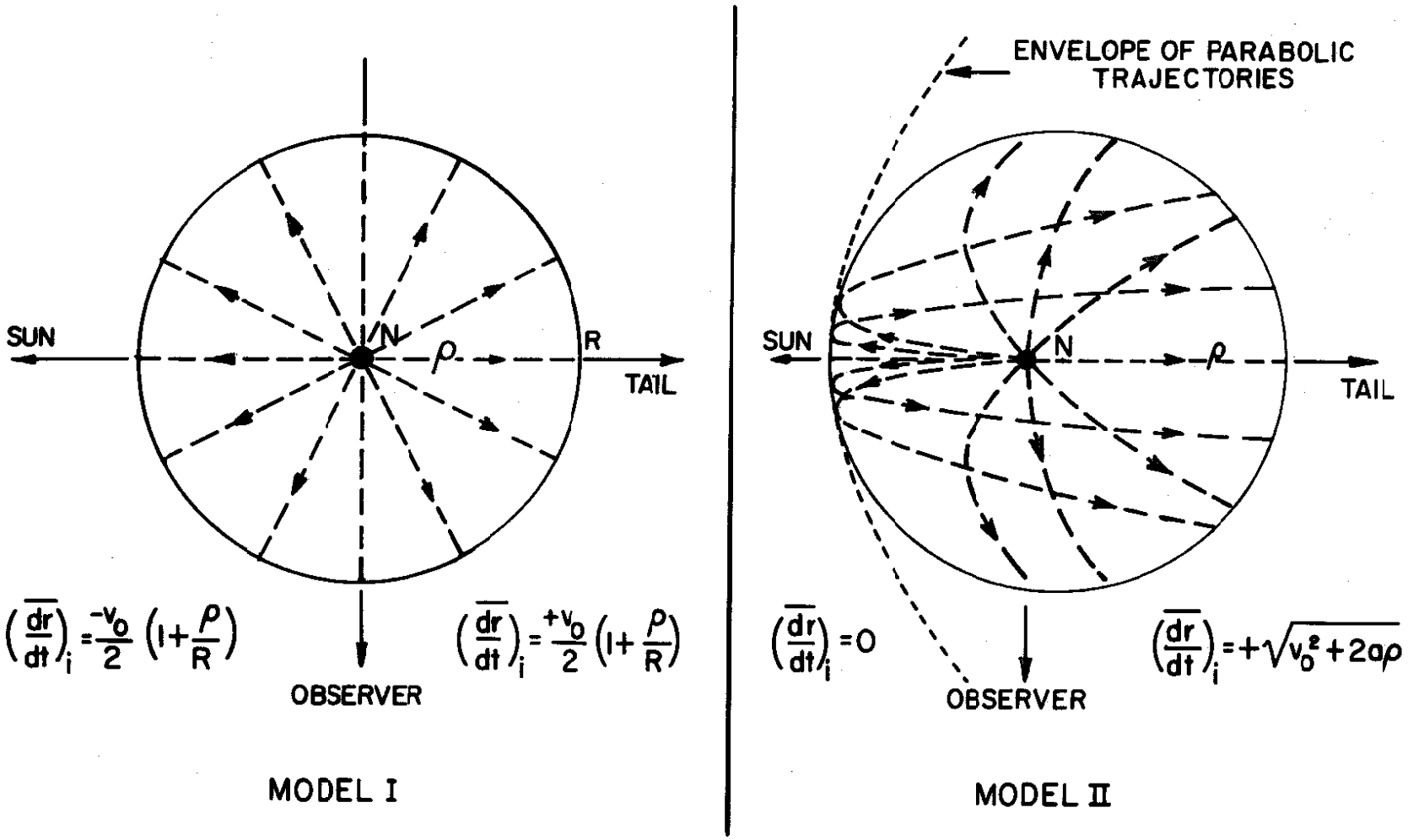

Fig. 8. **Simple models of a comet's head.** The phase angle (sun-comet-earth) is taken to be 90° (this condition was fulfilled by Comet Seki-Lines near the end of April, 1962).

relative to the sun. It is easy to evaluate the mean "internal" radial velocity $\left(\frac{dr}{dt}\right)_i$ as a function of ρ in each situation. The formulae are given in figure 8. In the first case the particle density decreases as the inverse square of the distance from the nucleus so that the dispersion around the mean $\left(\frac{dr}{dt}\right)_i$ is rather small. The distribution of molecules being flatter in the fountain model (see Eddington, 1910, and Fokker, 1953) the mean $\left(\frac{dr}{dt}\right)_i$ is not so sharply defined.

In spite of this difference and the difference in the expressions for $\left(\frac{dr}{dt}\right)_i$ we shall see that it is not easy to distinguish between model I and model II from a study of the structure of the rotational lines. It is useful in such a study to construct "radial profiles" of the lines, like those shown in figure 9, which are obtained by tracing the spectrum along the direction perpendicular to the dispersion and adjusting the length of the slit of the recording microphotometer so as to cover only one line at a time. The shape of these profiles is fixed both by the variation of the integrated number $N(\rho)$ of CN radicals with the projected distance ρ from the center of the nucleus and by the variation of the effective radial velocity, which governs the amount of energy available to excite the individual lines. Thus it is necessary to consider the dependence of what we may call the "excitation function" for level K, e_K, given by:

$$e_K = x_K \cdot \frac{K+1}{2K+1} \cdot r_\lambda^R + x_{K+2} \cdot \frac{K+2}{2K+5} \cdot r_\lambda^P \qquad (26)$$

(also equal to $y_{K'=K+1}$) upon $\left(\frac{dr}{dt}\right)_i$. Some examples can be found in

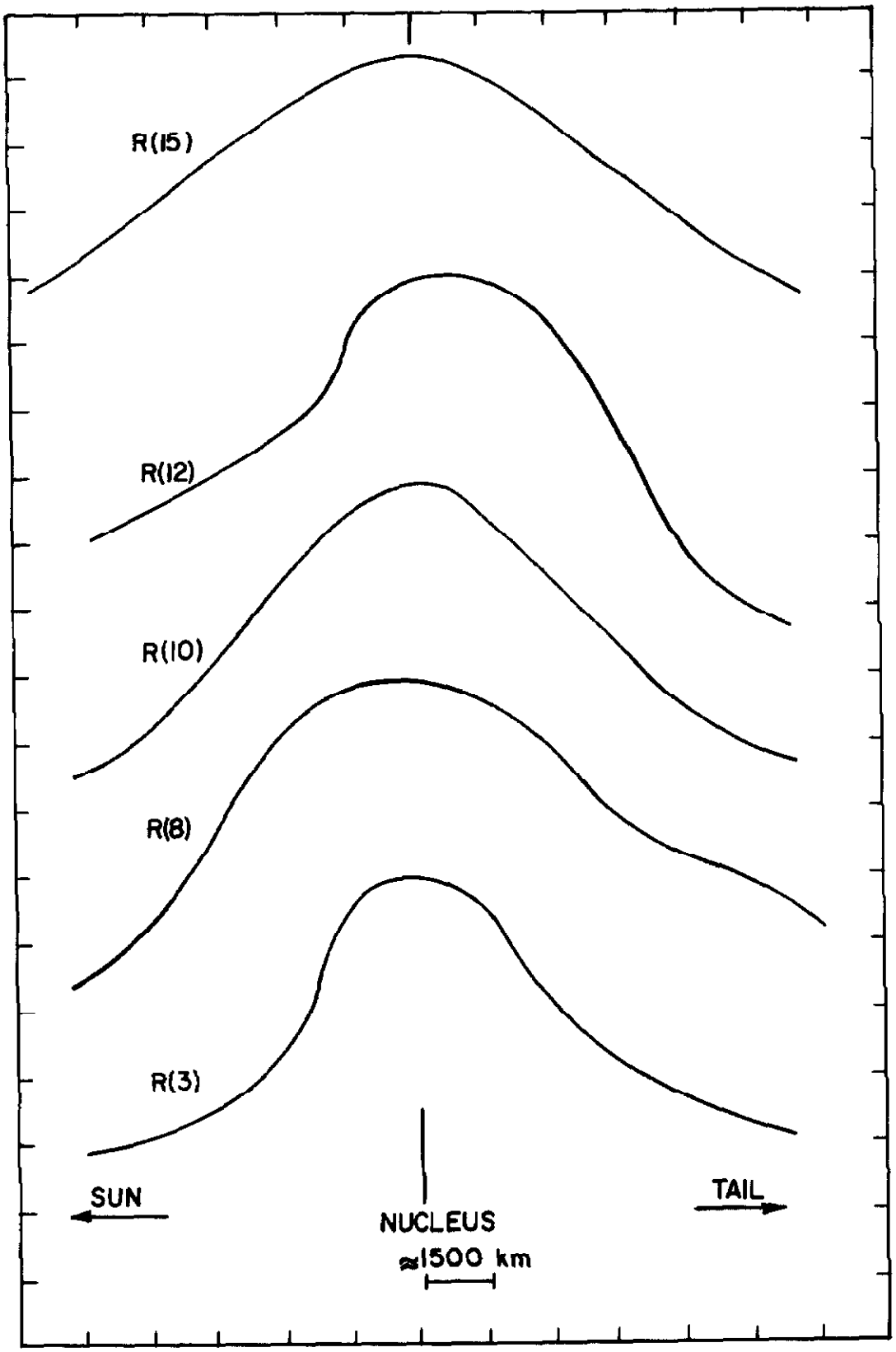

Fig. 9. Radial profiles of rotational lines (density tracings).

figure 10. From this diagram we see that the lines that are the most likely to provide information about the way in which $\left(\frac{dr}{dt}\right)_i$ changes with ρ are R(8), R(9), and R(12), since these are the only lines for which e_K varies appreciably in the neighborhood of $\left(\frac{dr}{dt}\right)_i = 0$. The fact that R(8) and R(9) are somewhat stronger on the sunward side, in the close neighborhood of the nucleus, than on the tailward side, while R(12) is weaker on the sunward side can apparently be accounted for by either model provided that we assume an ejection velocity v_o of about 3 km/sec, a value somewhat large compared with the usual estimates, but not unreasonably so. We cannot hope to make use of the explicit dependence of $\left(\frac{dr}{dt}\right)_i$ on ρ in order to discriminate between the models because the distances ρ involved here are too small -- of the order of several thousand kilometers -- and, in the case of model II, because any possible acceleration imparted to the CN radicals is probably very small, as the very nearly circular character of the observed images of these radicals suggests. Furthermore, the slow increase of $\left(\frac{dr}{dt}\right)_i$ would presumably be masked by the more rapid decline of $N(\rho)$ as ρ increases. Although both models are expected to be over-simplifications of the actual comet head -- e.g., only because they assume a unique velocity of ejection -- it might be argued, at first sight, that model II includes a particularly unrealistic feature in that it regards the repulsive force exerted on the neutral particles as acting continuously, whereas the interaction is more likely to be an impact phenomenon involving either photons or corpuscular radiation. In this respect model I would be closer to reality if, for example, the repulsive

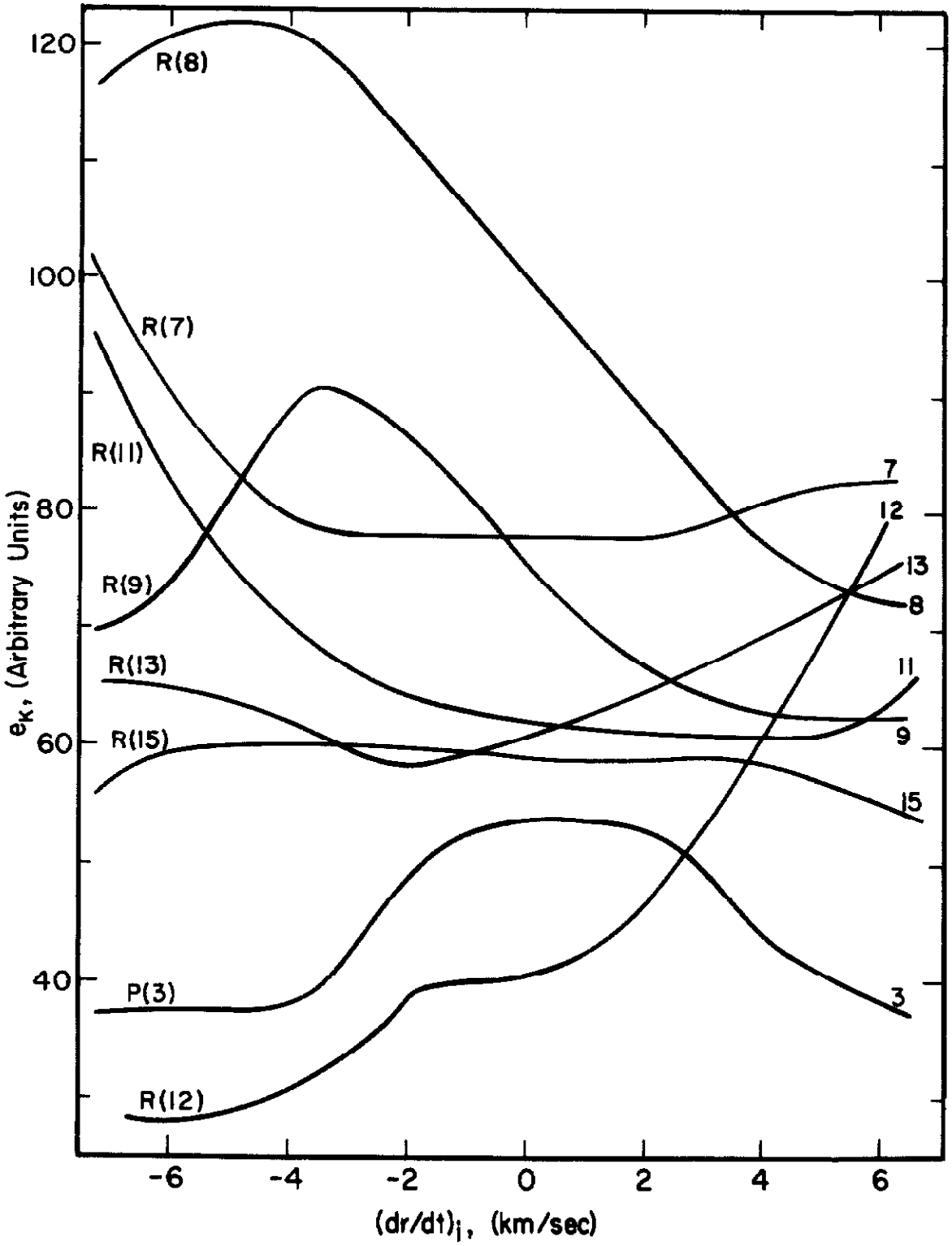

Fig. 10. Excitation functions obtained by means of equation 26. The x_K's include the effect of the Fraunhofer lines (Comet Seki-Lines, April 22, 1962).

force under consideration destroyed the fluorescing particles (ionization, dissociation) at the time of collision. However, the absorptions in the λ3883 band, during which the CN radicals acquire some momentum in the direction opposite to the sun, are much more frequent than the destructive collisions just mentioned (ultraviolet radiation, corpuscules). We shall return to this question in chapter IV. For the time being we note that, in the final analysis, the fountain model seems more probable than the isotropic expansion model.

In any case, in addition to the orderly motions considered so far there is some definite evidence for the existence of internal motions of a more random nature. Thus, for instance, referring to figure 7, we notice that the lines P(3), R(1), R(3), R(9), R(10), R(12), all undergo a discontinuity at a distance of about 2000 km sunward of the nucleus as indicated in this figure (position marked d). Figure 10 then tells us that the only velocity for which P(3), R(9), R(12) together become particularly weak is around -5 to -6 km/sec. It can be verified that, for the same value of $\left(\frac{dr}{dt}\right)_i$, there is a dip in the excitation curves of R(3) and R(10) as well, while R(1) is obviously associated with P(3). On the other hand, almost all other lines are either not or virtually not affected when $\left(\frac{dr}{dt}\right)_i$ changes from about -2 km/sec to about -5 km/sec. An exception is R(11), which should be stronger: this, indeed, is observed. A severe criterion that has to be satisfied when assigning a certain velocity component to a given region in the comet is, of course, that the effects produced by such a velocity on all lines of the band be all consistent with each other. Thus, if we adopt model I, which would

seem the better in this connection, there should be an additional sunward component of radial velocity of some 3 to 4 km/sec at the above-mentioned position in the comet.*

That model I is capable of explaining some observations, while model II is not, does not agree with what has been said above concerning the respective ability of each of these models to represent the actual situation. It is possible that the combined effect of errors in the orbital radial velocity (the orbit used in the determination of $\frac{dr}{dt}$ is not definitive) and in the solar tracings be responsible for this contradiction. For example, a change of $\frac{dr}{dt}$ by -2 km/sec, which would shift the $\left(\frac{dr}{dt}\right)_i$ scale by two units to the left in figure 10, would lead to the conclusion that the fountain model is more adequate to account for all the observations mentioned than the isotropic expansion model. However, such a change in $\frac{dr}{dt}$ seems somewhat large.

A few additional examples of random motions can be given. Thus, negative radial velocity components of about - 2 km/sec seem to be required near 5000 km tailward of the nucleus, which would account for a secondary maximum observed at this place in the radial profile of R(3), and of - 4 km/sec at 9 to 10,000 km towards the tail in order to explain why R(8) is still so strong there while R(12) is so weak. We notice that the internal motions that we have to assume in order to understand the relative intensity fluctuations in the comet head are all directed toward

*The corresponding motions are nearly parallel to the tail axis since no large velocity component relative to the earth is observed. The difference between the observed and computed values for $d\Delta/dt$ may be real, but it is small anyhow (1 to 2 km/sec).

the sun, while the comet was moving away from the sun at the time of the observations. It is tempting to add that this might be consistent with the hypothesis of an interaction between the cometary gas and the resisting force of condensations of interplanetary particles which would oppose the motion of this gas. Yet it would be difficult to go far beyond this point without going into purely speculative considerations.

In a thorough and very accurate investigation one would determine as many "radial profiles" as possible, on an intensity scale. This would give $S(\rho)$, the surface brightness, as a function of ρ. This is not yet directly comparable with the computed intensity referred to one particle, $I^c\left[\left(\frac{dr}{dt}\right)_i\right]$, which is proportional to i_K^R or i_K^P expressed in formulae 24 and 25, for $S(\rho)$ contains a factor $N(\rho)$ representing the dependence on the distance ρ of the number of particles integrated over the line of sight through a column of unit cross section. The determination of $N(\rho)$ makes use of lines such as R(15), for which e_K is very nearly constant over a wide range of $\left(\frac{dr}{dt}\right)_i$: then, indeed, we are sure that the essential factor determining the radial profile is $N(\rho)$, so that $S(\rho)$ is proportional to $N(\rho)$. Knowledge of $N(\rho)$ yields at once the observed energy emitted per particle, $I^o(\rho)$, equal to $S(\rho)/N(\rho)$. A detailed comparison of $I^o(\rho)$ with $I^c\left[\left(\frac{dr}{dt}\right)_i\right]$ should then enable one to derive the relation between $\left(\frac{dr}{dt}\right)_i$ and ρ along the line that was seen by the spectrograph. Repeating this study for spectra of a comet or comets -- preferably dust free! -- observed with the slit of the spectrograph oriented in various positions, and, possibly, combining this with information concerning $\left(\frac{d\Delta}{dt}\right)_i$ obtained from a study

of the usual profiles of the lines at different places in the comet, one would gain a comprehensive view on the internal velocity field in comets and thus compile a set of data which might be valuable for the study of the general structure of cometary atmospheres. The amount of work required to carry out the analysis briefly outlined above, together with the high resolution now achieved in cometary spectra would be disproportionate to the relatively poor degree of accuracy of the reference material concerning the solar spectrum that is generally available at present. In some cases it is found that r_λ varies by a factor of 2 or 3 for a change in λ_{exc} by an amount which, at the wavelength of the CN violet band, corresponds to a velocity of 3 to 4 km/sec. This is illustrated in figure 11. It need hardly be mentioned that it is highly desirable in such cases to possess solar tracings of very high dispersion.

A final remark should be made about the values of x_K to be introduced into equation 26. The rotational line R(12) provides a strong confirmation for the necessity to take consideration of the Fraunhofer lines from the outset of the computation of the theoretical intensities or excitation functions. The transitions capable of exciting this line both fall near the bottom of Fraunhofer lines, as shown in figure 11. Should one use the relative population distribution as determined when no allowance is made for the solar absorption lines, it can be shown that he would derive a very small value for the intensity of R(12) corresponding to an effective radial velocity equal to the orbital velocity alone ($\left(\frac{dr}{dt}\right)_i = 0$) and that it would consequently be necessary

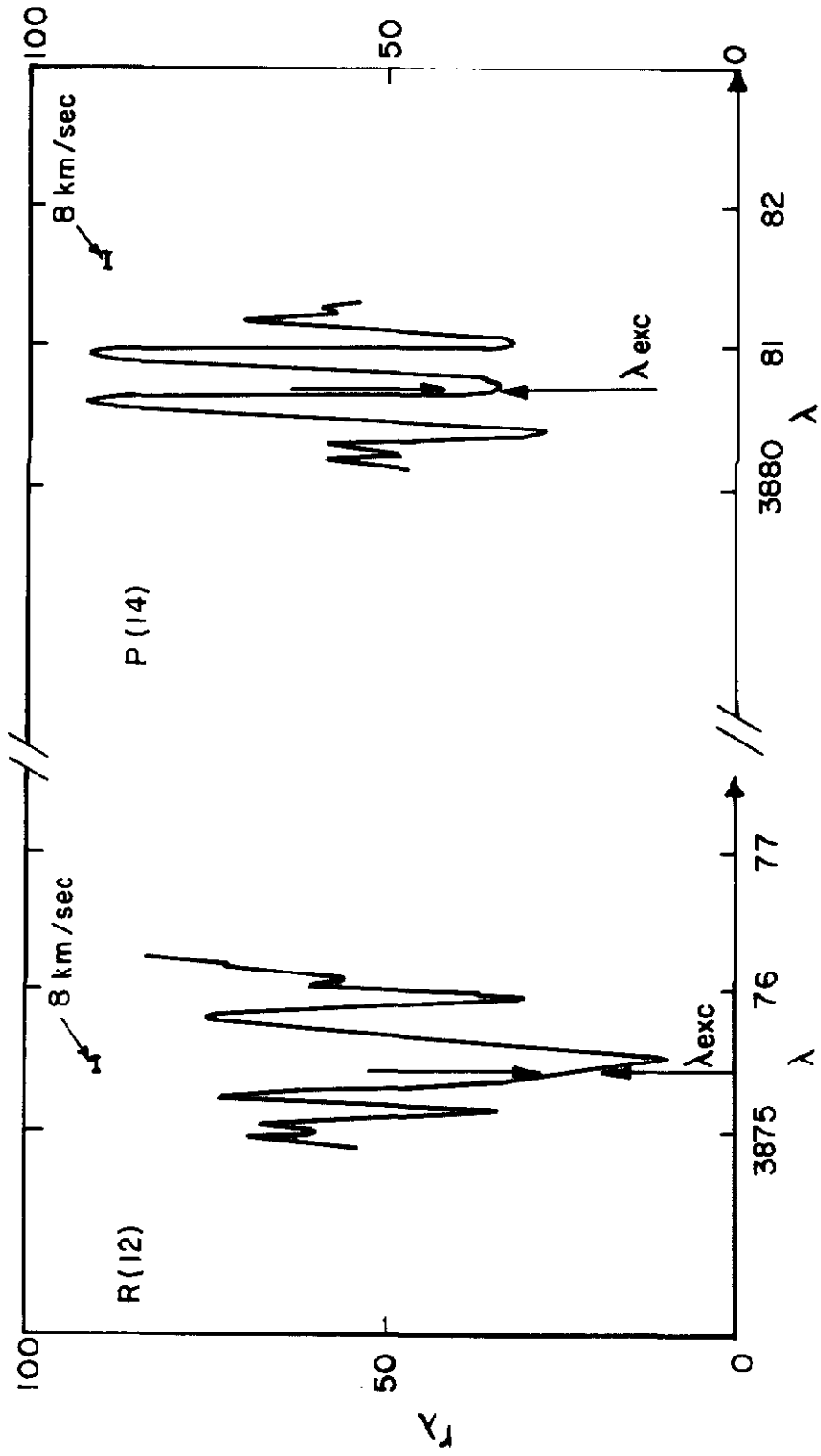

Fig. 11. Excitation of the rotational line R(12) of the violet (0, 0) band of CN in Comet Seki-Lines (1962c). Notice the velocity scale.

to consider anomalously large internal velocities (> 20 km/sec) in order to account for the observation that R(12) is almost as strong as its neighbors near the nucleus of the comet. On the other hand we have already seen that no such difficulty is encountered if the x_K-distribution used itself contains the effect of the Fraunhofer lines.

We are not in a position as yet to provide any detailed explanation for the Greenstein effect. Such an explanation will become possible only after several accurate investigations of the differential motions in a number of bright comets have been carried out by using a method similar, for example, to that which has been proposed above and, possibly, by iterating the procedure in order to obtain a more correct x_K-distribution which corresponds originally to $\left(\frac{dr}{dt}\right)_i = 0$.

2. Visual Region (C_2, NH_2)

The results of two independent measurements of Pd 6552 are given in table 7. The wavelengths listed in the first column have been corrected for the shift associated with the relative motion of comet and earth. The identifications have been made on the basis of the same references as those used by Greenstein and Arpigny (1962) for their analysis of the spectrum of Comet Mrkos (1957d). For the great majority of the emissions the wavelength appearing in the third column is the corresponding wavelength as measured in the spectrum of Comet Mrkos (also corrected for the Doppler shift); only the symbol of the molecule or radical responsible for the emission is then added, the complete identifications being given in the above-mentioned paper. Since Comet

Table 7. The Visual Region of the Spectrum of Comet Seki-Lines (1962c)

λ	I	Identifications
4697.00	1N	97.40 C_2 (3, 2) Head
4714.64	2N	14.80 C_2 (2, 1) Head
36.67	3n	37.16 C_2 (1, 0) Head
5013.68	0N	13.97 (2) C_2
29.85	1N	30.07 (2N) C_2
33.90	0?	33.95 (1N) C_2
37.65	1n	37.76 (2) C_2
41.22	1n	* 41.40 C_2 $R_1(49)$, $R_2(48)$, $R_3(47)$
45.25	0N	45.21 (1) C_2
48.39	0n	48.79 C_2 $R_1(47)$, $R_2(46)$?
49.65	0N	49.74 (0) C_2
52.86	1N	52.77 (3) C_2
56.27	1N	55.94 (3d) C_2
59.85	1	59.80 (2) C_2
61.75	1N	* 61.55 C_2 $R_3'(31)$; 61.45 $R_2'(32)$, $R_1'(33)$
63.07	1N	63.15 (2) C_2
64.96	0N	64.58 C_2 $R_3'(32)$?
66.81	1N	66.82 (1) C_2
70.23	2	70.12 (2) C_2
71.92	0	71.65 C_2 $R_1''(15)$; 71.96 $R_2''(14)$; 72.20 $R_3''(13)$
73.48	1n	73.47 C_2
75.28	0	* 75.42 C_2 $R_3(26)$; 75.02 $R_2(27)$; 74.94 $R_1(28)$
76.66	2N	76.77 (1) C_2
80.04	2	80.17 (2) C_2
83.03	2N	82.94 (2N) C_2
84.78	0	84.92 (1) C_2
86.64	2n	86.65 (1n) C_2
89.29	2	89.33 (3) C_2
92.43	2n	92.41 (2) C_2

Table 7. Continued

λ	I	Identifications
5093.93	0n	
95.41	2	95.34 (2) C_2
97.61	2N	98.16 (2) C_2 (2, 2) Head
5101.07	2N	01.14 (2) C_2
03.64	2n	03.58 (2N) C_2
05.19	0N	
06.61	2	* 06.46 (2) C_2
08.24	0	
09.25	2n	09.30 (1) C_2
11.68	2n	11.68 (2) C_2
13.29	0	13.03 (0) C_2
14.35	2	14.36 (2) C_2
15.82	0	15.88 (1) C_2
16.86	2	16.74 (2) C_2
19.37	2	18.97 (1N) C_2
21.52	2n	21.32 (2) C_2
24.01	2	* 23.76 (0N) C_2
25.86	2N	26.05 (2N) C_2
28.75	6N	28.42 (5), 29.11 (5) C_2 (1,1) Head
32.53	2	* 32.38 C_2 R_1(18)
34.24	1N	* 34.19 (0) C_2, NH_2
36.51	1n	36.16 (1) C_2
38.14	1n	38.24 (1) C_2
39.70	1n	39.47 (1) C_2
41.90	1n	41.41 (2n) C_2
43.20	1d	* 42.98 (0) C_2
44.96	1N	44.73 (2) C_2
46.28	1n	46.06 (1) C_2
47.80	1n	47.82 (1) C_2
49.36	1n	49.26 (1) C_2

Table 7. Continued

λ	I	Identifications
5150.63	1n	50.64 (2) C_2
52.01	1	51.97 (1) C_2
53.27	1	53.33 (1) C_2
54.45	1	54.47 (1) C_2
55.68	1	55.57 (1) C_2
56.74	0	* 56.71 (1) C_2
57.95	1	57.70 (1) C_2
58.65	1	58.39 (1d) C_2
62.61	5N	61.69 (3N), 64.08 (10N) C_2
64.84	20N	64.71 C_2 (0,0) Head
86.25	0	86.21 (0n) NH_2
91.75	0n	
94.14	0	94.17 (1) NH_2
5318.27	1N	18.32 (2) C_2
27.65	0N	27.49 (0n) C_2
32.81	1	32.47 (1N) C_2
83.24	1d	83.42 (1n) NH_2
98.76	1N	99.00 (2n) NH_2
99.94	0?	
5401.66	0N	
13.35	1N	13.11 (1N) C_2
17.00	0N	* 17.03 (1n) NH_2
18.93	1	19.08 (2) NH_2
23.92	0N	23.74 (1) NH_2
28.67	3	28.87 (5n) NH_2
41.09	0N	
43.61	2N	43.70 (1) NH_2
46.90	0N	* 46.50 C_2 R_1(55)?
51.87	0n	* 51.91 (2) C_2
56.84	0n	57.16 (1) C_2
58.63	0	59.16 (1) C_2

Table 7. Continued

λ	I	Identifications
5460.60	0	60.92 (0) C_2
62.41	1N	62.63 (2) C_2, NH_2
69.64	2N	69.88 (2N) C_2
72.63	2N	72.73 (3n) C_2
75.68	0N	75.96 (1) C_2, NH_2
77.55	0N	* 77.29, 77.66 NH_2 $^2_{20}$- $^1_{10}$
82.12	1N	82.46 (2n) C_2
87.63	1N	87.90 (2) C_2
89.57	0n	89.77 (0) C_2
92.15	2n	92.16 (3N) C_2
97.03	1N	97.01 (3n) C_2
98.97	0?	99.04 (0) C_2
5501.26	3n	01.28 (5d) C_2 (3,4) Head
06.53	2N	06.24 (3) C_2; 06.80 NH_2 (1,7,0) $^2_{21}$- $^3_{31}$
08.16	0	08.53 (1) C_2
10.63	2N	10.90 (2) C_2
12.67	0N	12.74 (0) C_2
14.79	2	14.91 (2) C_2
16.59	1	16.94 (0) C_2
21.50	0	21.57 C_2 $R_1(29)$; 21.40 $R_2(28)$; 21.48, 21.63 NH_2 (1,7,0) $^4_{23}$- $^5_{33}$
23.78	2N	23.90 (2n) C_2, NH_2
27.75	2N	27.73 (3) C_2
30.80	0	30.53 (0N) C_2
32.18	2	32.29 (2) C_2
36.16	2	36.29 (2) C_2
40.22	5N	40.02 (6nd) C_2 (2,3) Head; 40.21 NH_2 (0,11,0) $^2_{21}$- $^3_{31}$
45.90	0?	
46.96	0?	* 46.90 C_2 $R_1'(18)$; 47.08 $R_2'(17)$

Table 7. Continued

λ	I	Identifications
5551.65	2N	51.59 (2) C_2
55.50	1N	55.45 (1n) C_2
58.89	1	59.13 (2) C_2
60.21	1	59.87 C_2 P_3^1 (36); 60.53 NH_2 (0,11,0) 4_{23} - 5_{33}
62.35	2N	62.46 (3) C_2, NH_2
65.64	2N	65.66 (3) C_2
67.63	0?	67.45 (0) C_2
69.32	2	69.34 (2) C_2
72.55	2N	72.38 (3n) C_2
75.99	2d	75.60 (3N) C_2
78.46	1	78.61 (3) C_2
82.10	2	82.16 (2N) C_2
84.91	6	85.01 (10N) C_2 (1, 2) Head
87.69	1	* 87.53 C_2 R (21)
88.42	1	88.23 (2) C_2
90.68	2	90.67 (3) C_2
93.44	2n	93.55 (2) C_2
95.74	2n	96.13 (2d) C_2
98.62	1N	98.37 (1n) C_2
5600.96	2n	00.96 (2) C_2
03.48	1	03.17 (1) C_2
05.70	2n	05.95 (3) C_2
07.91	1N	08.17 (1n) C_2
10.17	1n	10.27 (2) C_2, NH_2
12.31	1n	12.29 (1N) C_2
14.36	1	14.42 (2) C_2
16.11	1N	* 16.15 C_2 P_1(34), P_2(33); 16.31 P_3(32)
18.05	1N	17.78 (2) C_2
19.65	1	19.64 (1) C_2

Table 7. Continued

λ	I	Identifications
5621.20	0n	21.31 (1) C_2
22.91	1N	22.92 (1) C_2
24.32	1n	24.29 (1) C_2
25.58	1	25.83 (1) C_2
28.12	0	28.55 (0N) C_2
28.84	0	29.05 C_2 P_1(25), P_2(24); 29.24 P_3(23)
35.06	6	C_2 (0,1) Head
82.05	0	82.24 (1) NH_2
93.51	1n	93.34 (2n) NH_2
5701.08	0n	00.40 (1n) NH_2
03.04	2	02.98 (3) NH_2
07.64	0?	07.19 (0) NH_2
10.12	0n	
21.49	1n	20.56 (3n) NH_2
31.67	4	31.63 (3n) NH_2
41.37	2	41.28 (2) NH_2
52.75	1	52.57 (1) NH_2
5928.47	0N	26.61 (2) NH_2
31.06	0N	31.05 (0) C_2
41.99	0?	
45.56	0N	
48.52	1n	47.99 (1) C_2
52.10	0?	51.95 (1N) C_2
61.06	0N	60.99 (2) NH_2, C_2
62.75	0N	62.65 (2) NH_2
76.60	8d	76.69 (6) NH_2
84.61	2N	84.61 (1) NH_2
94.99	5	95.00 (5) NH_2, C_2
6004.33	0N	04.69 (2n) C_2 (3,5) Head
06.86	2	07.00 (2) C_2
18.53	1	18.58 (1) C_2

Table 7. Continued

λ	I	Identifications
6020.17	3	20.13 (4) C_2
22.11	0n	22.15 NH_2 (0, 9, 0) $^2_{20}$- $^1_{10}$
27.46	1N	
28.59	1n	28.79 (1) C_2
33.55	1N	33.40 (3n) C_2, NH_2
37.92	1	37.50 NH_2 (0, 9, 0) $^2_{21}$- $^2_{11}$
39.05	1	39.19 NH_2 (0, 9, 0) $^2_{21}$- $^2_{11}$
59.37	1n	59.12 (1N) C_2 (2, 4) Head
68.04	0?	
71.73	0?	71.64 (0) C_2
75.05	0n	74.45 (1) C_2?
77.19	0?	77.34 (0) C_2, NH_2
86.97	0?	86.71 (0N) C_2, NH_2
89.53	0N	89.48 (1) C_2
91.99	0N	92.15 (0) C_2
94.70	0N	94.67 (0) C_2
96.69	3	96.56 (3) NH_2
98.20	4	98.39 (3) NH_2
6100.76	0N	01.30 (0N) C_2?
08.83	1	08.89 NH_2 (0, 9, 0) $^3_{21}$- $^4_{31}$, $^3_{22}$- $^4_{32}$
10.08	1n	09.78 (0) C_2, NH_2
21.45	2N	21.30 (2N) C_2 (1, 3) Head, NH_2
29.54	0	
76.87	0	77.20 (0) C_2?
78.71	0n	78.80 (0) C_2
82.77	0N	C_2?
85.29	0N	C_2?
90.69	1N	90.54 (2n) C_2 (0, 2) Head

Table 7. Continued

λ	I	Identifications
6288.06	1n	88.17 (3) NH_2
97.09	1N	97.18 (2N) NH_2
98.50	1n	98.58 (1) NH_2
6300.28	3	00.44 (10) NH_2 [OI]
32.81	0n	32.71 (1) C_2
34.44	2n	34.61 (3) C_2
60.25	0N	60.43 NH_2
62.31	0N	
63.76	0N	63.88 [OI]

Seki-Lines and Comet Mrkos had somewhat different heliocentric radial velocities, some features may be appreciably shifted in the spectrum of one of these comets with respect to its position in the spectrum of the other (the center of gravity of a blend may be effectively displaced by a change in the relative intensitics of exciting radiation for the different components of this blend). The fact that such shifts only seldom occur in any important degree is undoubtedly in agreement with the low efficiency of the solar light to produce intensity anomalies in the visual range. In the case of the emissions which were not reasured in Mrkos the identifications appear in detail in table 7. Since the lifctime of a rotational level of C_2 against pure rotation transition is approximately proportional to $1/J^3$ -- the difference between J and K is irrelevant here since we are dealing with very high values of these quantum numbers -- while the life-time against absorption varies as r^2, the highest J-value observed should be proportional to $r^{-2/3}$. This is roughly what we observe if we compare Comet Seki-Lines (highest $J \approx 55$, $r = 0.82$) with Comet Mrkos (highest $J \approx 75$, $r = 0.60$). Similarly, the vibrational excitation is lower in Comet Seki-Lines than in Comet Mrkos owing to the larger heliocentric distance of the former. There are a few other important differences between the spectra of these two comets -- lines that are present in one spectrum while absent from the other, or lines that are weaker in either of the spectra; these are denoted by asterisks in table 7. These differences can be understood in terms of radial velocity shifts which bring λ_{exc} in or off a strong solar absorption, thus weakening or enhancing the corresponding lines. For example, the

line $R_1(17)$ of the (0, 0) band of C_2 at $\lambda 5134.34$ is weak in Comet Mrkos, while it is strong in Comet Seki-Lines: one of the two radiations exciting this line is seen by the cometary molecules at $\lambda 5133.70$ (Rowland intensity 4), in the case of the former comet, whereas it is seen at $\lambda 5133.56$, outside the solar absorption in the case of the latter. It would, of course, be necessary to consider the line $P_1(19)$ which, like $R_1(17)$, originates in level $K' = 18$ in order to see whether this line shows a behavior similar to that of $R_1(17)$; however, this is not possible because $P_1(19)$ falls in a strong blend near the head of the (0, 0) band.*

On the contrary, the blend $P_1(31)$, $P_2(30)$ of the same band at $\lambda 5156.59$ is stronger in Mrkos than in Seki-Lines: λ_{exc} falls at 5156.00 Å, where r_λ is large for Comet Mrkos, but the heliocentric radial velocity of Comet Seki-Lines exceeding that of Comet Mrkos by about 10 km/sec, λ_{exc} is shifted to 5155.80 Å, near the center of the solar line $\lambda 5155.77$ of Ni (Rowland intensity 2). The R-lines associated with the two lines just considered give rise to an interesting feature. The blend formed by $R_1(29)$ ($\lambda 5106.42$) and $R_2(28)$ ($\lambda 5106.50$) together with $R_3(27)$ ($\lambda 5106.60$) does not seem to be very much weakened in Comet Seki-Lines. However, further inspection reveals that this blend is measured at $\lambda 5106.46$ in Comet Mrkos, while it appears at $\lambda 5106.61$ in Comet Seki-Lines. Thus the center of gravity of the blend has been displaced to the red by about 0.15 Å, indicating that $R_1(29)$ and $R_2(28)$

*We recall that in the case of a line issued from a rotational level in the vibrational state $v'=0$ the excitation occurs principally in (0, 0) itself, so that the corresponding transitions in (0, 1), (0, 2), etc. can be disregarded.

have, indeed, a lower intensity relative to $R_3(27)$ in the spectrum of Comet Seki-Lines. Furthermore, $R_1(29)$ and $R_2(28)$ themselves are affected to some extent by the Fraunhofer line $\lambda 5105.55$ (4) in the case of Comet Seki-Lines, but not in the case of Comet Mrkos.

Chapter III

COMET HUMASON (1961e)

About two years ago an uncommon object made its appearance in the sky. It soon won fame: Comet Humason had very high intrinsic luminosity and exhibited exceptionally intense activity, its brightness fluctuations being conspicuous both for their often large amplitude and for the suddenness with which they sometimes occurred (see e.g. Van Biesbroek, 1962). The spectrum of this comet was not less remarkable: the outstanding feature was the overwhelming strength of the "comet-tail bands" of the molecular ion CO^+ even in the region of the comet's head (Greenstein, 1962; Dossin and Rousseau, 1962). A preliminary study of two spectra taken by Greenstein at the prime focus of the 200-inch telescope (N 1965 and N 1702, dispersion 180 Å/mm) has already been published (Greenstein, 1962). Comet Humason was 2.6 A.U. distant from the sun at the time of these observations. A higher-dispersion spectrum (Pd 6741, 18 Å/mm) mentioned in the paper just referred to will also be analysed here. This plate is, unfortunately, underexposed, showing only the major part of the rotational structure of the (3, 0) and (2, 0) bands of CO^+, together with the heads of the (4, 0) and (1, 0) bands of the same ion, and some patches, just barely detectable, at the position of the (0, 0) bands of N_2^+ and CN. Nevertheless, we shall try and derive some information from it concerning the possible fluorescence excitation of CO^+, especially since this is the first time these bands are resolved so much and also the first time one can hope to gain some insight into the question of the excitation mechanism responsible

for the CO^+ emissions.

The Excitation of the Comet-Tail Bands

The list of wavelengths in the (3, 0) and (2, 0) bands of CO^+ measured both on Pd 6741 itself and on tracings of this plate made at different positions along the spectral lines is presented in table 8. The second column of this table gives intensity estimates, while the third contains the identifications, for which the notations used conform to those of Rao (1950) and are indicated in the energy-level diagram for the $A\ ^2\Pi - X\ ^2\Sigma^+$ transition reproduced in figure 12. The latter will be useful when we consider the fluorescence processes. From table 8 we see that the rotational lines of a given branch are seen out to about K = 6 or 7. (The individual rotational lines are labelled with the rotational quantum number K, equal to K", indicated between parentheses in table 8.) On a normally exposed plate we should, of course, expect the intensity distribution to extend farther; from the observed shapes of the bands on intensity tracings of the lower dispersion plates N 1695 and N 1702 it appears that the last line corresponds to a K-value around 10.

It seems interesting to make a comparison between CO^+ and CN here. These two systems are quite similar in some respects. They have the same electronic configurations, and, in particular, the same type of electronic ground state, $^2\Sigma^+$. They represent a situation which is intermediate between the case of the hydrides CH, NH and OH on the one hand, and the homonuclear molecule C_2 on the other hand. There is a gradual increase of symmetry from the highly

Table 8. Rotational structure of comet-tail bands in the spectrum of Comet Humason (1961e)

a. (3, 0) band

λ	I	Identifications
3997.70	1n	R_{21} Head 97.69 (3); 97.45 (4), (5)
99.84	6	R_2 Head 99.71 (2), (3); 99.89 (4); 4000.19 (5)?
4000.91	3	00.63 R_2 (6); 00.95 Q_2 (2)
01.65	2	01.61 Q_2 (3)
02.50	2	02.42 Q_2 (4)
03.38	2	03.34 Q_2 (5)
04.33	2n	04.42 Q_2 (6)
05.54	2	05.63 Q_2 (7)
17.95	2	R_1 Head 17.78 (4), (5); 17.89 (3); 17.98 (6); 18.17 (2)
18.69	1n	18.60 R_1 (1)
19.91	6	19.81 Q_1 (1); 19.86 (2); 20.07 (3);
21.00	2	20.94 Q_1 (5)
21.73	2	21.74 P_1 (3); 21.60 Q_1 (6)
22.58	2	22.62 P_1 (4)
23.58	2	23.61 P_1 (5)

Table 8. Continued

b. (2, 0) band

λ	I	Identifications
4248.95	1n	R_{21} Head 48.93 (5), (6); 49.02 (4); 49.26 (3)?
49.65	0	49.67 R_{21} (2)
51.73	6	R_2 Head 51.63 (2), (3); 51.78 (1), (4); 52.10 (5)?
53.04	2	53.05 Q_2 (2); 53.16 R_2 (7)
53.80	1	53.78 Q_2 (3)
54.63	2	54.65 Q_2 (4)
55.67	2	55.67 Q_2 (5)
56.66	2n	56.84 Q_2 (6)
58.24	2	58.16 Q_2 (7)
72.75	2N	R_1 Head 72.97 (1); 72.47 (2)
73.61	0	73.64 R_1 (0)
74.49	6	74.38 Q_1 (1); 74.42 (2); 74.62 (3)
75.95	2	75.80 P_1 (2); 76.23 Q_1 (6)
76.66	2	76.56 P_1 (3)
77.54	2	77.50 P_1 (4)

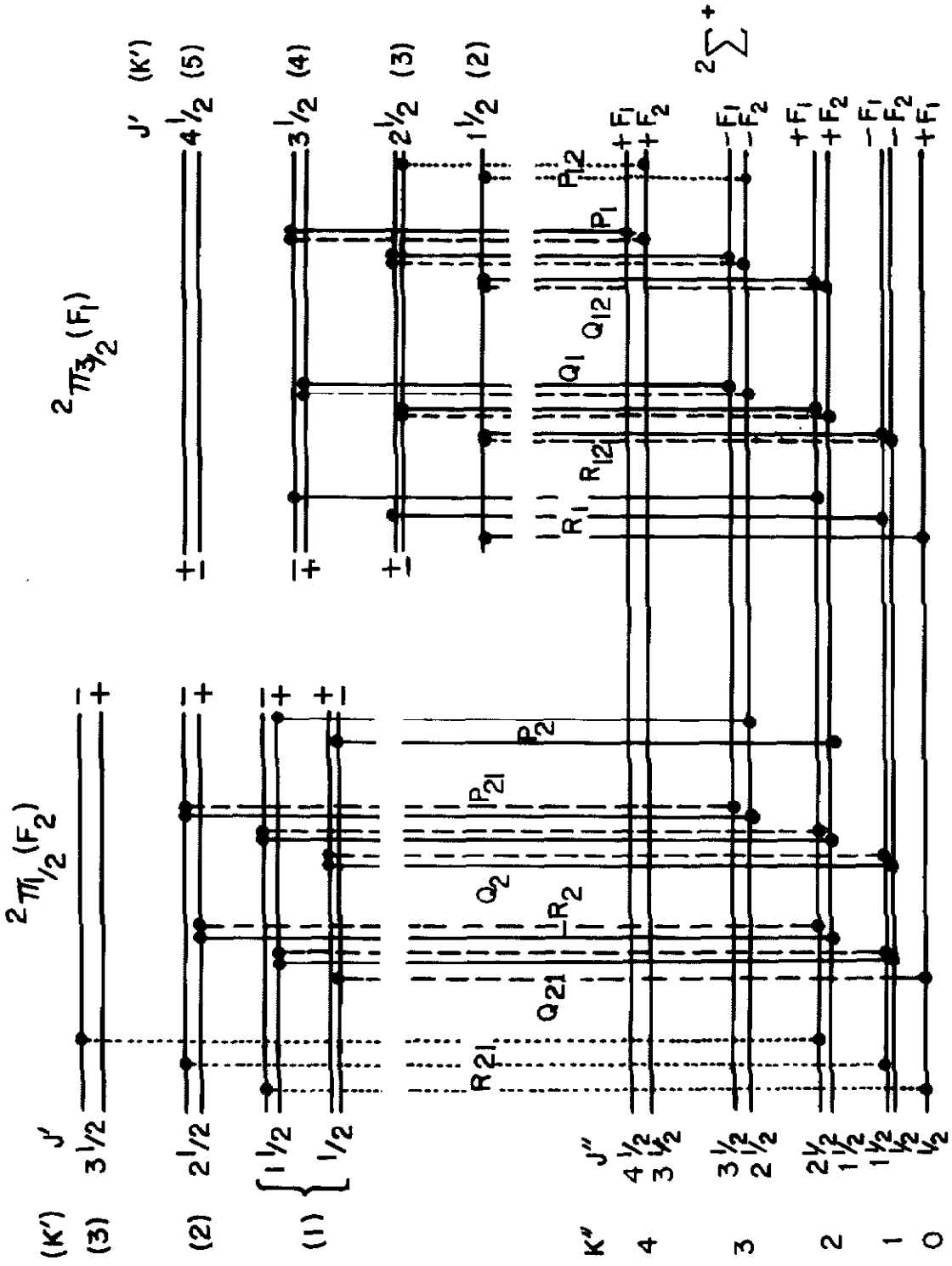

Fig. 12. Energy level diagram for the CO^+ comet-tail system.

asymmetrical hydrides, to the slightly asymmetrical CN and CO^+, to the completely symmetrical C_2. The hydrides are characterized by large rotation transition probabilities; thus the bands of these radicals are limited to their very first members (e.g. to K = 2 or 3, for a heliocentric distance of 1 A.U.) in cometary spectra. On the contrary, C_2 is able to retain much of the rotational energy acquired in the absorption processes owing to the absence of a permanent electric dipole; as a result, the Swan bands are remarkably well developed in the light of comets (typically up to K-values of the order of 50, for r = 1 A.U.). As far as CN is concerned the last lines observed when the comet is near 1 A.U. correspond to K-values from 20 to 25. As already mentioned, no high-resolution cometary spectrum showing CO^+ had been secured before Greenstein's recent observations of Comet Humason. However, from the widths of the bands observed at low dispersion one can infer that CO^+ has, indeed, a behavior similar to that of CN as far as K_ℓ is concerned. Furthermore, we have theoretical reasons to believe that such is the case. It is true that there exists an appreciable difference between CN and CO^+, namely that the spacing between the electronic states ($X\ ^2\Sigma^+$, $A\ ^2\Pi$, $B\ ^2\Sigma^+$) is roughly twice as large in CO^+ as in CN,* with the result that the band systems which are prominent in the photographic or visual regions of the spectrum correspond to different transitions for these two molecules ($B\ ^2\Sigma^+ - X\ ^2\Sigma^+$ for CN; $A\ ^2\Pi - X\ ^2\Sigma^+$ for CO^+). However, although this circumstance

*This fact is, of course, a consequence of the larger effective nuclear charge in the case of CO^+.

has important consequences with regard to the treatment of the fluorescence mechanism as we shall see later on, it can be seen that it is not likely to be of importance here. Indeed, although the comet-tail system extends over a larger wavelength range than the violet system, it can be assumed that the intensity of the solar light is of the same order for both systems at a given heliocentric distance and that consequently, the essential factor governing the rate of absorption is the "strength" or the f-value of the system.* It is shown in Appendix C, b that the lifetimes against absorption in the comet-tail system and in the violet system differ by a factor of about 3. Considering, on the other hand, the pure rotation transition rates, we can conclude that these are likely to be similar for the ground states of CO^+ and CN, in the same way as they are very nearly equal for CH, NH, and OH (Hunaerts, 1959b) as well as for OH^+. Now our calculations indicate that, at $r = 2.6$ A.U., K_ℓ is near 12 for CN (cf. Appendix A). Allowing for the difference in τ_{abs} between the ground states of CN and CO^+ we then find that K_ℓ should be roughly equal to 9, which is to be compared with the observed value of about 10. This provides a theoretical confirmation for the similarity between the comet-tail system and the violet system suggested by the observations. Had we taken $f(CO^+) = 0.002$, the value which is usually quoted (Grudzinska, 1960; Wurm, 1961), we should have predicted a value of 5 or 6 for K_ℓ, which is definitely too small.

*See Appendix C, b for a precise definition of what is to be understood here by the "f-value" of a molecular band system.

In contrast with the general parallelism between CN and CO^+ that we have just indicated, there exists an important difference between the violet system and the comet-tail bands as far as the arrays of relative vibrational transition probabilities associated with these two molecular systems are concerned. This difference, which is, of course, connected with the fact that the systems under consideration do not correspond to similar electronic transitions, in turn produces considerable differences in the details of the fluorescence excitation, as will presently appear. In the ideal case of a band system possessing an infinitely narrow principal Condon parabola (see figure 13(a)) the fact that a band (v', v'') with $v' \neq 0$ is observed with appreciable intensity in the cometary spectrum can be interpreted as indicating that the lower level $v'' = v'$ in the ground state of the molecule is populated in some appreciable way under the steady-state conditions assumed to be achieved. Indeed, the upper level v' can be fed virtually only by the transition $(v', v'' = v')$, since the vibrational transition probabilities are very low for transitions outside the principal diagonal of the $p_{v'v''}$ array. In this case the transition $(v', v'' = v')$ itself will certainly be strong in the comet's spectrum. The CN violet system provides a typical example for such a situation. For instance, if (1, 0) and mainly (1, 1) were relatively strong,* we could infer that level $v'' = 1$ would be appreciably populated. The situation is very different when the main Condon parabola is very wide as in the case of the

*Or more precisely, if, for example, I_{11}/I_{00} were appreciably larger than ≈ 0.10, which is the maximum value corresponding to negligible population of $v'' \geq 1$ - vide infra.

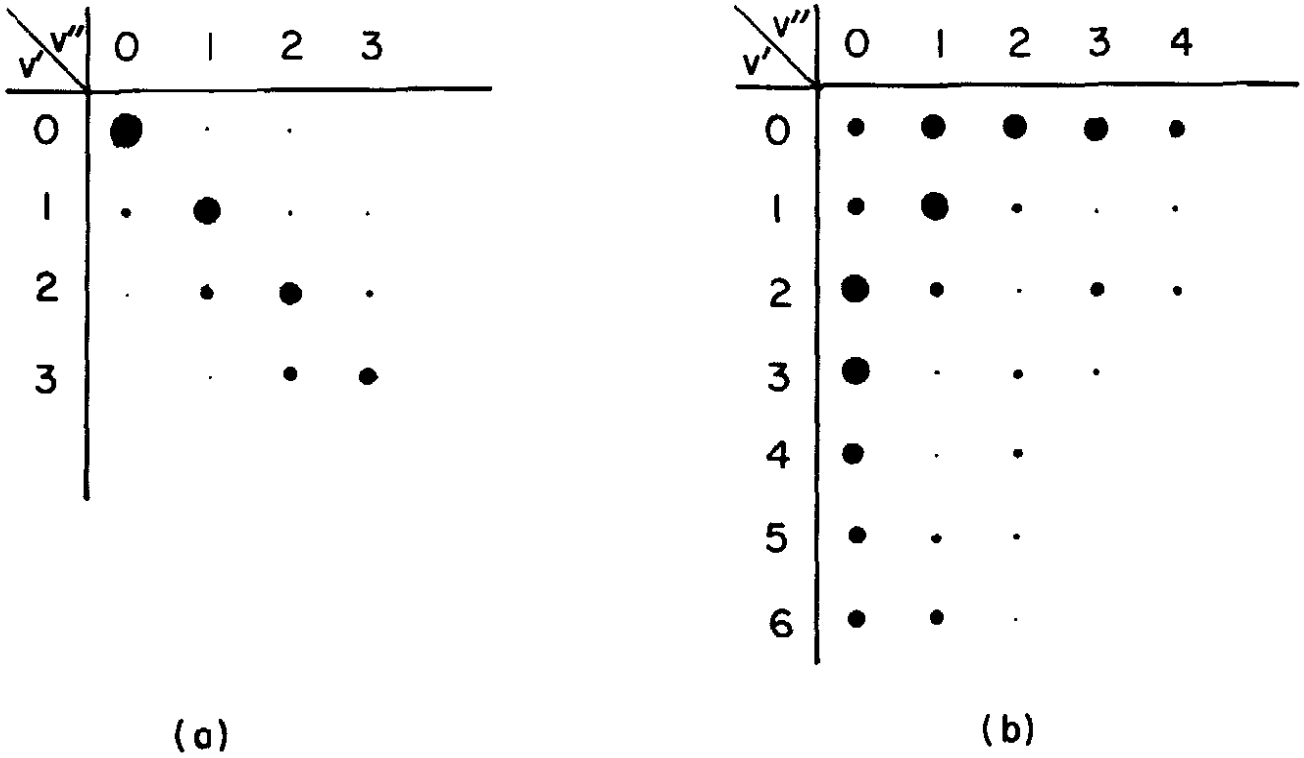

Fig. 13. Schematic representation of the arrays of relative vibrational transition probabilities for (a) the CN violet system and (b) the CO^+ comet-tail bands. The size of the dots is roughly proportional to the value of the corresponding transition probabilities.

comet-tail system of CO^+ (see figure 13(b)). Here over a large range of v'-values (from $v' = 1$ up to 5 or 6 in the comet-tail system) the presence in the cometary spectrum of a transition falling outside the Condon parabola (as, for instance, (3, 2)) does not, in general, allow us to conclude at once that the corresponding v''-level has a non-negligible population. This is due to the fact that, for these values of v', the population $N_{v'}$ is achieved in a fluorescence process essentially, or at least to a very large extent, by transitions $(v', 0)$ originating in the very lowest vibrational level. In this case it is not until we have studied the fluorescence mechanism in detail that we are able to draw any conclusion as to the relative populations of the vibrational levels in the ground electronic state. We shall come back to these considerations later on.

In order to study some possible effects of the resonance-fluorescence mechanism on the intensities of individual rotational lines it is, of course, necessary to have some knowledge about the relative populations of the vibrational levels in the lower electronic state of the comet-tail system, as this will determine the number of transitions to be included when the population of a given upper level is evaluated. A possible way to tackle this problem obviously consists in assuming various relative populations, $N_{v''}$, in the ground state (for instance, a Boltzmann distribution!), calculating the corresponding sets of theoretical intensities and then choosing the best set of values for $N_{v''}$ from a comparison of the predicted intensities with the observed ones. Instead of using such a method -- in which, in a sense, one "does not play the

game fully" -- it seems more justified to follow a procedure which adopts the resonance-fluorescence excitation mechanism as a working hypothesis and to keep to it throughout, computing the relative populations of the vibrational levels in the lower and upper electronic states, and thus also the relative intensities of the vibrational bands directly from a solution of the appropriate steady-state equations and concluding in favor of or against the fluorescence mechanism according as these computed intensities agree with the observed ones or not.

Before involving ourselves in rather lengthy computations, however, it may be worthwhile to look for a possible simplified method which would make use of readily derivable or measurable quantities. Thus, for example, let us assume that we introduce in the formula giving the intensity (more precisely, the rate of emission per cm^3 per sec) of a band (v', v''):

$$I_{v'v''} = N_{v'} A_{v'v''} h\nu_{v'v''} \tag{27}$$

the expression for $N_{v'}$ derived from the steady-state questions:

$$N_{v'} = \frac{\sum_{v''} N_{v''} C_{v'v''}}{\sum_{v''} A_{v'v''}} , \tag{28}$$

where $A_{v'v''}$ and $C_{v'v''}$ are the transition rates given by equations 7 and 9 respectively (see also table 9 below), and where we have lumped together all the rotational lines of a band, as we shall use the low-dispersion plates N1695 and N1702 for the intensity estimates. We see that, for instance, we can hope to obtain the populations N_1'' and N_2''

relative to N''_o e.g. (or $x''_1 = N''_1/N''_o$ and $x''_2 = N''_2/N''_o$) from the determination of two intensity ratios such as:

$$\frac{(v'_1, v''_1)}{(v'_2, v''_2)} = \frac{I_{v'_1 v''_1}}{I_{v'_2 v''_2}} = \frac{C_{v'_1 0} + C_{v'_1 1} x''_1 + C_{v'_1 2} x''_2}{C_{v'_2 0} + C_{v'_2 1} x''_1 + C_{v'_2 2} x''_2} \cdot \frac{A_{v'_1 v''_1}}{\sum_{v''} A_{v'_1 v''}} \cdot \frac{\sum_{v''} A_{v'_2 v''}}{A_{v'_2 v''_2}} \qquad (29)$$

for which $v'_1 \neq v'_2$, provided we assume that the lower vibrational levels are populated only up to $v'' = 2$. Should it appear necessary to include terms in x''_3 as well, we should, of course, only have to consider a third intensity ratio and thus to solve a system of three linear equations in three unknowns. Such a method would be especially valuable if it turned out that an approximate knowledge of the intensity ratios sufficed for a fairly accurate determination of the x's, for this would probably make all the work involved in intensity calibrations unnecessary. Unfortunately such is not the case, as the following unfruitful attempts will reveal:

(a) Using (2, 0), (3, 0), (4, 0)

Trying to solve the corresponding equations for x''_1 and x''_2 we find that such a solution is very sensitive to the value of (4, 0)/(3, 0). For instance, when this varies from 0.7 to 0.8 the values of x''_1 and x''_2 change by a factor of 2 to 3, depending on the value of (2, 0)/(3, 0). When the latter is equal to 1 a change of (4, 0)/(3, 0) by some 25% produces a change in x''_1 by almost one order of magnitude. Since it is impossible to reach the necessary degree of accuracy in the determination of relative intensities, we have to look for a more suitable combination of band intensities.

(b) (4, 0), (5, 0), (6, 1)

The advantage of this combination comes from the fact that it does not involve x_3'' at all because $C_{v'3}$ is virtually zero for $v' = 4$, 5 and 6, so that we are certain that we can include only two unknowns in this case (x_3'' could possibly be determined separately). However, it can be shown that a physically acceptable solution, namely one that yields positive values for x_1'' and x_2'', exists only in a short interval of values of (5, 0)/(6, 1), i.e. from 3.35 to 3.44. Now when this ratio varies by only 3% over this interval from end to end, x_1'' goes from 0 to ∞! Needless to say that this choice of band intensities is again hopeless.

(c) (1, 0), (2, 1), (3, 1), (4, 2)

This combination would lead to the determination x_1'', x_2'' and x_3''. It is interesting because the bands involved extend over a rather short wavelength interval, which tends to reduce the uncertainties associated with plate sensitivity and atmospheric extinction. A slight difficulty arises from the fact that the longward component of (4, 2) (R_1 and Q_1 branches) coincide with the shortward component of (1, 0) (R_2 and Q_2 branches), but this can be overcome if we notice that (4, 2) must have the same $(R_1 + Q_1)/(R_2 + Q_2)$ ratio as (4, 0). Nevertheless, (4, 2) was finally abandoned because the observed ratio (4, 2)/(4, 0) was found to be appreciably different from its theoretical value $(A_{42}\lambda_{40})/(A_{40}\lambda_{42})$. Substitution of (6, 1) or (5, 0) was tried but the same problem of the very high sensitiveness of the solution to the values of the intensity ratios was encountered once again.

In view of the definite lack of success of the method outlined above, which would otherwise have been very simple, we now turn to the solution of the complete fluorescence problem in which, be it repeated, we regard each vibrational band (doublet) as a whole. The steady-state equation for vibrational levels in the upper electronic state is expressed in equation 28. As for vibrational levels of the lower electronic state the equation contains additional terms because we have to consider pure vibration radiative transitions, in much the same way as we had to consider pure rotation transitions when studying the resonance-fluorescence in the hyperfine rotational structure of the CN violet band:

$$N_{v''}\left(\sum_{v'} C_{v'v''} + D_{v'', v''-1}\right) = N_{v''+1} D_{v''+1, v''} + \sum_{v'} N_{v'} A_{v'v''} , \qquad (30)$$

where $D_{v'', v''-1}$ is the rate of the pure vibration transitions $v'' \rightarrow v'' - 1$. The final solution will be the result of the competition between absorptions and pure vibration transitions. The relative importance of the latter with respect to the former is not known a priori. It is clear, from what has been said previously about the array of vibrational transition probabilities for the comet-tail bands, that it is not possible to determine the ratio $D_{v'', v''-1} / \sum_{v'} C_{v'v''}$ in a manner similar to that in which one obtains the relative importance of pure rotation transitions (using the last observed rotational line). Consequently, the procedure will be to carry out the computations for various values of this ratio and to discriminate the best value from its ability to reproduce the observations satisfactorily. The dependence of $D_{v'', v''-1}$ on v'' can be

computed by using the wave functions for vibrations described by a Morse potential (see Appendix C, a). Furthermore, the selection rule $\Delta v'' = 1$ used in equation 30 can be shown to hold in a good approximation. Since we are interested in the relative populations $x_{v''}$ and $y_{v'}$ (here normalized in such a way that $x_o = y_2 = 1$), we can neglect all the physical constants and thus replace the absolute coefficients $A_{v'v''}$; $B_{v'v''}$; $C_{v'v''}$; $D_{v'',v''-1}$ by the corresponding relative quantities $a_{v'v''} \propto p_{v'v''}/\lambda^3_{v'v''}$; $b_{v'v''} = p_{v'v''}$; $c_{v'v''} \propto p_{v'v''}\eta_{v'v''}(\lambda^2 F_\lambda)_{v'v''}$; $\delta_{v''v''-1}$. The transition probabilities $p_{v'v''}$ include the dependence of the electronic transition moment on the internuclear distance as they should (Robinson and Nicholls, 1960). It is also important to note that the coefficients $c_{v'v''}$ now themselves contain the effect of the Fraunhofer lines in the factor $\eta_{v'v''}$ (cf. chapter II for the case of CN where the rotational lines were considered individually and the effect of the solar absorption lines was separated from $C_{v'v''}$ and represented by r_λ). This factor $\eta_{v'v''}$, which is thus intended to represent the overall effect of the solar absorptions over the whole band (v', v''), could be called the "mean Fraunhofer weakening coefficient" for this band. It seems natural to evaluate this coefficient by taking the average of the residual intensities r_λ corresponding to the individual lines of the band weighted according to the strengths of these lines and the relative populations of the levels in which they originate. Thus we write:

$$\eta_{v'v''} = \frac{\eta^{(1)}_{v'v''} + \eta^{(2)}_{v'v''}}{2} \quad , \tag{31}$$

where

$$\eta^{(i)}_{v'v''} = \frac{\sum_{K} N''_K \bar{S}^{(i)}_K}{\sum_{K} N''_K S^{(i)}_K} \quad , \tag{32}$$

with

$$S^{(i)}_K = \sum_{R,P,Q} S^{(i)}_{J'} = K + \frac{1}{2} \tag{33}$$

and

$$\bar{S}^{(i)}_K = \sum_{R,P,Q} r^J_\lambda S^{(i)}_{J'} \tag{34}$$

The symbol $\sum_{R,P,Q}$ represents a summation over the six branches included in one component of the doublet, while the superscript (i) designates the component that is considered. Thus, for example, for the longward component of a band we have to include the lines $R_1(K)$, $R_{12}(K)$, $Q_1(K)$, $Q_{12}(K)$, $P_1(K)$, and $P_{12}(K)$, all of which are issued from level $K\ (= K'')$. The strengths of the rotational lines, $S_{J'}$, are given in Appendix C, c. The heliocentric radial velocity used in determining the r_λ's is $\frac{dr}{dt} = -11.0$ km/sec. The populations N''_K are, of course, unknown. However, since $\eta_{v'v''}$ is only a correction factor and since we are not directly interested in the details of the intensity distribution in a band here, but rather in the intensity of a band as a whole, we can safely assume any reasonable distribution of populations for the rotational levels in the ground electronic state, the departure of the adopted distribution from the true distribution representing only a second order effect in the present context. Thus, we may use a Boltzmann formula

with a temperature parameter determined as follows. The line strengths in various branches are fitted by means of formulae of the form $(2J + 1)^n$. Then, the "equilibrium temperature" that would correspond to the observed maximum in the intensity distribution can be written:

$$T = 0.72 \frac{B}{n} (2J_M + 1)^2 \quad {}^{o}K \tag{35}$$

where J_M is the rotational quantum number at which the maximum occurs. J_M has been determined for (1, 0), (2, 0) and (3, 0) both from the low-dispersion plates and from the high-dispersion plate, leading to the result:

$$T = (120 \pm 30) \quad {}^{o}K \tag{36}$$

On the other hand, the value of the parameter T predicted for CN at r = 2.6 A.U. through formula 23 is equal to 115 ^{o}K. Besides, it is encouraging to note that the calculations based on three different values for T, namely 70, 90 and 135 ^{o}K, give essentially the same results for the various η's within a few percent.

Combining equations 28 and 30 we now obtain

$$x_{v''} \epsilon_{v''} = \sum_{v'}^{v'_\ell} y_{v'} \gamma_{v'v''} \tag{37}$$

where

$$\epsilon_{v''} = \sum_{v'}^{v'_\ell} c_{v'v''} + \delta_{v'', v''-1} \tag{38}$$

and

$$\gamma_{v'v''} = a_{v'v''} + \sum_{v_1''=v''+1}^{v_\ell''} a_{v'v_1''} \cdot \prod_{v_r''=v''+1} \left(\frac{\delta_{v_v'', v_r''-1}}{\epsilon_{v_r''}} \right), \quad (39)$$

v_ℓ'' and v_ℓ' being the last levels considered. It is sufficient to include 4 levels in the ground state and 7 levels in the upper electronic state of the transition. The relevant data concerning $a_{v'v''}$, $p_{v'v''}$ and $c_{v'v''}$ are listed in table 9 together with the mean wavelengths of the transitions $\bar{\lambda}_{v'v''}$. Table 10 gives the values of η separately for the two components of the strongest bands of the comet-tail system. We shall refer to this later. Two methods can be followed in order to determine the x's. On the one hand, we can make use of the observational material itself and determine the relative populations of the vibrational levels in the upper state:

$$y_{v'} \propto \frac{I_{v'v''} \lambda_{v'v''}^4}{p_{v'v''}} \quad (40)$$

by measuring the relative intensities of bands corresponding to $v' = 0$ up to 6. It then suffices to introduce the values obtained for the y's into equation 37 to derive the x's. Actually, however, as stated earlier, we do not know the coefficients $\delta_{v'', v''-1}$ occurring in equation 37. The computations are, accordingly, carried out for five different values of the parameter

$$q = \frac{\sum_{v''=0}^{3} \delta_{v'', v''-1}}{\sum_{v''=0}^{3} \sum_{v'=0}^{6} c_{v'v''}} \quad (41)$$

Table 9. Relative transition probabilities and wavelengths of the comet-tail bands

v' \ v''	0	1	2	3
	4900	5480	6215	7125
	0.060	0.133	0.104	0.055
0	0.071	0.219	0.250	0.200
	0.087	0.321	0.399	0.275
	4552	5056	5673	6480
	0.199	0.241	0.059	-
1	0.188	0.312	0.108	-
	0.186	0.355	0.165	-
	4260	4697	5229	5878
	0.330	0.156	0.003	0.065
2	0.255	0.162	0.005	0.131
	0.176	0.172	0.006	0.206
	4008	4391	4851	5411
	0.370	0.025	0.108	0.065
3	0.238	0.021	0.124	0.103
	0.162	0.022	0.141	0.150
	3787	4128	4505	
	0.311	0.013	0.184	
4	0.169	0.009	0.168	
	0.073	0.008	0.159	
	3592	3898	4222	
	0.205	0.091	0.097	
5	0.095	0.054	0.073	
	0.027	0.028	0.054	
	3424	3700		
	0.100	0.140		
6	0.040	0.071		
	0.014	0.029		

Legend:

$\overline{\lambda}_{v'v''}$

* $a_{v'v''}$

$p_{v'v''}$

* $c_{v'v''}$

---

* $a_{v'v''}$ and $c_{v'v''}$ contain arbitrary scale factors. The values given above have been computed by means of:

$$a_{v'v''} = \left(\frac{p}{\lambda^3}\right)_{v'v''} \times 10^{-13} \quad \text{and} \quad c_{v'v''} = (p\eta)_{v'v''} \times \frac{(\lambda^2 F_\lambda)_{v'v''}}{(\lambda^2 F_\lambda)_{20}},$$

$\lambda_{v'v''}$ being expressed in cm.

Table 10. Mean Fraunhofer weakening coefficients of comet-tail bands

Band	$\eta^{(1)}$	$\eta^{(2)}$
(1, 0)	0.88	0.89
(2, 0)	0.67	0.73
(3, 0)	0.80	0.78
(4, 0)	0.37	0.73
(5, 0)	0.70	0.37

Table 11. Relative intensities of comet-tail bands observed in the spectrum of Comet Humason (1961e)

Band	i	Band	i
(0, 0)	0.12	(3, 2)	0.25
(1, 0)	0.60	(4, 0)	0.64
(2, 0)	1.00	(4, 2)	0.26
(2, 1)	0.43	(5, 0)	0.40
(3, 0)	1.16	(6, 1)	0.16

Table 12. Relative populations of the vibrational levels of the ground electronic state of CO^+ ($x_{v''}$)

q	v'' = 0	1	2	3
0	1.00	0.354	0.224	0.144
0.1	1.00	0.338	0.214	0.130
1.0	1.00	0.240	0.142	0.065
10.0	1.00	0.055	0.028	0.009
∞	1.00	0.000	0.000	0.000

expressing the ratio of the sum of the rates for pure vibration transitions to the sum of the absorption rates. The best value for q is determined by requiring the introduction of the computed x's into:

$$y_{v'} \cdot \sum_{v''} a_{v'v''} = \sum_{v''} x_{v''} c_{v'v''} \qquad (42)$$

to reproduce as well as possible the starting values adopted for the y's in agreement with the observations. The second method consists in eliminating $y_{v'}$ from equations 37 and 42 to obtain

$$\sum_{v''} x_{v''} \beta_{v''v_1''} - x_{v_1''} \epsilon_{v_1''} = 0 \quad (v_1'' = 0, 1, 2, 3) , \qquad (43)$$

where

$$\beta_{v'' v_1''} = \sum_{v'} \left[\frac{c_{v'v''}}{\sum_{v''} a_{v'v''}} \cdot \gamma_{v'v_1''} \right] \qquad (44)$$

Taking 3 of the 4 equations represented by 43 and remembering that $x_o = 1$ we are led to solve a system of three linear equations in three unknowns x_1, x_2, x_3. Relation 42 can then be used as previously to derive the y's. We shall follow the first scheme to begin with and then use the second method as a check.

The first method leads us into the problem of the calibration of the photographic plates (N 1695 and N 1702). The relative intensities have been determined in three independent ways using three different reference stars, LDS 785A, AP Ser and the sun, whose spectral energy distributions are fairly well known. LDS 785A is a DB white-dwarf which has a negligible Balmer jump. Thus, its energy distribution can

be well represented by that of a black body at a temperature determined by using the relation between color index B-V and temperature for black bodies (Arp, 1961; Weidemann, 1963). The B-V color of LDS 785A itself is not known, but the BD white dwarfs for which colors have been determined accurately fall in a rather narrow B-V interval (- 0.14, - 0.05) (Greenstein, 1958). Accordingly, a value of - 0.10 was adopted for LDS 785A and a temperature of 17,000 ^{o}K was deduced. This will be justified a posteriori by the agreement of the results obtained from the use of this star with the other results. AP Ser is a subdwarf whose colors (B - V = + 0.60, U - B = + 0.01) kindly communicated to me by Dr. Eggen, indicate that it is very similar to the G0 subdwarf β Com. Thus, the energy distribution of the latter star (Melbourne, 1959) was adopted for AP Ser. The intensities of the most important bands of the comet-tail system derived by these first two determinations agree very well (within 10 to 15 %) with each other and are given in table 11. These intensities can also be evaluated by using the continuous cometary spectrum whose energy distribution is assumed to be identical with that of the sun. The results obtained in this way agree with the values given in table 11 within the same limits. This shows that the continuous spectrum is indeed a pure reflection continuum. We shall make use of this result later on. Finally, the star Giclas 6723 (DA white dwarf), which was also observed in the same conditions as the comet, could not be used directly to calibrate the comet plates because its colors were not known. However, the calibration obtained by means of the other stars was used to predict the colors of this white

dwarf. These predicted colors (B - V = + 0.15, U - B = - 0.75) were confirmed very recently by Eggen in a private communication (B - V = + 0.19, U - B = - 0.69), which shows once again that the relative intensities contained in table 11 are quite reliable. The relative populations of the vibrational levels in the $A\,^2\Pi$ state derived from the relative intensities appear in the seventh colum of table 13 below.

We are now in a position to resume our semi-theoretical calculations of the relative populations of the vibrational levels in the ground electronic state by the first method outlined above. Table 12 contains the numerical results corresponding to the following values of the parameter q defined previously: 0, 0.1, 1.0, 10.0, ∞, which, it is hoped, will eventually help us determine whether the pure vibration transition rates are appreciably smaller than, about equal to, or much stronger than the absorption rates. As expected, the x-distribution is quite different according to the relative importance of the radiative vibrational de-excitations in the ground state. The relative populations $y_{v'}$ predicted by each of these x-distributions are given in table 13 (columns 2 to 6). Column 7 of this table contains the $y_{v'}$ observed in the spectrum of Comet Humason (1961e), while the last column gives the corresponding values for laboratory conditions for comparison. We notice at once the agreement between column 5 and 6 on the one hand, and column 7 on the other hand, indicating that the vibration transitions are strong compared to the absorptions of solar light. The relative populations of the uppermost vibrational levels are very insensitive to the value of q but those of the lower ones do depend on the relative

Table 13. Relative populations of the vibrational levels of the electronic state $A\ ^2\Pi$ of CO^+

v'	Computed					Observed	
	q=0	0.1	1.0	10.0	∞	Comet	Laboratory
0	1.92	1.88	1.53	0.93	0.76	0.80 ± 0.25 *	0.87
1	1.42	1.45	1.42	1.21	1.15	1.07 ± 0.11	0.97
2	1.00	1.00	1.00	1.00	1.00	1.00	1.00
3	0.87	0.86	0.85	0.91	0.93	0.97 ± 0.05	0.68
4	0.49	0.50	0.48	0.47	0.49	0.55 ± 0.08	0.45
5	0.28	0.28	0.26	0.28	0.27	0.38 ± 0.07 †	0.37
6	0.22	0.23	0.24	0.24	0.24	0.32 ± 0.08 ‡	0.29

*Probable errors.

†y'_5 has been corrected for the presence of bands of N_2^+ and of OH^+ which are blended with the (5, 0) band of the comet tail system.

‡The agreement between observed and theoretical values ($q \gtrsim 10$) is not so good for the large values of v'. This is probably due to the lower accuracy of the intensities of the corresponding bands, which fall in a region where the plate sensitivity is already appreciably reduced, as well as to the occurrence of the blends. In the case of v' = 6 another uncertainty arises from the fact that no rotational analysis of bands issued from this level is available, so that η_{60} and η_{61} are rough estimates.

importance of the pure vibration transitions, i.e. on the $x_{v''}$-distribution. In particular y'_0 and y'_1 become large as soon as x''_1 and/or x''_2 are non-negligible because the (0,1), (0,2), (1,1), and (1,2) transitions have large relative probabilities. The second, purely theoretical method mentioned earlier has also been applied and the $x_{v''}$-distributions, and hence the $y_{v'}$-distributions, derived are essentially the same as the ones obtained by the first method, which corroborates the result that q is large for CO^+.*

Going back to the comparison between CO^+ and CN, we note incidentally here that the pure vibration de-excitation is important in the ground state of CN too. In order to show this, two opposite, extreme cases can be treated in which q is either negligible or very large and in which two vibrational levels are considered in each of the $B\,^2\Sigma^+$ and $X\,^2\Sigma^+$ states of CN. It is found that for very small q the intensity ratio I_{11}/I_{00} of the (1,1) and (0,0) bands of the violet system tends towards:

$$\frac{p_{11}}{p_{00}} \approx 0.8 ,$$

*It is clear that q cannot be determined accurately by the present analysis. The only conclusion that can be drawn is that q is greater than about 10. However, from the similarity between the molecular characteristics of the ground states of CO and CO^+ we may expect the variations of the electric dipole moments of these two molecules with internuclear distance to be similar (the electric dipole moments $\mu(r_e)$ of CO and CO^+ are indeed about equal -- see Kopelman and Klemperer (1962): $\mu \approx 0.10$ Debye). Then, assuming the dipole moment to be linear in the region where the wave-functions are appreciably different from zero, we can show that q is probably of the order of several thousands (cf. Matheson (1932): the vibrational transition rate $D_{10} = 56\ \text{sec}^{-1}$ for CO). This should be regarded as a confirmation of our finding, from the study of the fluorescence of CO^+ in Comet Humason (1961e), that q is large.

while for large q it approaches the value:

$$\frac{p_{11}p_{10}}{p_{00}^2} \approx 0.07 .$$

Since the observed intensity ratio (1,1)/(0,0) is always < 0.1, we conclude that the pure vibration transitions $v'' = 1 \rightarrow v'' = 0$ in CN are strong compared with the absorption rates $C_{v'v''}$ in a comet at the usual heliocentric distances. We may expect intensity ratios like (1,1)/(0,0) in the CN violet system or (0,0)/(2,0) and (1,0)/(2,0) in the comet-tail system to be higher in comets observed at 0.5 A.U. than in comets observed at 2.5 A.U. e.g.

In addition to the very satisfactory agreement between the observed values for $y_{v'}$ and those predicted under the assumption of fluorescent excitation, there is a number of features observed in the spectrum of Comet Humason which definitely speak in favor of a fluorescence mechanism. In the first place we draw the attention to the striking differences in intensities between the two components of the comet-tail bands (5,0), (4,0), (3,0) for instance (a reproduction of N 1695 and N 1702 appears in the paper by Greenstein (1962)). The shortward component of (5,0) is weaker than its longward component, the opposite is the case for (4,0), while the two components of (3,0), (2,0) and (1,0) have more nearly equal strengths. This can be readily understood if we refer to table 10 where the relevant values of $\eta^{(1)}$ and $\eta^{(2)}$ are given. Thus, it appears that the relative intensities of the components of the various bands are strongly correlated with the corresponding relative amounts of energy available in the solar radiation

to excite them. On the other hand, the splitting between the two components of the $A\ ^2\Pi$ state represents such a small energy difference that a collisional excitation could not be expected to produce such effects on the relative intensities of the two components of the band. It is also worthwhile mentioning that the observed relative intensities of the bands of the comet-tail system could not have been reproduced if we had evaluated the intensity of the sunlight simply by taking F'_λ as given by a solar spectral energy curve which takes account of the Fraunhofer lines by averaging their effect in a certain number of bandpasses. In other words, the effect of the solar absorption lines has to be allowed for according to the exact way in which these lines occur in the fluorescence processes. This means, for instance, that η will be a function of r and $\frac{dr}{dt}$. A conspicuous example is provided by the intensity of (3, 0) relative to that of (2, 0): the fact that (3, 0) is relatively much stronger in the cometary spectra than in the laboratory source could not have been accounted for if we had not introduced the factor η. A large intensity ratio (3, 0)/(2, 0) was observed in earlier comets. In particular, this ratio was even larger in Comet Bester (1947k) (Swings and Page, 1950) than in Comet Humason (1961e). Considering the differences in heliocentric distance and heliocentric radial velocity between these two comets at their respective dates of observation, it can be seen, using the Atlas of the Solar Spectrum again, that η_{30}/η_{20} was indeed larger in Comet Bester than in Comet Humason.

A final confirmation of the fluorescent character of the excitation mechanism responsible for the CO^+ emission is obtained when one examines the details of the rotational structure of the (2, 0) and (3, 0) bands

as shown by the high-dispersion plate Pd 6741. Examples of weakened and unweakened lines can be found which correspond to smaller or larger values of the relevant r_λ's. Having established previously that $x_{v''}$ is negligible for $v'' \geq 1$ we can safely consider only transitions in the $(v', 0)$ band. On the other hand, the manner in which the various branches should be associated can be derived by inspection of figure 12 and is outlined in table 14 where the first column contains the designation of the upper level one is concerned with in the different cases. It is easier to work with K $(= K'')$ rather than with J because, to a single value of K there correspond two different values of J in the case of blended branches such as R_2 and Q_{21}, or Q_1 and R_{12}.

Table 14. The various branches of a band in the CO^+ comet-tail system grouped according to the kind of upper level which they correspond to

Upper level		Branches
$^2\pi_{\frac{1}{2}}$	$J' = K + \frac{1}{2}(\pm)$*	$R_2(K)$, $Q_{21}(K)$; $P_2(K+2)$
	$J' = K + \frac{3}{2}(\pm)$	$R_{21}(K)$; $Q_2(K+2)$, $P_{21}(K+2)$
$^2\pi_{\frac{3}{2}}$	$J' = K + \frac{1}{2}(\pm)$	$Q_1(K)$, $R_{12}(K)$; $P_{12}(K+2)$
	$J' = K + \frac{3}{2}(\pm)$	$R_1(K)$; $P_1(K+2)$, $Q_{12}(K+2)$

*The upper sign is to be taken when K is odd.

Table 15 provides a few examples of rotational lines that are affected by solar absorptions (a) or not (b). The last column gives the quantity:

$$\bar{r}_\lambda = \frac{\sum S_K r_\lambda}{\sum S_K} ,$$

where the summation has to be carried out over the three relevant branches. This quantity represents the relative amount of radiation capable of exciting the line under consideration when we neglect the difference between N''_K and N''_{K+2}.

Table 15. Resonance-fluorescence effects in the (2, 0) band of the comet-tail system in Comet Humason (1961e)

Lines	λ_{exc}	$\bar{r}_{\lambda}$
	a. Weakened lines	
Q_1 (3)	4274.78	0.55
Q_1 (5)	75.68	0.50
R_1 (0)	73.79	0.48
$\left\{ \begin{matrix} R_1 (4) \\ R_1 (5) \end{matrix} \right\}$	72.10	0.62
Q_2 (1)	52.63	0.62
Q_2 (3)	53.93	0.50
R_2 (1)	50.38	
	b. Unweakened lines	
Q_1 (6)	4276.38	0.91
R_1 (1)	73.13	0.85
P_1 (3)	76.72	
R_2 (1)	51.94	0.92
P_2 (3)	55.53	
R_2 (2)	51.78	0.86
P_2 (4)	56.77	

Part Two

PHYSICAL PROPERTIES OF COMETS.

CHEMICAL COMPOSITION OF THE COMETARY GAS.

Chapter IV

CRITICAL STUDY OF SOME CHARACTERISTICS OF COMET HEADS AND TAILS

In this last chapter I wish to present a critical discussion of physical and chemical properties of comets. This discussion is not intended to be complete. Very recent review articles by distinguished specialists in the field of cometary physics (Wurm, 1963; Biermann and Lüst, 1963) contain some detailed descriptions of the observations and of the phenomena involved. Accordingly, no systematic account of all the aspects of the physics of comets is given in the following sections. Rather, a few topics have been selected which seem to be particularly important or which will require further study; these are concerned with the models of comae* and tails (forms, brightness distributions, motions), the problem of ionization, the determination of abundances. Some new results derived from a study of the spectra of Comet Humason (1961e) and concerning the distribution of particles and the abundances of some molecules are also included.

1. The Comae

a. Simple Models

The simplest models of cometary atmospheres have already been described briefly in chapter II in connection with the study of the Greenstein effect in the spectrum of Comet Seki-Lines: the isotropic expansion

*The term "coma" designates the atmosphere (gas or dust) surrounding the nucleus, while the word "head" is usually intended to describe the nucleus and the coma, as well as the various formations often present in the neighborhood of the nucleus.

model (IEM) and the fountain model (FM)* which have been sketched in figure 8 (p. 48).

The motions of the particles are, of course, entirely different in these two models. FM is probably more realistic than IEM. Indeed, we know that a momentum transfer mechanism does exist which certainly affects the cometary molecules, namely that of the radiation pressure due to sunlight. How strong is it, and how effective? A molecule absorbing a quantum $h\nu$ receives a momentum $\frac{h\nu}{c}$, i.e. its velocity component in the direction away from the sun is increased by an amount $\frac{h\nu}{m_n c}$, m_n being the mass of the neutral molecule. This is of the order of 5 cm/sec for CN and C_2 (absorbing in the photographic and visual regions). Since these molecules absorb a quantum every tenth second or so when the comet is 1 A. U. distant from the sun, the corresponding acceleration is of the order of 0.5 cm/sec^2. That FM offers a better description than IEM comes from the fact that, as long as the velocities are of the order of 1 km/sec, the molecules travel a distance of about 10 km in the interval separating two successive absorptions. The corresponding angular distance as seen from the earth is generally well below the resolving power of the usual instruments. IEM would be more adequate, for instance, if the characteristic time for absorption were 10^5 sec, or if destructive collisions were more frequent than the absorptions.

The Apparent Shape of the Coma of a Comet

In figure 8 the boundary of the image of the coma has been taken to be a circumference centered on the nucleus (only approximately so in

*This model is a special case of the Bessel-Bredichin theory which is outlined e.g. in Wurm's article mentioned above.

the case of FM), in agreement with the observations. As far as IEM is concerned, this apparent boundary is determined either by the distance $v_o\tau$ travelled by the particles in a time equal to their mean life τ, or by the distance R_1 at which the brightness (which, of course, decreases outward) is equal to the limit of sensitivity of the detector used. The latter distance is usually the shorter and hence is equal to the apparent radius. It is obvious that, by reason of symmetry, the boundary of IEM as well as its isophotes will always be circular.

The situation is not so simple for FM. In that case the locus at time t of the particles emitted at time $t = 0$ in all the directions contained in a plane going through the radius vector from the sun is a circumference whose radius equals $v_o t$ and whose center moves with velocity gt along the axis of the parabolic envelope away from the sun. On the other hand, the isophotes are circumferences centered on the nucleus, as we shall see. Thus, the observed contour of the coma will be circular if the sensitivity is not particularly high. This is generally the case. However, it might be made of a section of the parabolic envelope (which is the envelope of the loci of the particles at time t as well as of the trajectories) and of a portion of the circumference which would be either the isophote corresponding to the limit of sensitivity, or the circumference reached by the molecules at a time equal to their lifetime τ. Thus, by using a highly sensitive material or by making the exposure long enough, in "monochromatic" light isolating the emission of a given molecule, one might hope to derive some information concerning the lifetime of that molecule. Reference to figure 14(a) shows that in

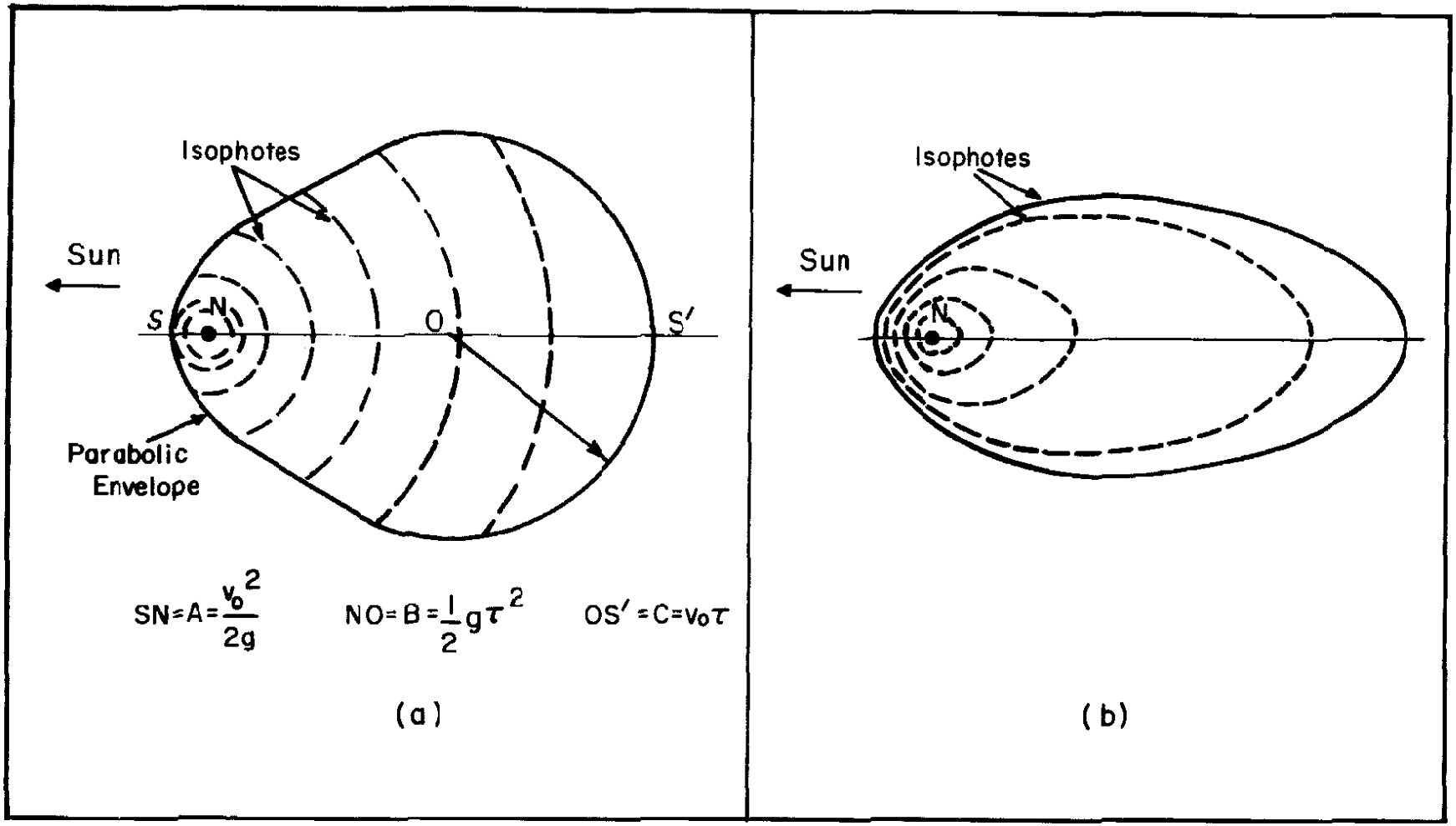

Fig. 14. The "fountain model" of the coma:
(a) contour determined by envelope and by lifetime τ of the molecule
(b) effect of dispersion of ejection velocities; contour determined by isophote.

principle one should be able to estimate the three quantities v_o, g and τ by measuring three geometrical parameters ($A = v_o^2/2g$, $B = \frac{1}{2} g\tau^2$, $C = v_o\tau$). This would be very valuable, for it might furnish some clue as to the process or processes by which the molecules are destroyed. One should try and carry out such observations. This may turn out to be very difficult, if not impossible, owing to the presence of the sky background, as Wurm (1963) has pointed out. The comets for which elongated monochromatic images will be most easily observed are those which are characterized by high densities, small v_o, or large g, or by a combination of these. It should be noticed that these elongated images are wider on the side opposite to the sun than on the sunward side (see figure 14(a)). Elongated isophotes in which the reverse is the case (slightly narrower on the tailward side; see figure 14(b)) have been observed by Miller (1957) in Comet 1955g. These may be connected with the existence of a dispersion of ejection velocities (cf. infra).

When the observed contour of the coma is circular we can derive only lower limits for v_o and τ. For example, in the case of Comet 1942g the emission in the CN violet band was observed up to a distance of the order of 10^6 km and the isophotes as well as the boundary were circular (Vorontsov-Velyaminov, 1960). Since $g = 0.5$ cm/sec^2 for $r = 1$ A. U., we have

$$v_o^2 r^2 \geq R_1 ,$$

R_1 being the radius of the contour. With $r = 1.45$ A. U. and $R_1 \approx 10^6$ km we obtain:

$$v_o \geq 2 \text{ km/sec} \qquad (44)$$

Then, the inequality $v_o \tau > R_1$ gives

$$\tau_{CN} \gtrsim 5 \times 10^5 \text{ sec} \quad * \tag{45}$$

The Distribution of Particles

In the case of IEM it is clear that the particle density per cm^3, $n(R)$, decreases as the inverse square power of the distance R from the nucleus. As for FM, the formula for n was given by Eddington (1910) and will not be repeated here. We shall be more interested in knowing the integrated number of particles along a line of sight, $N(\rho)$, as a function of the projected distance ρ. The surface brightness $S(\rho)$ on the isophote of radius ρ will be proportional to $N(\rho)$ provided that the atmosphere is optically thin.

Let us first consider IEM, for which it is obvious that the isophotes are circular. If there is no appreciable particle decay over a distance R_2 large compared with the radius R_1 of the observed image ($R_2 \gtrsim 10\, R_1$), the inverse square law being valid over that distance, the coma may be considered as extending to infinity and it is found by integration that

$$N(\rho) = \frac{\pi n_o R_o^2}{\rho} \tag{46}$$

and that

$$N(0) = n_o R_o, \tag{47}$$

R_o being the radius of the nucleus and n_o being equal to $n(R_o)$. If, on the other hand, $R_1 < R_2 < 10\, R_1$ and if $n(R)$ is taken equal to zero

*Wurm (1963) has found a higher value for the lower limit of τ_{CN} because he has adopted for v_o the same value (1 km/sec) as that observed for Halley's comet.

for $R \geq R_2$, equation 46 has to be replaced by

$$N(\rho) = \frac{2n_o R_o^2}{\rho} \tan^{-1}\sqrt{\left(\frac{R_2}{\rho}\right)^2 - 1} \ , \tag{48}$$

while equation 47 is still very nearly valid. It is also interesting to evaluate the total number $\mathfrak{n}$ of particles present in the cometary atmosphere. If this atmosphere is bounded by a sphere of radius R_2 as above, the total number is given by

$$\mathfrak{n} = 4\pi n_o R_o^2 R_2 \ , \tag{49}$$

since R_2 is much larger than R_o.

It has been shown that, in the case of FM, the isophotes will always be circular and centered on the nucleus, whatever the angle between the line of sight and the axis of the parabolic envelope may be (see e.g. Wallace and Miller (1958)). The appropriate integration of the density n given by Eddington (1910) yields the following result:

$$N(\rho) = \frac{\pi Q_o}{v_o \rho} \ , \tag{50}$$

for isotropic ejection with velocity v_o, at the rate Q_o (per sec, per unit solid angle). We see that equation 50 agrees with equation 46, since $n_o R_o^2$ equals Q_o/v_o. Owing to this agreement and to the observed fact that the cometary images are generally circular, the formulae applying to IEM are quite useful in practice, in spite of the inadequacy of this model to represent the true situation.

Comet Humason provides an illustration of the $1/\rho$ law, as we shall see. Since plate N 1702 was well guided, we can hope to derive some information concerning the spatial distribution of CO^+, N_2^+ and

CN. For this purpose "radial profiles" were secured at the wavelengths of the (4, 0), (3, 0), and (2, 0) bands of the comet-tail system, the (0, 0) band of the first negative system of N_2^+, and the (0, 0) band of the CN violet system. This yields $S(\rho)$ or $N(\rho)$. Any possible "Greenstein effects" on individual rotational lines would be smeared out, since we are dealing with unresolved bands here. The results are shown in figure 15 where $N(\rho)$ is expressed in arbitrary units different for each molecule. The CN radicals have a distribution which is very close to the usual $1/\rho$ law. The CO^+ and N_2^+ distributions, which are considerably flatter and extend over a larger volume, will be dealt with later on.*

b. More Elaborate Models

The simple models we have been concerned with in the preceding section can be refined in three different respects. In the first place, it is possible to allow for the decay of the particles more rigorously than was done above for the derivation of equation 48. Secondly, one may consider the effect of a certain dispersion in the velocity of ejection around a mean value. Finally, in some cases it is necessary to take account of a non-negligible optical thickness in the central regions of the coma.

Particle Decay

If the disintegration of the particles can be characterized by a mean lifetime τ_o, the density will be proportional to $R^{-2} \cdot e^{-\beta_o R}$,

*It has been verified that the shallow gradient of the ion distributions cannot be attributed to a large optical thickness effect.

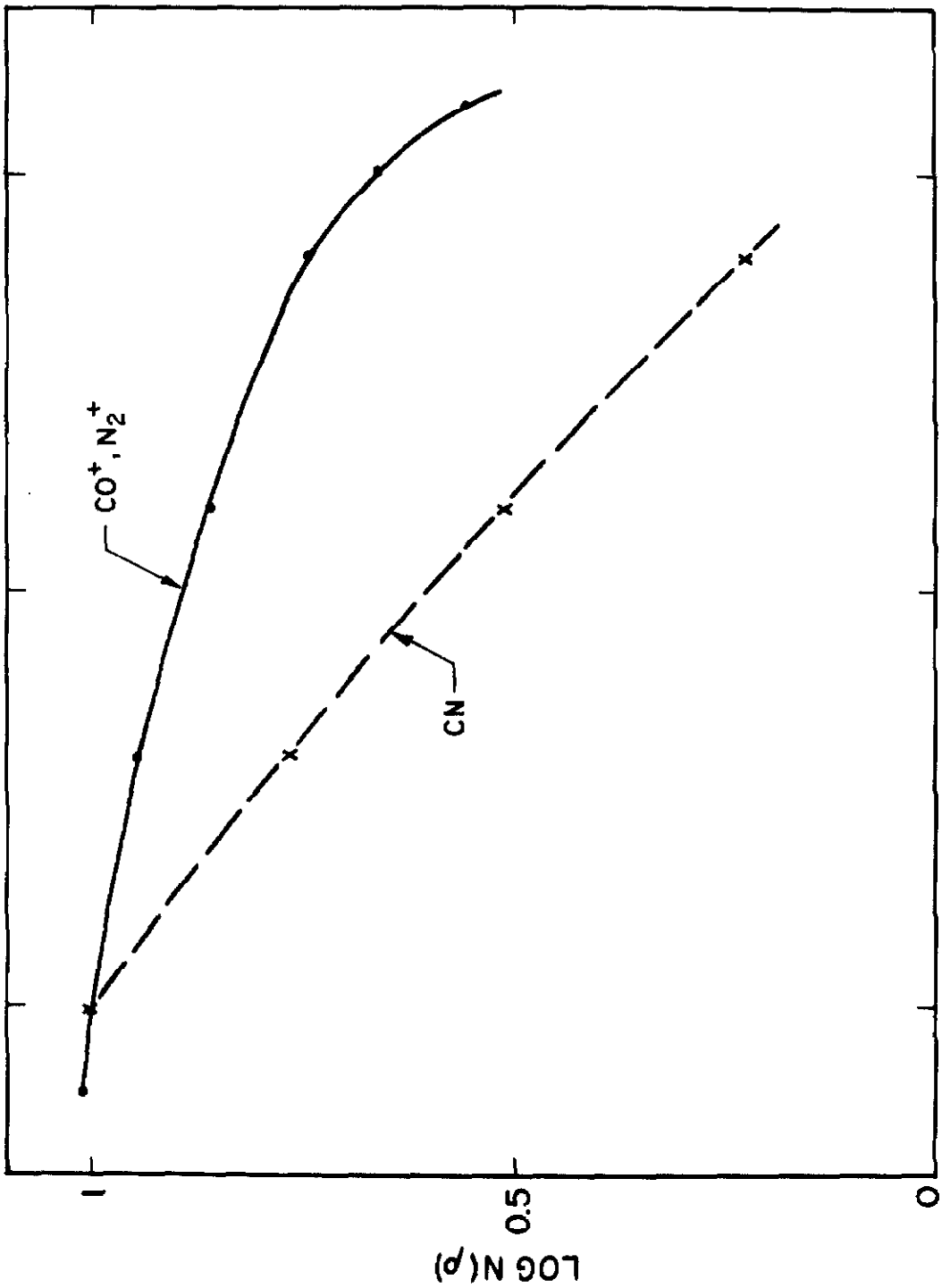

Fig. 15. Radial distributions of particles in Comet Humason (1961c).

β_o being equal to $(v_o\tau_o)^{-1}$. Haser (1957) has given the following formula for $N(\rho)$ valid in the case of IEM:

$$N(\rho) = 2n_o R_o^2 e^{\beta_o R_o} \frac{B(\beta_o \rho)}{\rho} . \qquad (51)$$

$B(x)$ is a decreasing function of x which is very nearly constant and equal to $\frac{\pi}{2}$ for $x \lesssim 0.1$ but decreases very rapidly as soon as x is $\gtrsim 1.0$. Thus, equation 51 becomes identical to equation 46 for very small β_o (i.e. for very large τ_o). The same is true for very small ρ, which shows that the "$1/\rho$ law" will always apply in a region whose outer boundary ρ_2 will be governed by the value of $\beta_o(\rho_2 \approx \beta_o^{-1})$. The relative distributions corresponding to equations 46 (with a cutoff at $\rho = \beta_o^{-1}$), 46 and 51 have been plotted in figure 16. They differ appreciably from each other when ρ becomes comparable with β_o^{-1}. However, $N(\rho)$ is already so low when this occurs that equation 49, which is based on the distribution represented by equation 46, will give a very good approximation for the total number of particles in any case.

Haser has also considered a two-component model in which both parent particles and dissociation or ionization products move radially with velocities v_o and v_1 and have mean lifetimes τ_o and τ_1 respectively. The formula for the integrated number of daughter particles involves the difference between $B(\beta_o\rho)$ and $B(\beta_1\rho)$ and this can lead to rather flat distributions when the ratio $\beta_1/\beta_o = v_o\tau_o/v_1\tau_1$ is not too different from unity. Omitting the factors $e^{\beta_o R_o}$ and $e^{\beta_1 R_o}$, which are very close to unity, we can write this formula

$$N(\rho) = \frac{2n_o R_o^2}{\rho} \beta_o \frac{v_o}{v_1} \frac{B(\beta_o\rho) - B(\beta_1\rho)}{\beta_1 - \beta_o} \qquad (52)$$

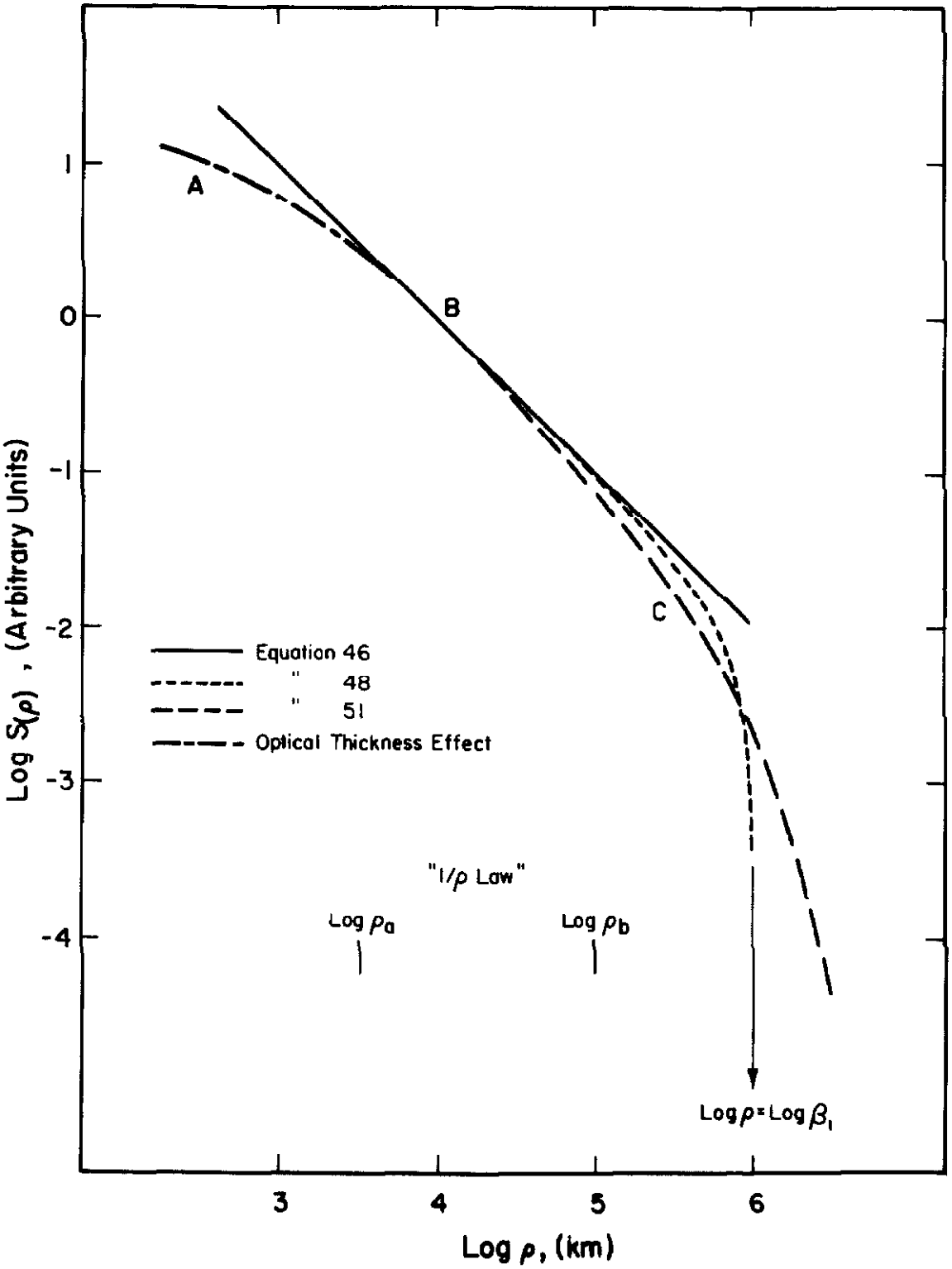

Fig. 16. Surface brightness distributions in comae ($S(\rho)$ is proportional to $N(\rho)$ except along AB).

Now this model is at least as unrealistic as IEM. Even if the parent molecules have a purely radial motion, the assumption that their disintegration products will also move radially is very questionable. Furthermore, in practice it is hardly possible to measure the relative surface brightness distribution over a range covering more than about one order of magnitude in ρ for a single observation and, accordingly, it seems that it might always be possible to find a suitable set of values of the two parameters β_o and β_1 in order to force the theoretical distribution to represent the observations over a relatively short interval of ρ. This in itself is not an argument against the two-component model, but it means that one should try and extend the observations over a range of ρ as large as possible. For example, surface brightness distributions in the light of C_2 have been determined for several comets by Miller (1961). This author concludes that the two-component model is not able to fit the observations. Using the same material, O'Dell and Osterbrock (1962) draw the opposite conclusion and state that in their opinion "the contradiction seems to result largely from a question of taste" (sic)! The best fit is obtained, according to these authors, for $\beta_o \approx 10^{-4} km^{-1}$ and $\beta_1 \approx 10^{-5} km^{-1}$.* Actually, it can be seen from equation 52 that the relative distribution is invariant with respect to an interchange of β_o and β_1. Thus, in the case of the observations just mentioned, in addition to the solution given by O'Dell and Osterbrock there exists a second one, namely $\beta_o \approx 10^{-5} km^{-1}$, $\beta_1 \approx 10^{-4} km^{-1}$. This is another unsatisfactory feature of the two-component model. Another one still appears when one compares the

*Note that O'Dell and Osterbrock have interchanged the meanings of the indices 0 and 1, while the notation used here agrees with Haser's.

values obtained for β_o and β_1 with the values suggested by other observations. Wurm (1961) has derived upper and lower limits for τ_o and τ_1 respectively, which lead to

$$\beta_o > 10^{-3.5}\,\mathrm{km}^{-1}, \quad \beta_1 < 10^{-5.5}\,\mathrm{km}^{-1}$$

Thus, the solution quoted by O'Dell and Osterbrock is the one that is the least in disagreement with the observations. The lower limit of β_o is uncertain, but the estimate for the upper limit of β_1 is more reliable and agrees with theoretical estimates of the ionization or dissociation probabilities of diatomic molecules found in comets.

We have seen in figure 15 that the distribution of the molecular ions CO^+ and N_2^+ was remarkably flat in Comet Humason. Any attempt to fit the observed distribution by means of the two-component model would be meaningless, for it is definitely certain that the ions do not move radially. We shall consider a possible interpretation of the flatness of the distributions of ions in section 2 of this chapter.

Dispersion of Ejection Velocities

If, as is probably the case in the actual situation, the ejected particles are not monokinetic, the observed surface brightness distribution will be the result of the superposition of the distributions corresponding to the various values of the velocity v_o. Thus, when we are concerned with IEM, by reasons of symmetry again, the $1/\rho$ law will hold for the resultant distribution since it does for the individual distributions.

Numerical integrations would be required for the determination of the form of the isophotes in the case of FM. However, the main

result can be anticipated by considering the variation of $N(\rho)$ along the axis of the parabolic envelope. Since the distribution corresponding to a given value of v_o follows the $1/\rho$ law and since, on the tailward portion of the axis, all values of v_o contribute to $N(\rho)$, the latter will be proportional to $1/\rho$. The situation is different on the sunward side of the nucleus. There indeed, although the individual contributions are still proportional to $1/\rho$, for a given value of v_o no contribution comes from particles with v_o's satisfying the inequality

$$\frac{v_o^2}{2g} < \rho$$

Thus, as ρ increases there are fewer and fewer contributions to $N(\rho)$ and as a consequence, $N(\rho)$ decreases more rapidly than $1/\rho$. These remarks suggest that we may expect the isophotes to be elongated in the direction of the tail. This is precisely what the detailed computations carried out by Wallace and Miller (1958) have shown (see figure 14 (b)).

If the values of v_o below a certain minimum v_m are not represented, the resultant distribution inside the parabola corresponding to v_m will be the same as if there were no spread of ejection velocities. In particular, the $1/\rho$ law will be valid on the sunward portion of the axis up to a distance equal to $v_m^2/2g$.

Optical Thickness

The foregoing considerations are based on the assumption that the cometary atmosphere is optically thin in the light of the particular molecule or atom under study. Owing to the low gaseous densities

prevailing in comets this assumption will be justified in the majority of cases. However, it may not be valid for a molecule or atom with a large f-value or, for molecules like CN, C_2, in the densest part of the coma near the nucleus. From the above discussion we can see that the optical thickness τ_y along the line of sight will in general decrease as $1/\rho$. If ρ_1 is the value of ρ for which τ_y becomes equal to 1, the observed surface brightness distribution will be rather flat for $\rho \lesssim \rho_1$. ρ_1 is usually of the order of 10^3 to 10^4 km or less.

Actually, we should consider not only the optical thickness τ_y along the line of sight, but also the optical thickness τ_x along the radial direction sun-comet. Let us assume for simplicity that this direction is perpendicular to the line of sight, as indicated in figure 17(a) which represents a cross section of the comet in the plane defined by the sun, the comet, and the earth. We shall assume further that we are dealing with a two-level atom or molecule. Then, if $n'(x, y)$ and $n''(x, y)$ are the densities, at point (x, y), of particles in the upper and lower levels respectively, the fluorescence is expressed by

$$n'(x, y)A = n''(x, y)C(x, y), \tag{53}$$

A and $C(x, y)$ being the emission and the absorption rates respectively. $C(x, y)$ can be written

$$C(x, y) = C_1 e^{-\tau_x(x, y)}, \tag{54}$$

where C_1 is a constant and

$$\tau_x(x, y) = \int_{-\infty}^{x} n''(\xi, y)\sigma \, d\xi \quad . \tag{55}$$

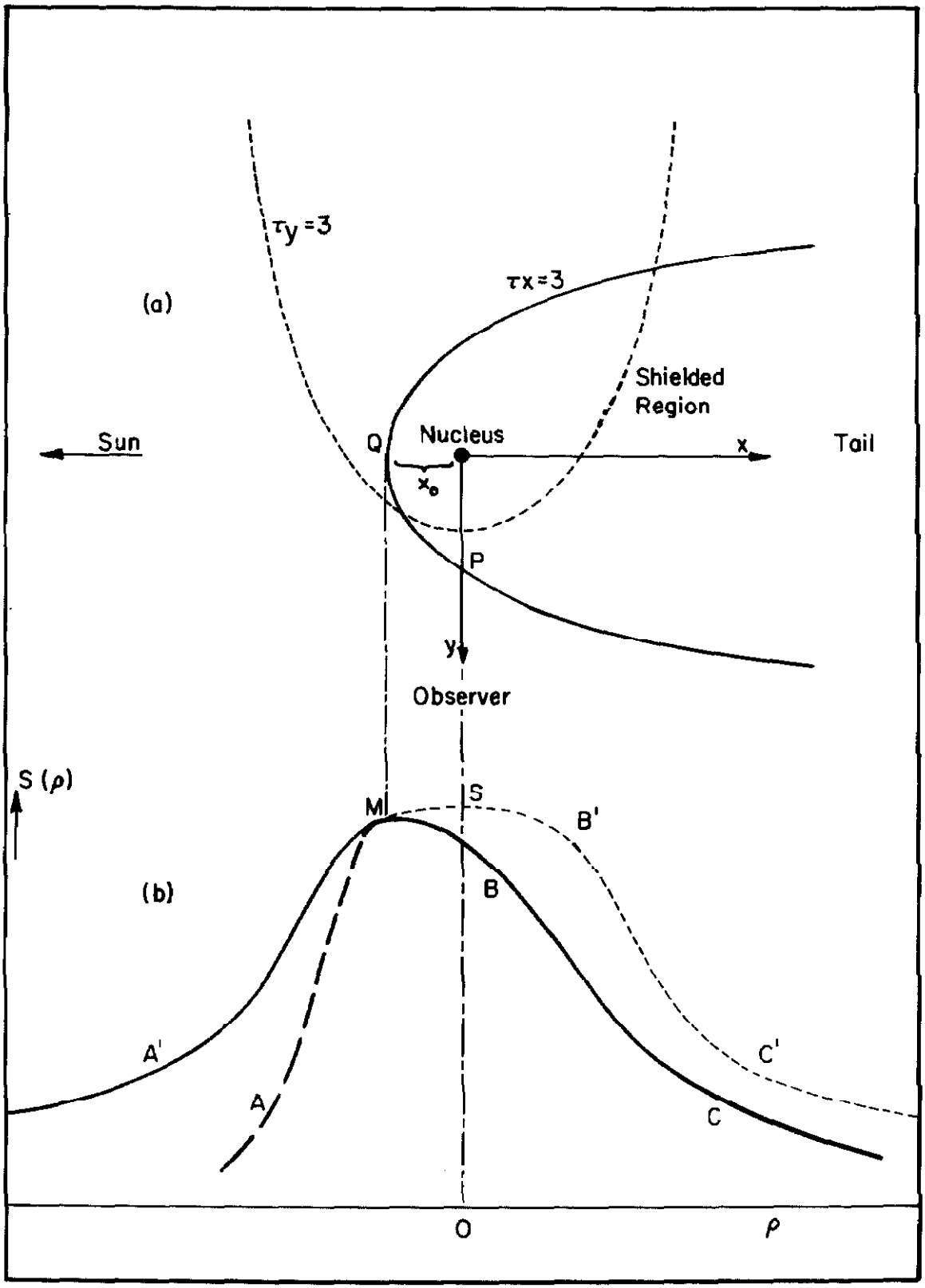

Fig. 17. Optical thickness effects.

In the last equation σ is the cross section for absorption in the transition considered. On the other hand, since C is always much smaller than A, we can write

$$n''(x,y) \approx n(x,y) = \frac{n_o R_o^2}{x^2+y^2} \tag{56}$$

Under these conditions, τ_x becomes

$$\tau_x(x,y) = n_o R_o^2 \sigma \int_{-\infty}^{x} \frac{d\xi}{\xi^2+y^2} \tag{57}$$

The curves of constant optical depth, $\tau_x = \tau_x^*$, are found to be represented by the following equation

$$y = \pm x \tan\left(\frac{y}{x_o}\right), \tag{58}$$

where

$$x_o = \frac{n_o R_o^2 \sigma}{\tau_x^*} \tag{59}$$

The + sign has to be taken for $|y| > \frac{\pi x_o}{2}$, the - sign for $|y| < \frac{\pi x_o}{2}$. These curves are U-shaped, as can be seen in figure 17(a). The surface brightness along the x-axis is obtained by integration:

$$S(x) = \frac{Ah\nu}{4\pi} \int_{-\infty}^{+\infty} n'(x,\eta) e^{-\tau_y(x,\eta)} d\eta . \tag{60}$$

Taking account of equations 53, 54, and 56 we can replace equation 60 by

$$S(x) = \frac{C_1 n_o R_o^2 h\nu}{4\pi} \int_{-\infty}^{+\infty} \frac{e^{-[\tau_x(x,\eta) + \tau_y(x,\eta)]}}{x^2+\eta^2} d\eta . \tag{61}$$

It will be recognized that even for the rather simple example treated here we cannot find any elementary analytic solution.

Nevertheless, it is possible to derive an important characteristics of the solution in the following way. Because of the presence of the exponential factor in equation 54, we may assume that all molecules inside the curve $\tau_x^* = 3$ (see figure 17(a)) are not affected by the solar radiation and thus do not contribute to the surface brightness $S(x)$, while outside the curve $\tau_x^* = 3$ everything is the same as if there were no attenuation of the solar exciting light. It is clear then that, on the tailward side, $S(\rho)$ ($\rho = |x|$) will decrease, as usual, as ρ increases. On the sunward side, however, $S(\rho)$ increases as ρ increases from 0 to $x_o = n_o R_o^2 \sigma/3$. Indeed, the integration involved in $S(\rho)$ being limited to the portion PQ of the curve $\tau_x^* = 3$, the path of the integration increases as ρ increases from 0 to x_o; moreover, the integration involves denser and denser regions. For $\rho > x_o$ $S(\rho)$ decreases as ρ increases. The decrease of $S(\rho)$ is slow at first because of the optical thickness τ_y along the line of sight. When ρ exceeds about πx_o, $S(\rho)$ is roughly proportional to $1/\rho$. The shape of the curve $S(\rho)$ is represented by the solid curve A'MBC in figure 17(b). The curve A'SB'C' shows the distribution which would be obtained if we had considered the effect of the optical thickness τ_y only, neglecting that of τ_x (assuming that we see only the particles outside the dotted curve in figure 16 (a)). The important result brought about by these considerations is that the maximum of $S(\rho)$ does not occur at the position of the nucleus, but is shifted slightly in the sunward direction.

Such a peculiarity has been observed in the intensity distribution of the Na D lines in the spectrum of Comet Mrkos (1957d) (Greenstein and Arpigny, 1962). The above treatment is not entirely rigorous, for it is based on the isotropic expansion model, which is certainly not applicable to the case of Na I owing to the large f-value of the D lines. However, replacing IEM by FM will make the mathematical formulae more complicated, but will not affect the general conclusions. In particular, we may expect the curves of constant optical thickness τ_x to be similar to those described above for the case of IEM and consequently, the maximum of the surface brightness distribution will be displaced in the sunward direction as previously. Thus, it seems that the usual radial intensity distribution of the Na I lines observed in Comet Mrkos* can be interpreted as an effect of the optical thickness of the atmosphere in the light of D lines. Actually, the observed distribution decreases more rapidly on the sunward side than on the tailward side of the nucleus and resembles the curve AMBC of figure 17 (b). The rapid decrease on the sunward side is probably due to a dispersion in the ejection velocity as discussed above. Wurm (1963a) has tentatively interpreted the shift of the maximum of $S(\rho)$ as a result of such a dispersion of velocities. According to this author the maximum of $S(\rho)$ would correspond to the maximum of the distribution of velocities v_o. Such an interpretation is not correct, however, for it is clear from our discussion of the dispersion of velocities that the existence of such a dispersion does by no means alter the position of the maximum of $S(\rho)$.

*The slit of the spectrograph was oriented along the tail when the spectra under consideration were secured.

c. The Variation of the Radius of the Coma with Heliocentric Distance

It is interesting to make some predictions as to the way in which the extent of the coma may be expected to vary with heliocentric distance r. We should first specify the meaning that is to be attached to the term "radius" of the coma. We shall assume that, by means of appropriate filters, we are observing the comet in the light of a given molecule. For instance, we take "monochromatic" pictures in the λ4737 band of C_2 or in the λ3883 band of CN. Besides, we assume that the isophotes are circular or very nearly so, and we define the radius R_1 of the coma as equal to the radius, in km, of the isophote corresponding to a given surface brightness S_1. We have

$$S(\rho) \propto N(\rho) \cdot C$$

or

$$S(\rho) \propto \frac{N(\rho)}{r^2}$$

and we may assume, by analogy with Arrhenius law used in chemical kinetics, that the production rate Q_o will depend on the temperature through an exponential factor involving some "activation energy" (evaporation or desorption heat) which will be designated by L. Then we can write

$$n_o R_o^2 = \frac{Q_o}{v_o} \propto r^{1/4} e^{-b\sqrt{r}} , \qquad (62)$$

where $b = \frac{L}{RT}$ and when we have taken

$$v_o \propto T^{1/2} \propto \frac{1}{r^{1/4}} . \qquad (63)$$

Equation 62 agrees with the formula first introduced by Levin (1948) in a study of the dependence of the brightness of comets on heliocentric distance. Finally, if we make use of equation 51, we see that the radius R_1 will be defined by

$$\frac{e^{-b\sqrt{r}}}{r^{1.75}} \quad \frac{B(\beta_o R_1)}{R_1} = k \ , \tag{64}$$

k being a constant involving S_1, b, $n_1 R_o^2$ (n_1 is the value of n_o for r = 1 A. U.), and some physical constants. Taking account of the dependence of β_o on r,

$$\beta_o = \frac{\beta_1}{r^{1.75}} \ , \tag{65}$$

we can transform equation 64 into

$$3.5 \log r - 0.43\, b\sqrt{r} + \log \frac{B(x_1)}{x_1} = \log k' \ , \tag{66}$$

where

$$k' = \kappa \beta_1^{-1}$$

and

$$x_1 = \beta_o R_1 \tag{67}$$

The relation $R_1(r)$ is derived as follows. The first two terms of the left-hand side of equation 66 are computed for a series of values of r. Thus, for a fixed log k' we have a set of values of log $B(x_1)/x_1$. From a plot of log $B(x)/x$ versus log x we then obtain x_1, whence R_1 is computed by means of equation 67. Some results corresponding to various values of b (b = 10 corresponds roughly to L = 6000 cal/mole) and of log k' have been plotted in figure 18. The maximum observed

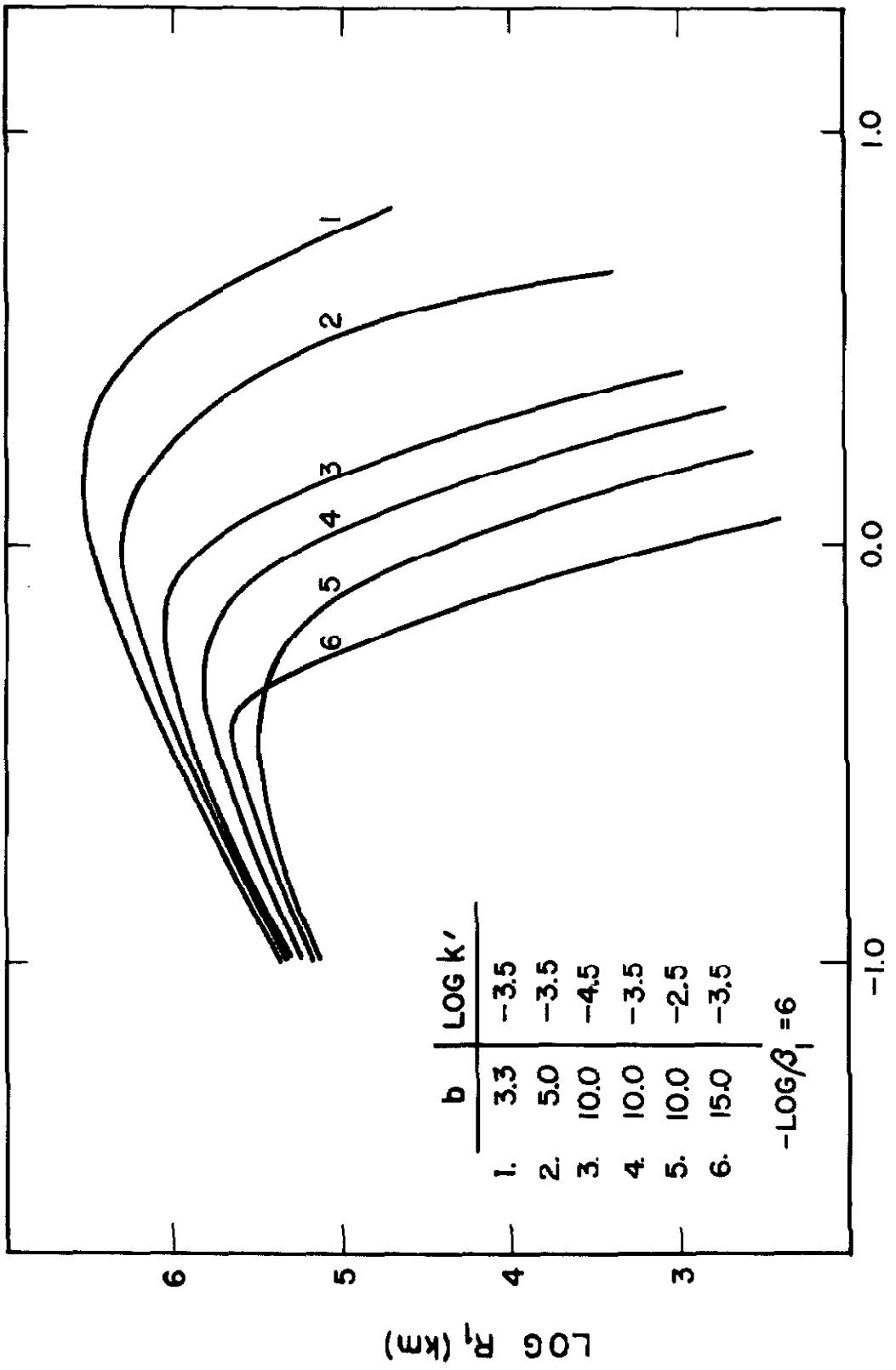

Fig. 18. The variation of the radius of the coma with heliocentric distance.

for each curve can be interpreted as resulting from the competition between the following effects: as r increases, the production rate and the amount of exciting radiation decrease, while the lifetime of the molecules increases. This is illustrated in figure 19 where a sequence of distributions $S(\rho)$ corresponding to increasing values of r (from top to bottom) is shown. Since the isotropic expansion model becomes less and less valid as r decreases, the curves shown in figure 18 can be useful only for r greater than a certain r_m depending on the particular value adopted for S_1. Furthermore, the comparison of theoretical curves such as those presented here with observed $R_1(r)$ relations cannot yield more than a relation between b and β_o (assuming the number of particles to be known in each case), for the latter is not well known. As yet such a comparison is not possible because we do not possess any series of monochromatic observations of comets. Such observations would be of interest. It is clear that the exposure time should be taken the same for all the observations of a given series. It would also be interesting to combine the study of $R_1(r)$ with that of $m_1(r)$, m_1 being the monochromatic magnitude of the comet referred to unit geocentric distance.

2. The Tails

a. Dust Tails

The curved, structureless tails of Types II and III made of dust particles which scatter the solar radiation are well understood as far as their dynamics is concerned. The "mechanical" theory developed by Bessel and Bredichin is able to account for their forms if the repulsive acceleration is identified with that produced by the radiation

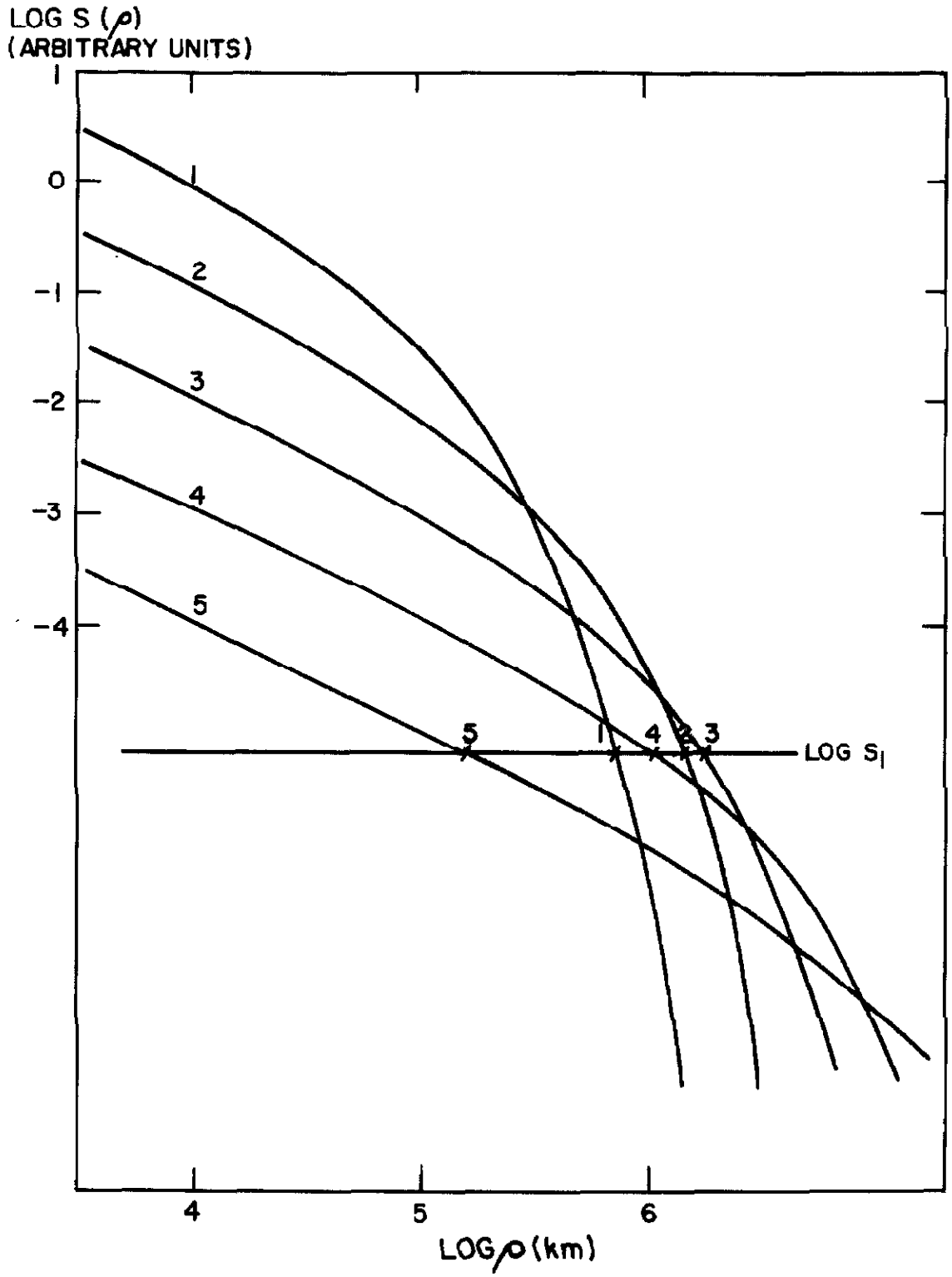

Fig. 19. Surface brightness distributions corresponding to various heliocentric distances (increasing from 1 to 5). It is seen that the radius at which $S = S_1$ goes through a maximum as r increases.

pressure due to the solar light. This acceleration is of the order of or, more often, smaller than the gravitational attraction of the sun. If the radius of the particles is a and their density d, we have accordingly

$$\frac{3p_r}{4adF_\odot} \lesssim 1, \tag{68}$$

p_r being the radiation pressure and $F_\odot$ the force of solar gravitational attraction. Inserting numerical values into equation 68, we obtain a lower limit for the size of the dust particles

$$a \gtrsim 0.1\mu, \tag{69}$$

corresponding to a density of the order of a few gm/cm^3. The recent investigation of the scattered light in the tails of Comets Arend-Roland (1956h) and Mrkos (1957d) by Liller (1960) has led to the conclusion that the size of the dust particles responsible for the scattering was of the order of 0.25 to 5μ, which is in agreement with inequality 69. Liller's work has also indicated that these particles might be iron grains with diameters around 0.6μ. Future studies of the tails of Types II and III will be concerned with the determination of the nature and size of the solid particles as well as of their abundances. They will be based mainly on spectrophotometric analyses and on polarization measurements.

b. Gas Tails

More fascinating and more puzzling are the straight, gaseous Type I tails consisting of molecular ions (mainly CO^+, N_2^+, and CO_2^+)

which are blown away with considerable velocities and accelerations in a direction deviating slightly from the radius vector sun-comet. These tails are usually highly active and may show a wide variety of appearances: straight thread-like rays stretching out laterally, very long (10^7 - 10^8 km) streamers, very turbulent or wavy patterns, clouds or knots. The whole configuration may change in a few hours, but the evolution is sometimes much slower.

The Rotation of the Rays

A system of rays nearly symmetrical with respect to the tail axis is observed in some comets. It has been stated (Wurm, 1963; Biermann and Lüst, 1963) that, without exception, the evolution of each of these rays is such that, while growing in length, it is turning towards the tail axis (which almost coincides with the radius vector), the axis of rotation going approximately through the nucleus, and the angle between the ray and the axis being rather large initially. While there is indeed a number of cases where such an evolution has definitely been observed, it should be emphasized that this number is very small (about half a dozen published cases in toto). This is due to the difficulty of identifying a given ray on successive plates beyond any doubt.

Besides the fact that the number of observations is too small for the rule to be deemed absolutely general, there do exist a few cases where this rule fails to hold. A conspicuous example may be found among photographs of Halley's comet published by Bobrovnikoff (1931). Comparing figures 41 and 43 (Plate XVIII of Bobrovnikoff's paper) we notice at once a striking resemblance between the patterns of five rays appearing on each photograph and we see that the rays make larger

angles with the axis of the later picture than in the earlier one, which is in contradiction with the rule under consideration. Although the two pictures are separated by about a day, it seems likely from the description given by Bobrovnikoff and from the analogy of the two configurations, that the identity of the rays in the two photographs is real. Bobrovnikoff's description also shows that, in spite of the rather simple patterns appearing on these photographs, the actual situation is more complicated in the central region of the head. The rays do not originate in or near a single nucleus but in different condensations or jets that are seen on short exposure photographs only.

Various plates of Comet Humason (1961e) obtained by Rudnicki and Kearns with the 48-inch Schmidt telescope provide further examples of departures from the rule concerning the rotation of tail rays. Pairs of plates taken on the following nights: July 30/31, July 31/August 1, August 25/26, and September 2/3, 1962, and separated by about 24, 3-1/2, and 1-1/2 hours, respectively, show that the rays are by no means coplanar (the angle between the line of sight and the tail axis was very small at the time of the observations) and that some rays, whose identification is certain, are turning away from the axis.

Very recently Malaise (1963) has reported his observations of the peculiar behavior of the tail of Comet Burnham (1959k), which also contradicts Wurm's rule concerning the turning of the rays. Comet Burnham's tail, which consisted of a single, rather sharp and straight streamer, was observed to "swing" about the direction of the radius vector with a period of approximately four days. This shows again that a tail ray can very well move away from the radius vector.

It should also be noted that in general, whether the rays turn toward or away from the axis, they do not turn around an axis going through the center of the coma. Actually, the prolongation of a ray intersects the tail axis at a point which is further from the nucleus, the smaller the angle this ray makes with the axis. To be sure, the observational material is still too scanty to allow any general conclusion as to the rotation of the tail rays. It seems that the rotation toward the axis is more common than the rotation away from the axis, but it is clear that it will be necessary to secure numerous series of photographs as close as possible to each other before we can settle the question.

Nevertheless, the existence of even a single known case of rotation away from the axis is important for the interpretation of this turning of the rays. Two different lines have been followed till now in order to explain this phenomenon. Wurm's attempt based on the fountain model is very implausible because it requires very peculiar conditions of ejection; furthermore, Stumpff (1959) showed that this model could not account for the observations in the case of Comet Morehouse. In the same paper Stumpff was able to interpret these observations by means of a hypothesis first suggested by Kopff according to which the turning toward the axis of the tail is due to the existence of a repulsive force increasing with the distance from the axis. This hypothesis is in close agreement with Biermann's corpuscular theory of comet tails which would explain the increase of the acceleration by the decrease in density of cometary matter as the distance from the axis increases.

Neither Wurm's nor Kopff's hypothesis would be able to explain a case of rotation away from the axis. In view of this we may look for another -- not necessarily exclusive -- explanation. For this we shall refer to what will be called the "magnetic model" of cometary tails. The suggestion made by Biermann in 1951 that a stream of ionized gas from the sun will probably carry a magnetic field along with itself was developed qualitatively by Alfvén (1957) who gave a picture which can be briefly described as follows. When a solar stream hits the comet's head the transverse magnetic field lines incurve progressively because of the higher resistance of the coma in the central regions (see figure 20 (a)). At the same time the field lines are decelerated and the final model is made of a series of field lines attached to the head as indicated in figure 20 (b). The rays or streamers are thought to be formed by the ejection of ions which are forced to move along the lines of force. In a highly idealized situation in which all orientations of the transverse field were represented, the lines of force would lie on surfaces of circular symmetry around the tail axis and one might expect the ions to undergo a drift due to the curvature of the field lines and to the gradient normal to these lines. This drift would result in a rotation of the rays around the axis of the tail. While it is very improbable that such regular and symmetrical conditions may really exist -- note, however, that the patterns we are trying to explain are sometimes very symmetrical themselves -- these considerations suggest that the rays might rotate in space rather than in a plane. In projection, then, we could observe rays that are

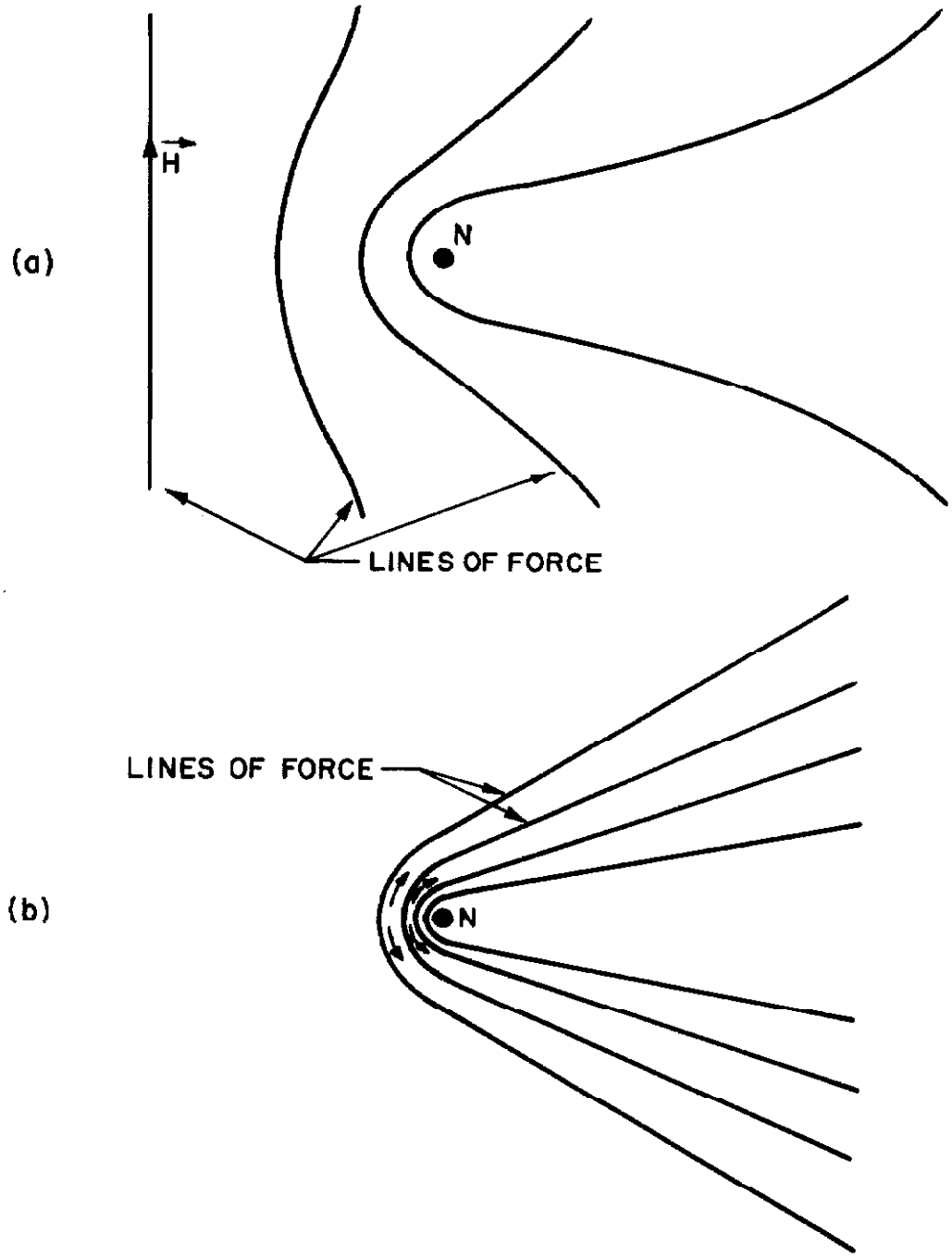

Fig. 20. The "magnetic model" of comet tails (after Alfvén, 1957).

approaching the axis as well as rays that are receding from it. It may be worth mentioning here that preliminary results from the Mariner II space probe indicate the existence of a transverse magnetic field of variable strength and orientation (Coleman et al., 1962). Finally, it should be noted that condensations and clouds have actually been observed to move away from the tail axis in the case of Comet Mrkos (1957d) (Lüst, 1962).

In connection with the magnetic model it is interesting to note that some U-shaped tails showing a continuous spectrum can be interpreted by means of this model if one assumes (1) that these tails are made of small particles capable of acquiring some electric charge, (2) that initially these particles are distributed spherically around the nucleus according to an inverse square law, and (3) that after its collision with the comet a given line of force takes a form such that all its points have encountered the same total number of particles on their way through the comet's head. We can refer to the first section of the present chapter where we had to deal with the same integration as the one which the above assumptions lead to. Thus, equations 57 and 58 and figure 17 (a) show that beyond a rather short distance from the nucleus the width of the tail will be nearly constant and equal to about 2 or 3 times the diameter of the head. This is in agreement with the observations.

Finally, going back to figure 15 where the radial distribution of the ions (CO^+, N_2^+) observed in Comet Humason (1961e) is plotted, we see that it is possible to interpret the flatness of this distribution by means of the magnetic model, since, according to this model, the

ions are ejected laterally along the field lines (we recall that Comet Humason was observed almost end-on, the angle between the line of sight and the radius vector being only about 12°).

The Velocities and Accelerations

Typical ion velocities near the head are of the order of 10 to 20 km/sec, while the velocities in the tail can reach 100 km/sec or more. The corresponding accelerations determined from the motions of condensations or rays are always found to be much larger than the solar gravitational attraction, as they range from about 30 to 300 cm/sec^2 or even more.

The solar radiation pressure is definitely out of the question because of low f-values or because of the weakness of the solar radiation in the ultraviolet region,where the f-values may be large. The electromagnetic radiation from the sun being inadequate, it is natural to consider the possibility of momentum being derived from the solar corpuscular radiation. Biermann (1951) attempted to explain the large accelerations by the interaction between the electrons present in the solar plasma and the cometary ions. This mechanism gives rise to accelerations that are about two orders of magnitudes too low. On the other hand, Biermann and Trefftz (1960) have shown that very little momentum is transferred from the solar protons to the cometary ions in the charge exchange process which produces CO^+ ions. Another possible mechanism for the coupling between solar and cometary particles has been sought in the occurrence of plasma instabilities resulting from the collision between the solar stream and the comet. Hoyle and Harwit (1962) have concluded that this possibility is negligible,

but this conclusion depends on the value adopted for the electron temperature and might be changed if the value adopted by Hoyle and Harwit were too high (Biermann and Lüst, 1963). Finally, a suitable magnetic field may be the agent responsible for the coupling. The presence of magnetic fields in comets seems very probable indeed (narrowness of the rays and streamers, helical and wavy patterns). Harwit and Hoyle have recently provided the magnetic model mentioned earlier with a semi-quantitative basis and they have been able to account for the rather large ejection velocities of the molecular ions. The magnetic field lines are decelerated because more and more ions (formed by charge exchange) become attached to them as they move through the comet's head and the transverse magnetic field lines serve to transmit the momentum from the protons to the molecular ions.

The picture drawn by Harwit and Hoyle is not entirely clear, however. For instance, at some stage of their reasoning these authors show that the velocity of the field lines must always be greater than a certain minimum value, which they identify with the ejection velocity of the ions, while later in their discussion they consider that these field lines are stopped in the head.

When the transverse field is weak the motion of the ions is determined by their interaction (characterized by a cross section σ) with neutral molecules. Then, the velocity of the ion when they enter the tail is found to be (after correction for an obvious error):

$$v = \frac{m_p v_p}{m_i (n_c D)\sigma} \quad , \tag{70}$$

where m_p and m_i are the proton and the ion mass respectively, v_p

the stream velocity of the proton, n_c a mean density of neutral molecules, and D a characteristic length of the order of the diameter of the coma. Actually, $(n_c D)$ is equivalent to the "surface density" $N(\rho)$ introduced previously, if ρ is the projected distance as seen from the solar stream. Thus, equation 70 becomes

$$v = \frac{m_p v_p}{m_i \pi n_o R_o^2 \sigma} \rho \,, \tag{71}$$

which shows that v is proportional to ρ. This property is similar to Kopff's hypothesis mentioned earlier. It might be used to explain the rotation of the rays. Taking v_p = 300 km/sec (in agreement with recent results from artificial satellites experiments -- see below), $n_o R_o^2 = 3 \times 10^{23}$ cm^{-2} (see next section) and $\sigma = 10^{-15}$ cm^2, we find that v is of the order of 10 km/sec at a distance of 10^4 km from the tail axis, while it reaches 100 km/sec at 10^5 km from the axis.

Harwit and Hoyle claim that their model also accounts for the high accelerations observed in the ionized gas tails, but this is incorrect. Dividing the momentum flux $n_p m_p v_p^2$ by the total mass per cm^2 through the tail as seen from the solar stream, Harwit and Hoyle obtain a quantity which, clearly, has the dimensions of an acceleration and which is of the order of 30 to 3×10^3 cm/sec^2 for conditions of enhanced solar activity (0.3 to 30 cm/sec^2 if we use typical values for "quiet" conditions). However, according to their model, the momentum transfer occurs only in the head, not in the tails where the lines of force become nearly parallel to the solar stream velocity.

A final remark may be in order. The momentum flux of the solar plasma is of the order of 10^{-8} to 10^{-7} CGS units under "normal" conditions

($n_p = 10\ cm^{-3}$, $v_p = 3 \times 10^2 - 10^3$ km/sec), while the momentum flux associated with the cometary ions is about $5 \times 10^{-8} - 5 \times 10^{-6}$ in the same units ($n_i = 10^2 - 10^3\ cm^{-3}$, $v_i = 30 - 10^2$ km/sec). On the other hand, for a total number of CO molecules of the order of 3×10^{34} (cf. next section), the rate of production of CO^+ by charge exchange is $\approx 3 \times 10^{28}\ sec^{-1}$, which is about what was observed in Comet Humason (1961e). Thus, it would seem that the solar corpuscular streams can provide approximately the required fluxes of momentum and of particles to explain the observations, although the values may be somewhat larger than the normal values suggested by the recent space probes. We need more observations, for instance, to establish on a firm basis whether or not the largest values of the tail accelerations are always correlated with high solar activity. In any case, the problem of the dynamics of the gaseous cometary tails remains an open one.

The Ionization of Cometary Molecules

The ionization of cometary molecules may be achieved by one of the following mechanisms:

(a) photoionization by far ultraviolet solar radiation

(b) interaction with solar corpuscular radiation: exchange of charge between solar protons and neutral cometary molecules (Biermann)

(c) unknown process intrinsic to the comet itself (Wurm)

The first of these mechanisms is usually considered as unimportant on account of the weakness of the solar radiation in the spectral range

involved (far ultraviolet). We shall see that this may not be justified. As to the second mechanism, it is opposed mainly by Wurm (1960, 1961, 1962, 1963) on the basis of a few arguments that we shall examine presently. From the observational facts (1) that important fluctuations in the intensity of the CO^+ ions in comet tails sometimes occur on a rather short time scale (of the order of $10^{3.5}$ sec) and (2) that the CO^+ ions appear already close to the nucleus of a comet (and not only in the tail itself, or at a large distance from the nucleus), Wurm concludes that the lifetime of CO, which is believed to be the parent molecule of CO^+, must be very short ($< 10^{3.5}$ sec). Comparing this with another common feature of comets, namely that the neutral molecules like CN, C_2, ... are distributed over large volumes (up to distances of $\approx 10^5$ km or greater), Wurm then draws the conclusion that there must exist two different groups of molecules in comets, one of which contains molecules that are readily ionized (CO, N_2, CH, ...), the other one molecules that have very long lifetimes ($\approx 10^6$ sec) against ionization (CN, C_2). On the basis of the same arguments Wurm favors the idea of an ionization process that would be due entirely to the conditions prevailing inside the cometary atmosphere itself, and thus independent of any phenomena having their origin outside the comet. The first of Wurm's conclusions (short lifetime of CO) is derived from point (1) above by making use of two simple differential equations which we repeat here for the sake of convenience (Wurm, 1943)*:

*In the most recent version Wurm (1963) has changed the notations and in so doing he has introduced an inconsistency. This appears in equations 37 and 38 (p. 610) which are obviously dimensionally incorrect.

$$\frac{dn_{CO}}{dt} = z - \lambda_{CO} n_{CO} = 0$$

$$\frac{dn_{CO^+}}{dt} = \lambda_{CO} n_{CO} - \lambda_{CO^+} n_{CO^+} = 0,$$

where z is the rate of production of CO, λ the inverse of the lifetime and where n is the total number of molecules present. Under steady-state conditions we obtain

$$I_{CO^+} \propto \frac{\lambda_{CO}}{\lambda_{CO^+}} n_{CO},$$

I_{CO^+} being the intensity in a CO^+ streamer. It can be shown readily that, if I_{CO^+} varies, say, by a factor of e over a time interval Δt, then

$$\tau_{CO} \lesssim \Delta t$$

provided that λ_{CO} is constant, the change in I_{CO^+} being assigned entirely to a change in n_{CO}. Now these considerations were first held at a time when the solar light was believed to be responsible for the ionization of CO, and the condition of constancy of λ_{CO} could not be doubted. If, however, CO^+ is formed by charge exchange involving solar protons, λ_{CO}, which will then be given by

$$\lambda_{CO} = (nv)_p \sigma , \tag{72}$$

may very well vary itself owing to fluctuations in $(nv)_p$. Thus the fluctuations of the intensity of CO^+ streamers would merely be due to variations in the flux of solar particles producing these ions. Such

variations are indeed expected and observed (Mustel, 1958, 1960; McNally, 1963), and a time scale of $10^{3.5}$ sec would not seem unreasonable for such variations. On the other hand, if the ionization of CO is completely "intrinsic" to the cometary atmosphere, as Wurm has suggested recently (Wurm, 1962), nothing is known about the process involved, and, at any rate it is impossible to draw any conclusion as to τ_{CO} at the present time. As far as the second point mentioned previously (appearance of CO^+ close to the nucleus) is concerned, it suffices to say that, since n_{CO^+} is likely to be proportional to n_{CO} and since CO, like the other neutral molecules, is likely to be densest near the nucleus, we should indeed expect CO^+ to appear rather conspicuously in the neighborhood of the nucleus, when it does appear at all. Furthermore, the fact that CO^+ is observed there does not imply that CO is completely ionized, as Wurm seems to believe (Wurm, 1960). In consequence, it seems that the value that is so often quoted for τ_{CO}

$$\tau_{CO} \lesssim 10^{3.5} \text{ sec} \tag{73}$$

should by no means be regarded as a definitive result. The actual lifetime of CO molecules may be very different from this. The answer to this question will presumably have to await the final determination of the ionization mechanism or the observation of CO itself. The importance of the above conclusion should be realized, as the acceptance of relation 73 leads to the strongest argument against the corpuscular

stream theory (see below) and sets a severe condition to be satisfied by any theory of the ionization in comets anyhow.

A controversy has opposed Wurm and Biermann for about a decade concerning the possible existence of important differences between the ionization of CN, C_2 on the one hand, and that of CO, N_2 on the other hand. On account of the closeness of the ionization potentials of the molecules of the two groups, Wurm maintains that the charge exchange cross sections should be similar for all of these molecules, and that, consequently, if the corpuscular theory of ionization were valid, the lifetimes of the molecules of both groups should also be similar. This is regarded by Wurm as a deadly argument against Biermann's mechanism because, according to this author, τ_{CO} is very different from τ_{CN}. Now this reasoning is questionable for two reasons. Firstly, as we have seen, it is not certain that we have any knowledge of the lifetime of the CO molecule at all. The time scale of one hour over which CO^+ streamers are sometimes observed to decay may very well reflect the time variation of the probability of ionizing CO, rather than this probability itself. Secondly, it is, in fact, very likely that, in spite of the similarity between CN and CO, the lifetime of these two molecules against ionization by solar protons (through the process of charge exchange) will differ by about one power of ten. This will be shown below.

Without going into the details of the theory and experimental facts concerning charge exchange processes, we may nevertheless recall briefly the essential results that will be of interest here. The basic

idea lies in Massey's "adiabatic hypothesis" (Massey, 1949) according to which the cross section for an inelastic collision involving atoms or molecules (or ions of these) will be small as long as the velocity of the oncoming particles, v, satisfies the inequality

$$\frac{vh}{a\Delta E} \ll 1 , \tag{74}$$

where a is a length which characterizes the interaction between the colliding particles, and ΔE is the absolute value of the difference in internal energy of the system between the initial and final states. As the energy E of the incident ion changes the cross section varies in a manner which is illustrated in figure 21 for typical cases. σ goes through a maximum for $E = E_M$, falls off steeply as E decreases, but decreases more slowly towards high energies. Clearly, the important parameter which will determine σ, in the case of charge exchange between protons and a cometary molecule, is not so much the ionization potential of this molecule, but rather the difference ΔE between this ionization potential and that of atomic hydrogen. This was pointed out by Rosen already in 1953 (Rosen, 1953). Furthermore, σ will depend on the electronic configurations involved in the transfer of charge. Considering $E = E_M$ and equating the left-hand side of equation 74 to 1, we can define a value of a, in Angstrom's units:

$$a(E_M) = 0.55 \frac{E_M^{1/2}}{m^{1/2}\Delta E} ,$$

if E_M is expressed in ev, m, the mass of the incident ion, in amu,

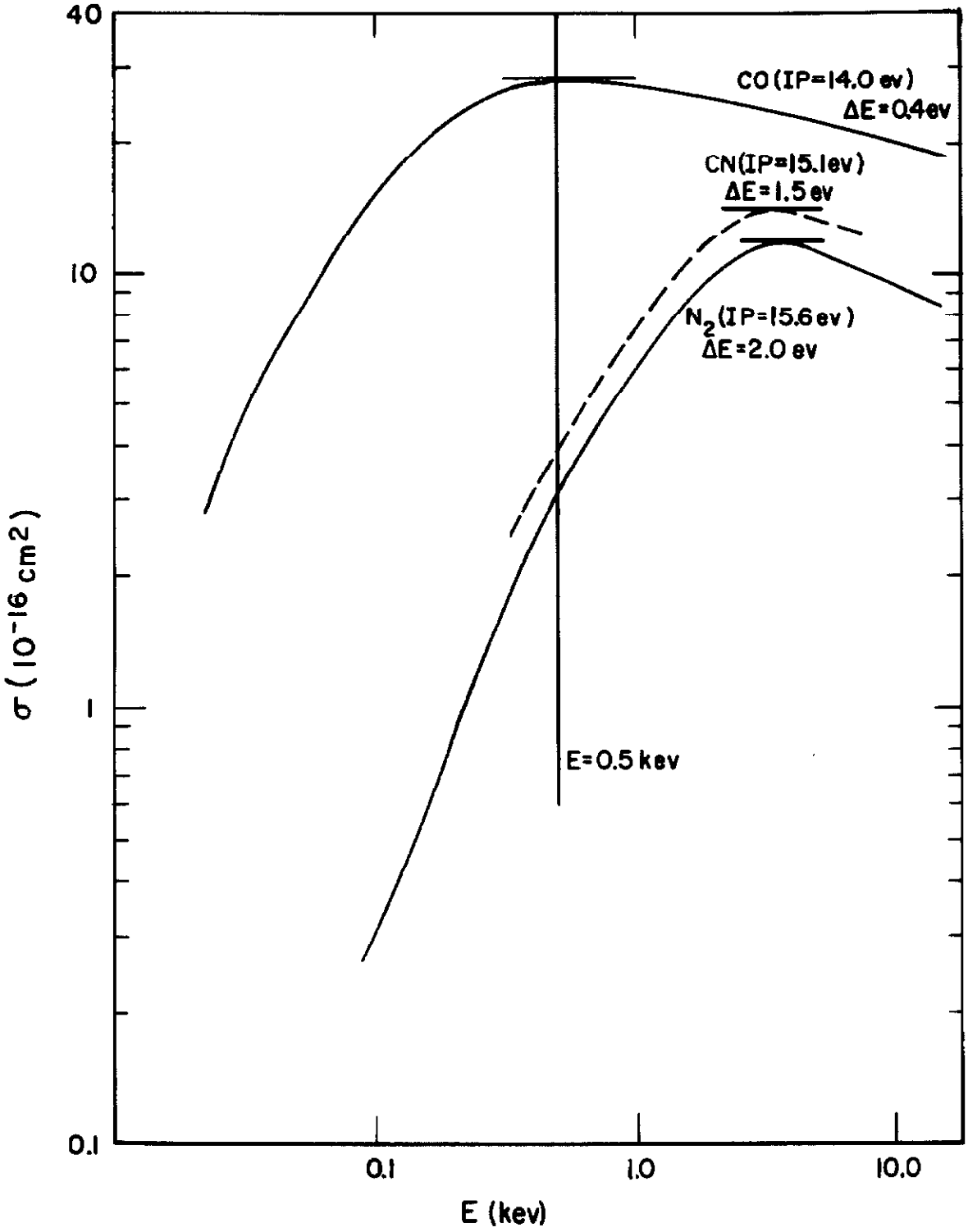

Fig. 21. Total charge exchange cross sections for interaction between protons and cometary molecules.

and ΔE in ev. For a rather large number of cases studied in the laboratory, it is found that $a(E_M)$ lies between about 7 and 28 Å, with a marked tendency for systems involving at least one molecule to have larger values of $a(E_M)$ (> 15 Å).* (Hasted, 1952; Stedeford and Hasted, 1955; Gilbody and Hasted, 1957) In particular, for (H^+, H_2), (H^+, N_2), and (H^+, CO), it is found that $a(E_M)$ is equal to 22, 16.5, and 23 Å respectively, when the smallest value of ΔE is considered (normal states of H_2^+, N_2^+, CO^+). The curves for (H^+, N_2) and (H^+, CO) are given in figure 21 (after the results of Carleton and Lawrence (1958) and Gustafsson and Lindholm (1960)). From these results it seems rather safe to assume that $a(E_M)$ = 20 Å for (H^+, CN), from which we obtain E_M = 3 kev. Now since the maximum value of σ usually decreases as E_M increases (Hasted, 1952), it appears that the (σ, E) curve for the exchange of charge between protons and CN radicals will presumably not depart very much from the dashed curve drawn in figure 21. The vertical line in this figure indicates a typical value for the energy of solar protons (0.5 kev, corresponding to 300 km/sec) as derived from observations of Lunik II and III, Explorer X and XII, and Mariner II. Thus, it is seen that the charge exchange cross section for (H^+, CN) will probably be smaller than that for (H^+, CO) by a factor of about 10 at the energies involved here. We notice that the same is true for (H^+, N_2) as compared with (H^+, CO). If the solar velocity is 100 km/sec the cross sections may differ by two orders of magnitude, while the cross section for CN becomes comparable with that for CO when v_p is of the order of or greater than 700 km/sec. The case of

*An exception to this rule is given by processes of the type $X^+ + H_2 \rightarrow X + H_2^+$, where X^+ is a heavy ion. For these a is of the order of 4 Å.

C_2 is omitted from the present discussion, as the ionization potential of this molecule is not known.

The rate coefficients for charge exchange involving CO, N_2, and CN calculated by means of formulae similar to equation 72 with $(nv)_p = 3 \times 10^8$ cm^{-2}sec^{-1} and E = 0.5 kev (for r = 1 A.U.) are given in table 16. These values correspond to the total charge exchange cross sections. They are due almost entirely to transitions to the ground states of CO^+, N_2^+, and CN^+, as these usually give the largest contribution to the total charge exchange cross section at the energies under consideration here. The case of CH provides an exception to this rule: the ionization potential of this radical being rather low (11.1 ev), the charge exchange cross section corresponding to the first excited state of CH^+, a $^1\Pi$, can be expected to be larger than the cross section for the transfer to the ground state of this ion, because its ΔE is smaller (0.5 ev as compared with 2.5 ev) (cf. Hasted, 1952). We notice that the time scale for ionization of CO by charge transfer is much larger than the value of 3×10^3 sec discussed earlier. Accepting the latter value as the true lifetime of CO, Biermann (1963) tries to explain it in the charge exchange scheme by the fact that the proton stream will be compressed when it hits the comet's head. However, while it is true that the density of the protons will increase, their velocity will decrease and this will affect σ strongly as can be seen from figure 21, so that the over-all effect will be to increase the time scale rather than to decrease it.

Also listed in table 16 are the values of the rate coefficients for

the photoionization of the molecules under consideration. The necessary values of the absorption coefficients have been taken from an article by Ditchburn and Öpik (1962), and the data on the solar radiation flux in the region 400 Å - 800 Å have been found in "Space Environment Handbook" (Johnson, 1961). It is seen that, if the charge exchange mechanism is important for the ionization in comets, the electromagnetic radiation from the sun may also play a role in some cases. For N_2 the photoionization is even more important than the process of charge exchange leading to N_2^+. We note that the lifetimes associated with the rates appearing in table 16 are about of the same order of magnitude ($\approx 10^6$ sec) as the lifetimes of the observed neutral cometary molecules.

Table 16. Rate coefficients (sec^{-1}) for ionization of CO, N_2, and CN by solar protons and by far ultraviolet solar light. Typical densities.

Molecule	CO	N_2	CN
λ (charge exchange)	10^{-6}	10^{-7}	10^{-7}
λ (photoionization)	2×10^{-7}	3×10^{-7}	$\approx 10^{-7}$ (?)
σ (cm^2)	3×10^{-15}	10^{-15}	10^{-15}
n_i/n_n	10^{-2}	3×10^{-3}	3×10^{-3}
n_n (cm^{-3})	10^5	3×10^4	$\underline{10^3}$
n_i (cm^{-3})	$\underline{10^3}$	$\underline{10^2}$	3

Underlined entries indicate values observed in comets.

On the other hand, it may be pointed out that, for instance, the number of CN^+ ions formed may be appreciably different from the number of CO^+ ions, not only because of the differences in the ionization rates, but also because the abundances of CO and CN may themselves differ from one another. For example, if we assume that the motion of the ions through the comet is determined by the pressure of oncoming solar protons and the interaction of these ions with the neutral molecules, it is possible to obtain a rough estimate of the ratio n_i/n_n, ion densities to neutral molecule densities for a given species, and hence one of these two densities from the observed value of the other one. Using the simple relations given by Harwit and Hoyle (1962), we derive

$$\frac{n_i}{n_n} \approx 30\, n_p \sigma D\ ,$$

where σ characterizes the interaction ion-molecule, and D is a characteristic length of the order of the dimensions of the comet's head. The factor 30 is intended to represent the ratio of the mass of the molecular-ion to that of the proton. Numerical results are given in table 16 for typical values of $n_i\ (CO^+)$, $n_i\ (N_2^+)$, and $n_n\ (CN)$ observed at a distance of, say, 10^4 km from the nucleus of a comet. Although the results given here are rather crude, it appears quite possible that the abundances of CO and CO^+ differ by at least one order of magnitude from those of CN and CN^+ in a given region of a comet. In this connection, we notice the interest that there would be to try and observe CO and CN^+ and to determine n_i/n_n ratios for CO and CN.

Finally, it may be mentioned that there exist several other reactions that might be of importance in some cases. These have been pointed out by Marochnik (1962). A reaction which is especially interesting is:

$$H_2^+ + N_2 \rightarrow N_2^+ + H_2 ,$$

because ΔE is very small (≈ 0.15 ev) in this case, so that the cross section is relatively large even for small velocities of the hydrogen molecular ions ($\approx 10^{-15}$ cm^2 from ≈ 0.1 to 0.5 kev). The problem is otherwise the same as before, as we have first to account for the formation of H_2^+. H_2 may be abundant, but the charge exchange cross section is rather low near $E_p = 0.5$ kev, while the photoionization rate is probably of the same order as that for N_2. Processes like

$$N_2^+ + N_2 \rightarrow 2N_2^+ + e$$

and

$$CO^+ + CO \rightarrow 2CO^+ + e$$

will probably be important only in the neighborhood of the nucleus ($R \lesssim 10^3$ km). Indeed, if we take the value of 10 km/sec for the ion velocity and $\sigma = 10^{-17}$ cm^2, which seem more realistic than the values given by Marochnik (ΔE is of the order of 15 ev here), we find that

$$\lambda = n_i \times 10^{-11} \text{ sec}^{-1} , \ *$$

*Apparently Marochnik has taken n_n instead of n_i in this relation, since he assumes an inverse square law distribution.

so that it is only if n_i were of the order of 10^4 to 10^5 cm^{-3} that the corresponding rate coefficients would reach values comparable to those given in table 16. Lastly, an ionization process involving collisions with electrons may compete with the processes mentioned so far if these electrons can be accelerated by electric fields produced by local irregularities in the cometary plasma (Alfvén, 1960; Huebner, 1961).

It should be emphasized that no attempt has been made here to establish the validity of any mechanism capable of explaining the ionization of cometary molecules. The main purpose of the foregoing remarks has been to draw the attention to the fact that the candidacy of the corpuscular theory to provide such a mechanism, at least in part, should still be retained in spite of the repeated attacks this theory has undergone in the last few years.

3. The Chemical Composition of the Cometary Gas

Ideally, the abundance of a given type of cometary molecules would be derived from "monochromatic" observations in the light of an emission band due to the particular molecule under consideration. Unfortunately, very few observations of this kind have been made so far and we often have to make use of rather imprecise estimates of the total visual magnitudes when trying to determine abundances. The use of such visual magnitudes inaccurate as it is, may nevertheless provide an order of magnitude estimate for the total abundance of C_2, $n(C_2)$, because the visual brightness of a comet with a weak continuum is determined essentially by emissions in the Swan system, the NH_2 emissions being virtually negligible. On the contrary, photographic magnitudes

are almost useless, since they include important contributions from at least three molecules (CN, C_2, C_3).

Since errors are found in the literature concerning this matter, it seems appropriate to write down explicitly all the equations to be used in the evaluation of abundances. If the total flux received from a portion of the comet limited by a diaphragm of the recording instrument is F, while F_* is the integrated flux received from the reference star through the same combination of telescope, filter, diaphragm, and photocell or photographic plate*, and if m and m_* are the corresponding magnitudes, obviously

$$F = F_* 10^{-0.4(m-m_*)}$$

and

$$F_* = \int_0^\infty f_\lambda P_\lambda \, d\lambda,$$

f_λ being the flux outside the instrument and P_λ the over-all sensitivity curve. Now if Δ is the geocentric distance of the comet we have

$$4\pi\Delta^2 F = \sum L_{v'v''} P_{\lambda_{v'v''}} \qquad (75)$$

$L_{v'v''}$ being the luminosity (total emission, per sec, of that part of the comet that is observed) in the (v', v'') band and the summation being extended over all bands. $L_{v'v''}$ is given by

$$L_{v'v''} = n_{v'}(Ah\nu)_{v'v''} , \qquad (76)$$

*The correction for atmospheric extinction is assumed to be allowed for separately.

so that $n_{v'}$ can be derived from equation 75 provided the ratios $\frac{n_{v'}}{n_{v''}}$ are known. Finally, the total number of molecules of the given type is

$$n = n_{v'} \sum_{v''} \frac{n_{v''}}{n_{v'}} \quad . \tag{77}$$

Since we know that the cometary emissions are excited by fluorescence, the ratios $\frac{n_{v''}}{n_{v'}}$ are to be computed by solving the relevant system of steady-state equations. The populations of the various levels in the excited electronic state have been neglected, as they are always very small.

Consider two different atoms or molecules which can both be regarded roughly as two-level systems and which we designate by means of indices 1 and 2. It follows from the steady-state equations that

$$\frac{n_2}{n_1} \approx \frac{n_2''}{n_1''} = \frac{(n'A)_2}{(n'A)_1} \frac{C_1}{C_2} \quad ,$$

the A's and the C's being the emission and the absorption rates respectively. If I_2/I_1 is the intensity ratio observed in a cometary spectrum and corrected for atmospheric absorption, this becomes

$$\frac{n_2}{n_1} \approx \frac{I_2}{I_1} \cdot \frac{\lambda_2 P_1}{\lambda_1 P_2} \cdot \frac{C_1}{C_2} \quad , \tag{78}$$

λ_i being the wavelength of the characteristic transition of molecule i and P_i the sensitivity of the photographic plate at λ_i. In the first approximation equation 78 can be used to derive an estimate of the relative abundances of the molecules CN, CH, NH, OH.

A critical revision of the available data concerning abundance determinations in comets has been carried out. The results (corrected whenever necessary) are presented in table 17 which also contains additional data obtained for Comet Humason (1961e) and a few other comets. H_o is the "absolute" visual magnitude (reduced to $r = \Delta =$ 1 A. U.). The last four columns give the total number of molecules $\mathfrak{N}$, the product $n_o R_o^2$ (derived from equation 49 with R_2 different for different molecules), the surface density N at $\rho = 10^4$ km (from equation 46), and the volume density n at $R = 10^4$ km. After a few general remarks which will be given below, some particular cases of comets referred to in table 17 will be considered. Finally, at the end of this section we shall discuss the problem of the forbidden oxygen lines in cometary spectra.

The approximate method given by Wurm (1963) for the determination of C_2 and CN abundances is actually valid only for the case of CN, since it is based on the assumption of a two-level molecule, while it is known that the C_2 Swan band system is well developed in comets. However, one finds that the values derived for $\mathfrak{N}(C_2)$ when the fluorescence is taken into account rigorously differ by less than a factor of two from the values obtained by means of Wurm's simplified formula. This is merely due to a numerical coincidence. For comparison, we give Wurm's formula

$$\mathfrak{N}(C_2) = \frac{3.9 \times 10^{-6} \times 10^{-0.4 m_v}}{(Ah\nu)_{oo}} \cdot 4\pi\Delta^2 \cdot \frac{\mathfrak{N}}{\mathfrak{N}'} , \qquad (79)$$

where $\mathfrak{N}/\mathfrak{N}'$ is evaluated in terms of a "radiation temperature"

Table 17. Molecular and Atomic Abundances in Comets

Comet	r [A. U.]	H_o	h	$n_o R_\rho^2$ [cm^{-1}]	$N(10^4$ km) [cm^{-2}]	$n(10^4$ km) [cm^{-3}]
			C_2			
Cunningham (1940c)	0.87	5.8	7×10^{31}	5.5×10^{20}	1.5×10^{12}	550
Van Gent (1941d)	1.25	6.9	2×10^{31}	1.5×10^{20}	5×10^{11}	150
* Whipple-Fedtke (1942g)	1.44	5.2	5×10^{31}	4×10^{20}	10^{12}	400
Bester (1947k)	0.84	6.6	1.5×10^{31}	10^{20}	4×10^{11}	100
* Mrkos (1955e)	0.72	6.8	10^{31}	8×10^{19}	2.5×10^{11}	80
Encke (1957c)	0.62	10.0	10^{30}	8×10^{18}	2.5×10^{10}	8
Mrkos (1957d)	0.60	3.6	10^{32}	8×10^{20}	2.5×10^{12}	800
* Burnham (1959k)	1.00	7.8	3×10^{30}	2×10^{19}	8×10^{10}	20
* Seki (1961f)	0.92	8.5	1.5×10^{30}	10^{19}	4×10^{10}	10

Table 17 Continued

Comet	r [A.U.]	H_o	n	$n_o R_o^2$ [cm^{-1}]	N (10^4 km) [cm^{-2}]	n (10^4 km) [cm^{-3}]
			CN			
Cunningham (1940c)	0.87	5.8	4×10^{32}	3×10^{21}	10^{13}	3000
Van Gent (1941d)	1.25	6.9	3×10^{32}	2.5×10^{21}	8×10^{12}	2500
* Whipple-Fedtke (1942g)	1.44	5.2	10^{32}	8×10^{20}	2.5×10^{12}	800
Bester (1947k)	0.84	6.6	4.5×10^{31}	4×10^{20}	1.5×10^{12}	400
Encke (1957c)	0.62	9.9	10^{31}	8×10^{19}	2.5×10^{11}	80
Mrkos (1957d)	0.60	3.6	1.5×10^{33}	10^{22}	4×10^{13}	10000
* Burnham (1959k)	1.00	7.8	10^{31}	8×10^{19}	2.5×10^{11}	80
* Humason (1961e)	2.60	3.0	2×10^{30}	1.5×10^{19}	5×10^{10}	15
			CH			
Cunningham (1940c)	0.87	5.8	10^{30}	8×10^{19}	2.5×10^{11}	80
Cunningham (1940c)	0.69	5.8	10^{31}	8×10^{20}	2.5×10^{12}	800
Bester (1947k)	0.84	6.6	1.5×10^{29}	10^{19}	4×10^{10}	10

Table 17 Continued

Comet	r [A.U.]	H_o	h	$n_o R_o^2$ [cm^{-1}]	N (10^4 km) [cm^{-2}]	n (10^4 km) [cm^{-3}]
			NH			
Bester (1947k)	1.05	6.6	4.5×10^{31}	4×10^{20}	10^{12}	400
			OH			
Bester (1947k)	1.05	6.6	1.5×10^{32}	4×10^{21}	10^{13}	4000
			Na			
Mrkos (1957d)	0.60	3.6	2×10^{31}	-	10^{12}	-
			CO^+			
Bester (1947k)	0.97	6.6	10^{32}	-	10^{12}	400
*Humason (1961e)	2.6	3.0	1.5×10^{33}	-	10^{13}	1000
			N_2^+			
*Humason (1961e)	2.6	3.0	1.5×10^{31}	-	10^{11}	10

Table 17 Continued

*The most accurate determinations are indicated by asterisks. The corresponding abundances should not be wrong by more than a factor of about 2. The references used in deriving the quantities listed in this table are as follows: Beyer (1942, 1950, 1958), O'Dell and Osterbrock (1962), Schmidt and van Woerden (1956), Swings and Haser (1956), Vorontsov Velyiaminov (1960).

It is seen that the molecular abundances vary appreciably from comet to comet both in relative and in absolute values.

characterizing the diluted solar radiation, and the correct formula

$$n(C_2) = \frac{3.9 \times 10^{-6} \times 10^{-0.4 m_v}}{(Ah\nu)_{oo}} \cdot 4\pi\Delta^2 \cdot \sum_{v''} \frac{n_{v''}}{n'_o} \cdot \frac{1}{\sum \left(\frac{i_{v'v''}}{i_{oo}}\right) P_{\lambda_{v'v''}}} \quad , \tag{80}$$

where P_λ represents the sensitivity curve of the human eye.

No determination of the abundances of CH, NH, OH has been made as yet. The method used here is rough, but it gives at least some indication as to the orders of magnitude involved. After the abundance of C_2 has been obtained by means of equation 80, that of CN is derived by comparing the intensity of CN violet (0,1) with that of C_2 Swan (2,0) on spectra found in the Atlas of Representative Cometary Spectra (Swings and Haser, 1956) and by making use of the results of the fluorescence computation. Then, the comparison of CH $A\,^2\Delta - X\,^2\Pi$ (0,0), NH $A\,^3\Pi_i - X\,^3\Sigma^-$ (0,0), and OH $A\,^2\Sigma^+ - X\,^2\Pi_i$ (0,0) with CN violet (0,1) is sufficient to yield $n(CH)$, $n(NH)$, and $n(OH)$ through equation 78 which is valid in all four cases because of the flatness of the Condon parabolae involved. The various values of R_2 used in equation 49 are as follows: C_2 (10^5 km), CN (10^5 km), CH (10^4 km), NH (3×10^4 - 10^5 km), OH (3×10^4 km). These values are estimated from the length of spectral bands which have about equal intensities. We note incidentally that the same value is used for C_2 and CN, whereas it is usually stated that CN has a shallower intensity gradient. This is a result of the great strength of the CN (0,0) band: in the case of CN violet all the emission is

concentrated in this band, while in the case of C_2 Swan, which has a comparable f-value, the light is spread over a rather large wavelength range. If we compare CN violet (0,1) and C_2 Swan (1,0). which have generally very similar intensities, one finds that the extensions of CN and C_2 are about the same.

An error which is commonly found in the literature results from a wrong interpretation of the meaning of molecular f-values determined experimentally. More details concerning this question are to be found in Appendix C, b. It will only be said here that this error is insignificant when we are concerned with a band system which has a flat Condon parabola, whereas it is large in a case like that of the CO^+ comet-tail bands where it amounts to a factor of about 3. A convenient and unambiguous definition of an f-value characterizing a whole molecular band system is proposed in Appendix C, b.

Let us now consider a few particular comets.

Comet Bester (1947k)

Grudzinska (1960) determined the ratio of the abundances of CN and CO^+ in this comet and found

$$n(CO^+) \approx 30n(CN) \qquad (81)$$

However, as mentioned previously, this result is affected by an erroneous use of the f-value for the comet-tail system (cf. Appendix C, b). Moreover, the assumption that the intensity of the exciting solar light is the same for the CN bands as for the CO^+ bands is also incorrect. Finally, correcting for these errors and using recent improved "relative transition probabilities" (Nicholls, 1956; Robinson and Nicholls, 1960),

we obtain

$$n(CO^+) \approx 3n(CN) \qquad (82)$$

If we compare this with the result derived below for Comet Humason (1961e), we see that the number of CO^+ ions relative to the number of CN radicals was some 25 times larger in Comet Humason than in Comet Bester. This seems quite reasonable if we compare the spectra of these two comets, one being cominated by CO^+, the other by CN (and C_2).

Comet Mrkos (1955e)

Using the results of photoelectric observations of this comet by Schmidt and van Woerden (1956), Houziaux (1960) evaluated the abundances of the C_2 molecules. Unfortunately, several errors are contained in this evaluation:

(1) A factor of 4π has been omitted in the transformation of the flux received at the earth into a luminosity (p. 1028 of the paper by Houziaux).

(2) The light received through Schmidt and van Woerden's C_2 filter has been assigned entirely to the (1, 0) Swan band, whereas this filter includes the whole $\Delta v = +1$ sequence (peak of the filter at λ4710; total width of filter at half peak transmission: 60 Å). Furthermore, it has been considered that the amount of energy transmitted by the filter depends on the profile of the (1, 0) band, while the sensitivity of this filter varies actually very little over the wavelength interval covered by the (1, 0) band.

(3) The statement, on page 1028, that the brightness B at 1 minute of arc from the nucleus was 0.1 on June 25, 1955 (in the unit defined by Schmidt and van Woerden) disagrees both with the results given in the

column headed "E(R)" in table II (p. 1031) and with the data given by Schmidt and van Woerden.

By means of the latter data* and by means of equations 75 through 77 it is found that the value given by Houziaux for the mean density in a sphere of radius $R = 5.35 \times 10^4$ km is overestimated by a factor of about 6 (the f-value adopted here is such that $(\bar{\lambda}f) = 0.130$, with $\bar{\lambda} = 5.165$ - cf. Appendix C, b). For $R = 0.535 \times 10^4$ km and $R = 1.07 \times 10^4$ km the densities have been overestimated by a factor of about 1.5 and 3 respectively.

Comet Mrkos (1957d)

It is difficult to estimate the abundance of Na because of the importance of self-absorption and because the high density of the available spectra (see Greenstein and Arpigny, 1962). However, since no attempt has been made till now to determine the amount of atomic sodium contained in a cometary atmosphere, it seems interesting to try and derive at least some indication here.

From the f-values of the Na D lines and of the C_2 Swan system it can be shown that

$$\frac{n(Na)}{n(C_2)} \approx 4.5 \times 10^{-3} \frac{I_{Na}}{I_{C_2}(0,0)} \qquad (83)$$

Now a study of spectra of Comet Mrkos (1957d) (r = 0.6 A.U.) reveals that $I_{Na}/I_{C_2}(0,0) \approx 30$. Combining this with $m_v = 2.5$ (Beyer, 1959) and considering that the contribution of the continuum is of the order of

*I am indebted to Dr. van Woerden for providing me with the original results concerning the observations referred to above. These results indicate that the data as given in Schmidt and van Woerden's paper (figure 1) are correct.

50%, we find

$$\eta(\mathrm{Na}) = 2 \times 10^{31} \tag{84}$$

and

$$\eta(C_2) = 1.5 \times 10^{32} \tag{85}$$

We can form another estimate of $\eta(\mathrm{Na})$ in the following way. The optical thickness in the light of the Na D lines is undoubtedly large in the central regions of the coma. However, at a distance of about 10^4 km from the nucleus in the direction of the sun this optical thickness becomes smaller than 1 since $D_2/D_1 = 2$ there. On the other hand, the cross section at the center of a Doppler broadened line is given by (Mitchell and Zemansky, 1961):

$$\sigma_o \approx 10^{-2} \frac{f}{\Delta\nu_D} \ \mathrm{cm}^2 \tag{86}$$

which becomes

$$\sigma_o \approx 10^{-12} \ \mathrm{cm}^2 \tag{87}$$

for $\bar{v} = 1$ km/sec. Hence we have

$$N(10^4 \text{ km}) \lesssim 10^{12} \ \mathrm{cm}^{-2} . \tag{88}$$

From the radial distribution of the intensity in the D lines we can obtain a lower estimate for the ratio of the total number of Na atoms to the surface density at $\rho = 10^4$ km on the sunward side. The final result is:

$$\eta(\mathrm{Na}) \approx 3 \times 10^{31}$$

The coincidence with equation 84 is, of course, accidental, especially

since the second estimate is very crude, but we may consider that the order of magnitude is confirmed.

Comet Halley (1910)

Schwarzschild and Kron (1911) measured the surface brightness of the tail of Comet Halley in cross sections perpendicular to the tail axis, whence they calculated the densities of the fluorescing particles. However, as Wurm pointed out (1943, 1961), the abundances derived by Schwarzschild and Kron were underestimated because their cross sections for fluorescence were much too large. Wurm applied a correction factor for this, but his own results are still incorrect, as they are based on unsound assumptions. In the first place, Wurm's treatment is equivalent to assuming a two-level model for CO^+, which is altogether unjustified. If we correct for this by treating the fluorescence rigorously, we find that the surface density at $\approx 3 \times 10^5$ km (i.e. $0.^\circ 5$) from the nucleus is about four times smaller than the value corresponding to Wurm's result. Wurm expressed his estimate in the form of a volume density, which is highly uncertain because the effective path length along the line of sight, p, is not known. Wurm assumed, after Schwartzschild and Kron, that the tail could be considered as a cylinder of diameter p; since p has been taken equal to 3×10^5 km, the volume density may have been underestimated by one or two orders of magnitude if the CO^+ ions were localized in streamers 10^3 to 10^4 wide. Furthermore, another uncertainty arises from the assignment of all the emission to CO^+, as Bobrovnikoff's photographs and descriptions (1931) for the dates of the observations in question show that a possible contribution of continuous scattered light is not at all excluded in some cases.

In conclusion, we may say that the abundance estimates of the CO^+ ions in Comet Halley appear to be very unreliable.

Comet Humason (1961e)

Having calibrated the spectra of Comet Humason in order to derive relative intensities, we were not very far from determining the absolute intensities of the various molecular emissions and hence, in turn, the particle densities in the comet. In view of the importance of such data for the study of cometary structures as well as of the outstanding character of Comet Humason (1961e) itself (especially as far as CO^+ is concerned), it is worthwhile our devoting a little additional effort to the determination of these densities.

The only available information concerning the total brightness of Comet Humason near the date of the observations is a visual magnitude by Kono who found (IAU Circ. 1806):

$$m_v = 6.8$$

on the 21st of August, 1962. Since this estimate is in agreement with the predictions of the ephemeris appearing in the IAU Circular 1798, we are justified in adopting the value given by the ephemeris for August 1, 1962, $m_v \approx 7.0$, bearing in mind, however, that an error of as much as one magnitude cannot be excluded a priori. (For instance, it has been observed that Comet Humason was brighter by about $1^m.3$ on November 16, 1962 than on the neighboring dates.)

Our problem, then, consists in providing a means for connecting the spectroscopic observations made in the photographic region to a visual estimate of the comet's brightness. We shall proceed as follows.

Since we have determined the relative populations $y_{v'}$ of the vibrational levels in the upper state of the transition corresponding to the comet-tail system, it is easy to evaluate the ratio (r_1) of the intensity of any band, (v', v''), of this system in the photographic region to the sum of the intensities of the bands of the same system which fall in the visual range -- each intensity being multiplied by the appropriate ordinate of the sensitivity curve for human vision. On the other hand, the ratio (r_2) of the amounts of continuous energy contained in a narrow bandpass (say, 10 Å wide) in the photographic region and in the bandpass corresponding to the visibility of the human eye can be readily obtained, as it has been recognized earlier that the reflection or scattering of solar radiation by cometary particles is undoubtedly non-selective in the case of Comet Humason (1961e) (see also below). A third link is established by measuring the ratio (r_3) of the intensity, at a given place in the comet, of the (v', v'') band to the intensity of the neighboring reflection continuum in a 10 Å bandpass. Thus we have, for example, with obvious notations:

$$r_1 = \frac{S^{CO^+}_{20}}{S^{CO^+}_{v}} \quad , \quad r_2 = \frac{S^{cont}_{\lambda_{20}}}{S^{cont}_{v}} \quad , \quad r_3 = \frac{S^{CO^+}_{20}}{S^{cont}_{\lambda_{20}}}$$

Then, with the aid of elementary algebra we obtain the following expression for the surface brightness in the light of one of the comet-tail bands:

$$S^{CO^+}_{v'v''} = r_1(v', v'')S^{\odot}_{v}\left(\frac{a_{\odot}}{a_{CO^+}}\right)^2 \cdot \frac{1}{1 + \left(\frac{r_1}{r_2 r_3}\right)\cdot\left(\frac{a_{cont}}{a_{CO^+}}\right)^2} \cdot 10^{-0.4(m_v - m_v^{\odot})} , \tag{89}$$

where $a_{\odot}$, a_{cont}, and a_{CO^+} are the angular radii of the solar disk,

the central reflecting part of the comet's head, and the CO^+ emissions respectively, and where we have used the sun as a standard for the conversion of magnitude into surface brightness. Each of a_{cont} and a_{CO^+} is an "equivalent" radius, i.e. the radius of the uniform disk whose surface brightness would be equal to the actual value of the respective surface brightness at the positions considered in the determination of the ratio r_3, and whose total brightness would be equal to the actual total brightness. These equivalent radii are determined by means of the radial profiles referred to previously. In practice only r_1 has to be known accurately. Indeed, the denominator of the fraction appearing in equation 89 will be very nearly equal to one, since the relative contribution of the nucleus to the total light of the comet is, at most, of the order of a few percent. Finally, the surface density of CO^+ ions at a distance ρ from the nucleus is related to the brightness by

$$N_{CO^+}(\rho) = (\bar{n}L)_{CO^+} = \frac{4\pi S^{CO^+}_{v'v''}(\rho)}{A_{v'v''}h\nu_{v'v''}} \cdot \frac{N''_o}{N_{v'}} \quad , \tag{90}$$

where $\bar{n}$ is the mean density per cm^3 and where L represents the net path length through the comet along the line of sight. We neglect the very small contribution to the total number of CO^+ ions from the populations of the vibrational levels $v'' \geq 1$ and of the electronic states $A\ ^2\Pi$ and $B\ ^2\Sigma^+$.

The last factor in equation 90 can be written:

$$\frac{N''_o}{N_{v'}} = \frac{\sum_{v''} A_{v'v''}}{\sum_{v''} x_{v''} C_{v'v''}}$$

or

$$\frac{N''_o}{N_{v'}} = \frac{hc^2}{W(\lambda^2 F_\lambda)_{20}} \cdot 10^{13} \cdot \frac{\sum_{v''} a_{v'v''}}{\sum_{v''} x_{v''} c_{v'v''}} \quad . \tag{91}$$

On the other hand, combining equations 90 and 91 and considering that $x_{v''}$ is usually negligible for $x_{v''} \geq 1$, we see that the average relative abundances of various molecules can be derived from

$$N \propto S_{v'v''} \cdot \frac{\lambda_{v'v''}}{C_{v'o}} \cdot \frac{\sum_{v''_1} A_{v'v''_1}}{A_{v'v''}} \quad ,$$

which is equivalent to

$$N \propto S_{v'v''} \cdot \frac{\lambda_{v'v''}}{(p\eta\lambda^2 F_\lambda)_{v'o}(\overline{\lambda f})} \cdot \frac{\sum_{v''_1} a_{v'v''_1}}{a_{v'v''}} \quad . \tag{92}$$

Three sets of calculations using the bands (3, 0), (2, 0), and (1, 0) of CO^+ successively have given very concordant results. Inserting numerical values into equation 89, we obtain for instance

$$S_{20}^{CO^+} = 0.007 \text{ erg cm}^{-2} \text{ sec}^{-1} \text{ (usa)}^{-1} , \tag{93}$$

at $\rho = 10^4$ km.* Equations 90 and 91 then yield:

$$N_{CO^+}(10^4 \text{ km}) = 2.5 \times 10^{13} \text{ cm}^{-2} .$$

In view of the uncertainty attached to the use of the visual magnitude m_v, two other independent procedures have also been followed

* usa stands for unit solid angle.

for the calibration of the comet spectra. On the one hand, since the CO^+ bands have been connected to the reflection continuum through the ratio r_3 defined earlier, the relative CO^+ intensities can be transformed into absolute intensities by means of the visual magnitude of the nucleus ($m_v^N = 14$ -- kindly communicated to me by Dr. Roemer). On the other hand, knowing the apparent magnitude of the star LDS 785 A as well as its spectral energy distribution, and comparing the intensities obtained under the same conditions of recording (same slit, same gain, etc.) for a CO^+ band and for the continuum of the white dwarf at the wavelength of this band, we can derive the absolute surface brightness of the comet in the CO^+ emission considered, provided that we allow for the differences in exposure time and in atmospheric extinction.

Table 18 gives the results of the three independent determinations of $S_{20}^{CO^+}$ as well as the corresponding surface densities for CO^+, N_2^+ and CN derived by means of equations 90 through 92. The necessary molecular data on "relative transition probabilities" have been taken from Fraser, Jarmain and Nicholls (1954), Nicholls (1956), and Robinson and Nicholls (1960); the f-values are given in Appendix C, b. The estimates of the mean densities per cm^3, which require the evaluation of effective path lengths, are rather uncertain in the case of the ions. Consequently, it would be preferable to quote only the surface densities, until we have a realistic model for the ionized part of a comet, which would enable us to actually calculate L. Nevertheless, since the results of previous investigations were expressed in the form of abundances per cm^3, the present results are also given in this form in table 18. The path length L_{CO^+} (as well as $L_{N_2^+}$) has been taken approximately equal to the

for the calibration of the comet spectra. On the one hand, since the CO^+ bands have been connected to the reflection continuum through the ratio r_3 defined earlier, the relative CO^+ intensities can be transformed into absolute intensities by means of the visual magnitude of the nucleus ($m_v^N = 14$ -- kindly communicated to me by Dr. Roemer). On the other hand, knowing the apparent magnitude of the star LDS 785 A as well as its spectral energy distribution, and comparing the intensities obtained under the same conditions of recording (same slit, same gain, etc.) for a CO^+ band and for the continuum of the white dwarf at the wavelength of this band, we can derive the absolute surface brightness of the comet in the CO^+ emission considered, provided that we allow for the differences in exposure time and in atmospheric extinction.

Table 18 gives the results of the three independent determinations of $S_{20}^{CO^+}$ as well as the corresponding surface densities for CO^+, N_2^+ and CN derived by means of equations 90 through 92. The necessary molecular data on "relative transition probabilities" have been taken from Fraser, Jarmain and Nicholls (1954), Nicholls (1956), and Robinson and Nicholls (1960); the f-values are given in Appendix C, b. The estimates of the mean densities per cm^3, which require the evaluation of effective path lengths, are rather uncertain in the case of the ions. Consequently, it would be preferable to quote only the surface densities, until we have a realistic model for the ionized part of a comet, which would enable us to actually calculate L. Nevertheless, since the results of previous investigations were expressed in the form of abundances per cm^3, the present results are also given in this form in table 18. The path length L_{CO^+} (as well as $L_{N_2^+}$) has been taken approximately equal to the

Table 18. Abundance estimates in Comet Humason (1961e)

Method	Surface Brightness $S_{20}^{CO^+}$ [erg cm^{-2}sec^{-1}(usa)$^{-1}$]	Surface Densities at 10^4 km from the Nucleus N_{CO^+}	$N_{N_2^+}$ [cm^{-2}]	N_{CN}	Corresponding Mean Volume Densities $\bar{n}_{CO^+}$	$\bar{n}_{N_2^+}$ [cm^{-3}]	$\bar{n}_{CN}$
m_v	0.0067	2.5×10^{13}	2.5×10^{11}	1.25×10^{11}	2500	25	37
cont	0.0022	7.2×10^{12}	7.2×10^{10}	3.6×10^{10}	720	7	11
*	0.0016	6.0×10^{12}	6.0×10^{10}	3.0×10^{10}	600	6	9
Adopted Values	0.0032	10^{13}	10^{11}	5×10^{10}	1000	10	15

apparent radial dimension of the comet in the light of CO^+, which can be estimated by inspection of Greenstein's spectra and of direct photographs taken by Rudnicki and Kearns with the 48-inch Schmidt telescope on the same dates as the spectra. The adopted value is 1.0×10^5 km (about 90% of the light is contained within a radius of 2' or 1.5×10^5 km). As far as CN is concerned it is possible to form a fairly reasonable estimate of L, for we can assume an ideal, spherically symmetrical model in which the density is inversely proportional to the square of the radial distance to the central nucleus, as we have seen earlier. It is clear that

$$N(\rho) = \pi \frac{n_o R_o^2}{\rho} = n(\rho)\pi\rho \quad . \tag{94}$$

This shows that, if L is taken equal to $\pi\rho$, which is about the case for the value used for L_{CN} (3.3×10^4 km), $\bar{n}$ is equal to $n(\rho)$. The last row in table 18 contains the final values adopted for the various abundances. The surface densities as well as $\bar{n}_{CN}$ are probably correct within a factor of 2 or 3.

It may be mentioned in passing that on the basis of the abundance determination for CO^+ and of the results obtained in the study of the fluorescence excitation of the comet-tail bands, it is possible to estimate the amount of infra-red energy emitted in the vibration transitions in the ground state of CO^+ -- essentially in the transition $v'' = 1 \rightarrow v'' = 0$, whose wavelength is about 4.6 μ. Of course, we should need to know q and x_1'' to determine this quantity. Actually, however, these two parameters enter the calculation only in the form of their product,

and it can be seen readily that, when q is large ($\gtrsim 10$), as has been shown to be the case, this product qx_1'' remains approximately constant and equal to about 0.5. Under these conditions one finds that

$$S_{IR}^{CO^+} \approx 7 \times 10^{-4} \text{ erg cm}^{-2} \text{ sec}^{-1} (\text{usa})^{-1}, \qquad (95)$$

a very large value indeed. The transition probability is much smaller in the case of the pure vibration transition than for the electronic transition, but this is compensated by a much larger number of emitting particles. The infra-red emission due to CN in a bright comet is probably of the same order of magnitude as the value given in equation 95 for CO^+.

Finally, we may try and evaluate the radius of the nucleus, R_o, since we know the magnitude of the nucleus and since we have shown that the continuous spectrum of Comet Humason was a pure reflection continuum. A remark concerning the latter point seems appropriate. Several spectrophotometric and polarimetric studies have established that, in the comets studied, the continuum was due to the scattering of sunlight by particles of diameters of the order of 0.5 μ. When such is the case, the scattering coefficient is proportional to λ^2, so that the scattered radiation is redder than the solar radiation. On the other hand, we have seen in chapter III that the relative intensities of CO^+ bands based on the assumption that the continuum had a spectral distribution identical to that of the sun agreed within 10 to 15% with the values derived in three other independent ways. Even if we consider only the wavelength range from about 3800 Å [(4,0) band] to about 4700 Å [(2,1) band], it seems that, if the scattering were selective and

proportional to λ^2, systematic differences would appear when we consider the successive bands from the (4, 0) band to the (2, 1) band. As a matter of fact, there would be a factor of about 1.5 between the ratios of the relative intensities of these two bands determined by means of the cometary continuum on the one hand, and by means of a star on the other hand. The errors involved in the calibration are certainly smaller than 50%. Furthermore, a direct calibration of the comet's continuum by means of the star LDS 785 A has been carried out independently. Figure 22 shows the resulting curve together with the spectral distributions of the sun and of the solar light scattered according to the λ^2 law (Mie scattering). Again we can conclude that the scattering was non-selective in the case of the nucleus of Comet Humason (1961e).

If we consider this as the reflection of sunlight by a sphere of radius R_o and albedo A (≈ 0.1), we find, from the usual formula

$$\log R_o = 0.2(m_\odot - m_\alpha) + \log r\Delta - 0.5[\log A + \log \varphi(\alpha)] ,$$

where we take $\log \varphi(\alpha) \approx 0$ (because the phase angle was very small), that

$$R_o = 6.6 \text{ km.}$$

This is of the same order as the value found for the nucleus of Comet Giacobini-Zinner (Mianes, Grudzinska, and Stawikowski, 1960), for instance.

If, on the other hand, it is assumed that the light received from the central region of Comet Humason was due mainly to the scattering of the solar radiation by a cloud of particles with diameters a of

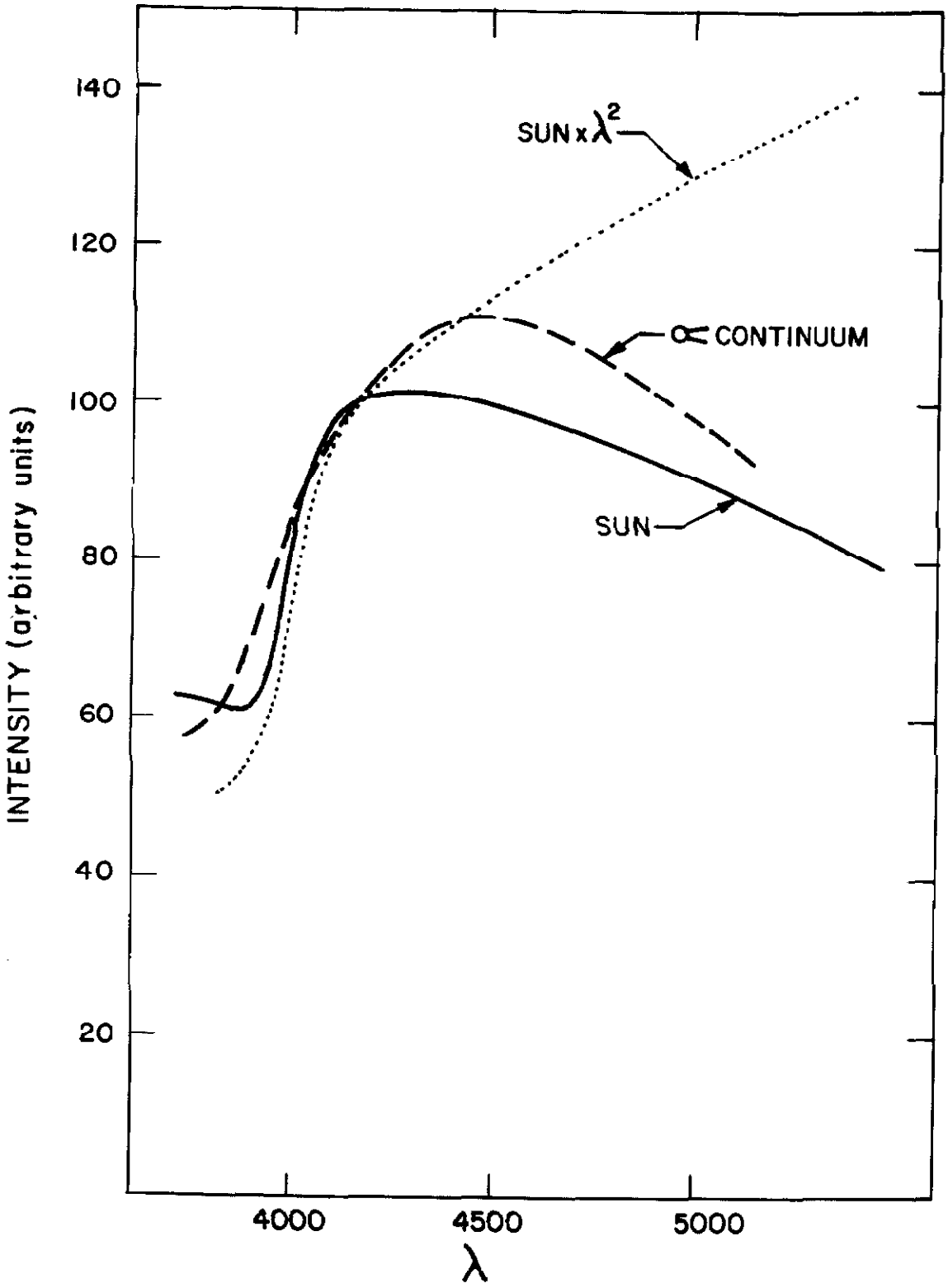

Fig. 22. Energy distribution in the continuous spectrum of Comet Humason (1961e), in the solar spectrum, and in the solar spectrum scattered according to a λ^2 law.

several microns, the equation

$$n \frac{\pi a^2 A \pi f^{\odot}}{2r^2 \Delta^2} = \pi f^{\mathscr{C}} ,$$

where $f^{\odot}$ and $f^{\mathscr{C}}$ are the fluxes received at the earth from the sun and from the comet respectively, yields the total number of grains:

$$n = 2 \times 10^{18} .$$

If the observed radius of the central condensation ($\approx 2 \times 10^3$ km) corresponds to the actual radius of the dust cloud, the mean particle density is

$$\bar{n} = 5 \times 10^{-8} \mathrm{cm}^{-3},$$

and if the specific mass is equal to 2 the total mass of dust is

$$\mathcal{M} = 2 \times 10^{10} \text{ gm.}$$

It does not seem impossible a priori that the dust grains have a certain range of sizes and that the predominant size be different in different comets. This could produce both reddened and unreddened scattered continuous spectra. Here again additional observations are certainly needed.

To conclude this section I should like to make a few comments concerning the forbidden oxygen lines in comets. That the [OI] lines often appear on cometary spectra has been known for a long time but the origin of these emissions remains uncertain. Are they purely terrestrial or is there any cometary contribution? It is difficult to answer this question on the basis of low-dispersion spectra because of the blends of the [OI]

lines with NH_2 or C_2 emissions. The first unambiguous case has been provided by Comet Mrkos (1957d). Studying high-resolution spectra of this comet, Swings and Greenstein (1958) have been able to show that the red doublet (λ6300, λ6364) and the green line (λ5577) (see figure 23) measured on these spectra are undoubtedly of cometary origin. A similar conclusion has been drawn by Swings and Fehrenbach (1962) concerning spectra of Comet Seki-Lines (1962c). Reexamining a series of low-dispersion spectra taken during the last two decades, Swings (1962) has found a number of other examples of cometary forbidden oxygen lines. The ratio I_G/I_R of the intensity of the green line to that of the red doublet seems to be highly variable; it is smaller than unity in one comet, greater than unity in another comet.

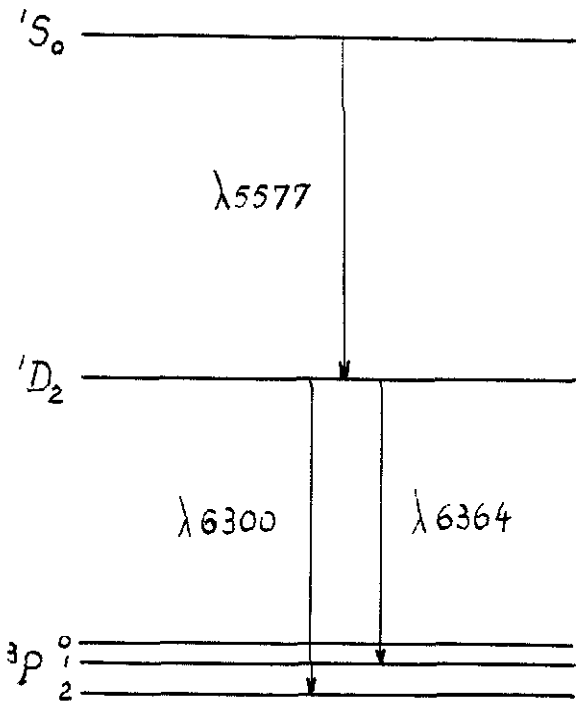

Fig. 23. Term diagram for the normal configuration of OI.

The problem of the excitation of these forbidden lines in comets cannot be solved as yet. The fluorescence mechanism can be ruled out on account of the low transition probabilities involved. For instance, in the case of Comet Mrkos (1957d) we have

$$\frac{I_O(\text{red})}{I_{C_2}(0,1)} \approx 0.15 .$$

If we introduce this into the following equation*:

$$\frac{n(O)}{n(C_2)} = \frac{I_O(\text{red})}{I_{C_2}(0,1)} \left(\frac{n'_o}{\sum n''} \right)_{C_2} \frac{A_{ol}}{C(^3P - {}^1D)} \frac{\lambda(^3P - {}^1D)}{\lambda_{ol}}$$

we obtain

$$\frac{n(O)}{n(C_2)} \approx 7 \times 10^6 .$$

Even if the estimate of $n(C_2)$ given by equation 85 were overestimated by a factor of 10 the corresponding value for $n(O)$ would be much too high to be acceptable.

The [OI] lines may be excited by electron collisions. It is also possible that the oxygen atoms are formed in the excited states ^1D and/or ^1S by photodissociation of O_2. If we assume that a steady state is achieved and if we consider only transitions produced by electronic collisions and, among them, only those transitions that have non-negligible probabilities for reasonable values of the electronic density and temperature (numerical values have been given by Remy-Battiau (1962))

*The transition ^3P - ^1S can be disregarded completely as far as the fluorescence is concerned.

$$n_P E_{PD} = n_D(A_{DP} + D_{DP}) + n_S A_{SP} \tag{96}$$

$$n_D(A_{DP} + D_{DP}) = n_P E_{PD} + n A_{SD} , \tag{97}$$

where the A's are the spontaneous emission rates, and where D_{DP} and E_{PD} are the collisional deactivation rate and the collisional excitation rate for transitions between the ^3P and ^1D states. Equations 96 and 97 are consistent with each other only if n_S is very small, which can be shown to be the case. Under these conditions, we have

$$\frac{n_D}{n_P} = \frac{E_{PD}}{A_{DP} + D_{DP}} . \tag{98}$$

For a reasonable value of the electronic temperature ($T_e \approx 10^4\ ^oK$) equation 98 becomes

$$\frac{n_D}{n_P} \approx 4 \times 10^{-8} \bar{n}_e \ ^* \tag{99}$$

On the other hand, the fluorescence calculations for the C_2 molecule show that

$$\left(\frac{n_o'}{\sum n''}\right)_{C_2} \approx \frac{3 \times 10^{-8}}{r^2} , \tag{100}$$

so that if we observe the ratio $I_O(\text{red})/I_{C_2}(0,1)$ in a cometary

---

*To be sure, in order to be rigorous we should consider the spatial variation of the various quantities considered here, but we have no model that would enable us to do so at present.

spectrum*, we can derive the relative abundance $n(O)/n(C_2)$ by means of:

$$\frac{n(O)}{n(C_2)} = \frac{I_O(red)}{I_{C_2}(0,1)} \cdot \frac{10^8}{r\bar{n}_e}, \qquad (101)$$

which will be valid if the [OI] lines are excited by electronic collisions. When this is the case the ratio I_G/I_R is always appreciably smaller than one for any reasonable set of values of T_e and n_e (Remy-Battiau, 1962). If cases in which $I_G/I_R > 1$ do really exist their interpretation will probably require photodissociation processes to be considered as well (or photoionizations followed by dissociative recombinations, which is equivalent). Unfortunately, the relevant probabilities are not known. However, the existence of such cases can be doubted, as will be seen shortly.

Very recently Biermann and Trefftz have made use of the remarks by Swings (1962) concerning the intensities of [OI] lines in cometary spectra in order to construct comet models in which chemical reactions occur according to these authors. By means of very simple considerations equivalent to the result expressed by equation 101 for instance, Biermann and Trefftz conclude that the total amount of gas contained in a cometary atmosphere is much larger than usually assumed. From the ratios I_O/I_{C_2} observed in some particular comets they derive $n(O)/n(C_2)$ and then from the value of $n(C_2)$ given by Wurm for a rather

*The observed intensity ratio, of course, to be corrected for the possible contributions of [OI] lines of telluric origin.

bright comet ($H_o = 4$) they derive $h(O)$. Now at least two objections can be raised against such a procedure. First of all, it should be noted that the remarks made by Swings concerning I_O/I_{C_2} are of a purely qualitative nature. On the other hand, the value of $h(C_2)$ used by Biermann and Trefftz may be rather different from the actual values corresponding to the particular comets under consideration and corresponding to the positions of these comets when they were observed. Furthermore, the results of Biermann and Trefftz's model computations are, of course, rather sensitive to the abundances of the reagents. For instance, the total production of CO^+ and the surface density of CO^+ depend on the product of the values adopted for the parameter Q_o/v_o for the two types of "parent" molecules. Quantitative observations of the dimming of stars by cometary atmospheres as well as spectra of stars seen through cometary atmospheres would provide valuable information concerning the total gas densities in comets. Another observational test which, at first sight, might seem interesting in this connection would consist in looking for possible collisional effects in the central regions of the coma: if the densities were high enough the results of the fluorescence calculations could be appreciably modified. Unfortunately, such high densities would, of course, be restricted to the immediate neighborhood of the nucleus and the effects of collisions would be masked because of the large optical thickness.

Finally, it should be mentioned that some doubts can be formulated as to the cometary origin of the forbidden oxygen lines in some cases. Let us examine for instance the series of spectra of

Comet Bester (1957k or 1948I) reproduced in Swings and Haser's Atlas of Representative Cometary Spectra (Plate III) and to begin with let us consider spectrum number 9, which corresponds to $r = 1.3$ A. U. . Adopting the visual magnitude given by Beyer (1950) and using a formula similar to equation 80, we obtain the surface brightness of the comet at 10^5 km from the nucleus in the light of the (0, 0) band:

$$S_{oo}^{C_2} \approx 3 \times 10^{-4} \text{ erg cm}^{-2}\text{sec}^{-1}(\text{usa})^{-1} .$$

On the other hand, the brightness of the night-sky [OI] λ5577 line is

$$(S_G^O)_O \approx 10^{-4} \text{ erg cm}^{-2}\text{sec}^{-1}(\text{usa})^{-1}$$

for the conditions of observation of the spectrum under consideration (Chamberlain, 1961; Swings and Page, 1950). Although these evaluations are far from being accurate, it seems that the two brightness in question are of the same order of magnitude -- especially since the brightness of $C_2(0, 0)$ has been slightly overestimated owing to the fact that the contribution to the continuum has been neglected. Since the intensity of λ5577 is comparable with that of $C_2(0, 0)$ at 10^5 km on the spectrum mentioned above, we can conclude that this forbidden oxygen line is of terrestrial origin. Moreover, this conclusion is confirmed by the uniformity of the λ5577 line on spectrum number 9. It is difficult to estimate relative intensities from an inspection of the spectra of the same comet at smaller heliocentric distances, for these spectra are so dense on the available reproductions. Nevertheless, it may be pointed out that if, for instance, at $r = 0.81$ A. U. (spectrum number 2) the comet was about three times brighter than at $r = 1.3$ A. U., the

night-sky λ5577 line was itself five times stronger because spectrum number 2 was taken much closer to the horizon than spectrum number 9. Thus, it is possible that the green line be purely telluric here again. The observed gradient could, of course, be explained by the superposition of $C_2(1, 2)$. Similar considerations apply to Comet Van Gent (1941d or 1941 VIII) whose spectra also show a rather strong green line.

The opinion expressed in the preceding paragraph can be reinforced by the following remark. If we compare a number of spectroscopic observations of the night-sky* with the cometary spectra discussed above and if we allow, as much as possible, for possible differences in the conditions of observation in the various cases (f-ratio of the telescope, spectral dispersion, emulsion type, zenith distance, exposure time) we can see that it is quite possible indeed that the strongest emission of the night-sky, λ5577, was recorded on the above-mentioned cometary spectra. Furthermore, the observations show that, as far as the night-sky emissions are concerned, λ5577 is always stronger than λ6300 and that it is sometimes as much as five times stronger. This, in turn, furnishes one further argument in favor of the existence of forbidden oxygen lines of cometary origin when the red doublet is observed to be stronger than the green line and when twilight effects can be excluded.

It will be necessary to obtain additional high-resolution

*See e.g. Blackwell, Ingham, and Rundle (1960), where a list of references to earlier observations can be found.

spectra of comets if we are to establish or to disprove the existence of cometary forbidden atomic oxygen emissions such that $I_G/I_R > 1$. This seems to be an important point because the difficulty of explaining such cases is considerable. On the other hand, while we are waiting for suitable comets to come to our neighborhood, it would be desirable that we make a quantitative analysis of the existing material, for this would enable us to test the validity of Biermann and Trefftz's models mentioned earlier.

CONCLUSIONS

The resonance fluorescence produced by solar light is a very efficient mechanism for exciting molecular emissions in comets. It has been shown here that the cometary emissions due to the NH_2 radical and the CO^+ molecular ion are caused by this process in the same way as those of the hydrides, the cyanogen radical and the C_2 molecule. Thus, it may certainly be said that all the molecular emissions observed in cometary spectra are produced by resonance fluorescence.

On the other hand, the study of the resonance-fluorescence excitation process in comets has now reached a stage of refinement in which not only first order effects, like those of the Swings mechanism, but also second order effects, like the Greenstein effect, can be analyzed in great detail. Significant progress, which could throw some light on the problem of the structure of comets, will be possible in this field when a series of high-resolution spectra of comet heads and tails, taken with very long slits, have been studied carefully by means of steady-state equations which include the effect of the solar absorption lines. Such studies should make use of solar intensity tracings of very high accuracy like those secured very recently by members of the staff of the Astrophysical Institute of the University of Liège at the Jungfraujoch Scientific Station.

While the interaction between cometary atmospheres and the electromagnetic radiation from the sun has been established beyond any doubt, the question of the correlation of fluctuations in the brightness of

comets with solar activity through the action of corpuscular streams seems to remain somewhat controversial. Of course, the anisotropy of the fluctuations in the solar corpuscular radiation field tends to make the number of observable effects rather small. On the other hand, if cases are observed in which important cometary brightness fluctuations occur which are not connected with any solar phenomenon, as has been the case for Comet Humason (1961e) (Roemer, 1962), then it is possible that processes having their origin in the comet itself are responsible for the changes in brightness and appearance.* A similar view has been advanced recently by Wurm concerning the ionization mechanism (Wurm, 1962).

An important distinction can be made between the interactions of the cometary molecules with the solar light on the one hand, and with the solar corpuscules on the other hand, as far as the time scales involved are concerned. The lifetimes τ_{abs} for absorption of solar light in the visible or photographic regions of CN, C_2, CO^+, ... are found to be of the order of 10 to 100 sec at a distance of 1 A.U., whereas the time scale associated with collisional processes,

$$\tau_{coll} = (nv\sigma)^{-1}$$

is about equal to or greater than 10^6 to 10^7 sec at the same heliocentric distance, if we adopt the most recent values for the flux of solar particles ($nv = 3 \times 10^8$ cm^{-2}sec^{-1}) and take $\sigma = 10^{-15}$ cm^2. We see that the absorption processes are very fast as compared with collision phenomena

*Unless the fluctuations observed in these cases can be entirely explained by variations in the solar corpuscular flux which might possibly occur to some extent even under normal, quiet conditions.

involving the solar particle fluxes encountered under "normal" conditions (not in strong bursts). As a result, it seems very likely that the steady-state conditions which are assumed to prevail, in the treatment of the fluorescence problem, are indeed readily established in comets, unless some unknown processes occurring on a very short time scale destroy this steady-state. This tells us, in turn, that if no such rapid process exists, any peculiarity in the distribution of molecules like $CO^{!}$ among their internal energy states that might be brought about at the time of their formation will be masked. Thus, it is not in the relative intensities of the bands of a given constituent, but rather in the relative intensities of the emissions of a constituent with respect to those of its "parent" that one should look for some clues to the mechanism of formation of this constituent. For example, it would be very interesting to be able to compare CO (which should have cometary emissions in the rocket ultraviolet) to CO^{+}, CN to CN^{+}(UV), especially if we could combine this with a theory which would predict the ratio of the number of molecular ions of a given kind to that of the corresponding parent molecules in terms of known cross section.

Many additional observations and many additional theoretical developments will be required before we achieve a full understanding of the cometary phenomena. In particular, the importance of "monochromatic" observations could not be stressed too much. Such observations will be necessary in order to test or to back up some of our ideas concerning the shapes of the comae and concerning the particle distributions in these comae. On the other hand, we know very little

about the cometary plasma and about its interaction with solar corpuscular streams, and the comet tails seem so reluctant to betray the secrets of their often spectacular and so varied behavior.

Finally, I should like to express the wish that the rather recent revival of the interest that is taken in the field of cometary physics be continued, not only for the sake of this field itself, but also for the possible profit of the various other fields with which it is connected, from the study of the interplanetary medium to low temperature physics, to plasma physics, and to space research.

APPENDIX A

ROTATIONAL LIFETIMES IN THE GROUND STATE OF CN

The probability A_K^{rot} of the pure rotation transition $K \rightarrow K - 1$ (see Figure A below) in a $^2\Sigma$ state can be obtained by combining the transition probabilities $A_K^{rot\,(1)}$ and $A_K^{rot\,(2)}$ of the two components of the transition. We have (Herzberg, 1950):

$$A_K^{rot\,(1)} = C \times \frac{K^3(K + \frac{1}{2})}{2(K+1)} , \tag{A1}$$

$$A_K^{rot\,(2)} = C \times \frac{K^2(K - \frac{1}{2})}{2} , \tag{A2}$$

with

$$C = \frac{512\,\pi^4}{3h}\,\mu^2 B^3 \tag{A3}$$

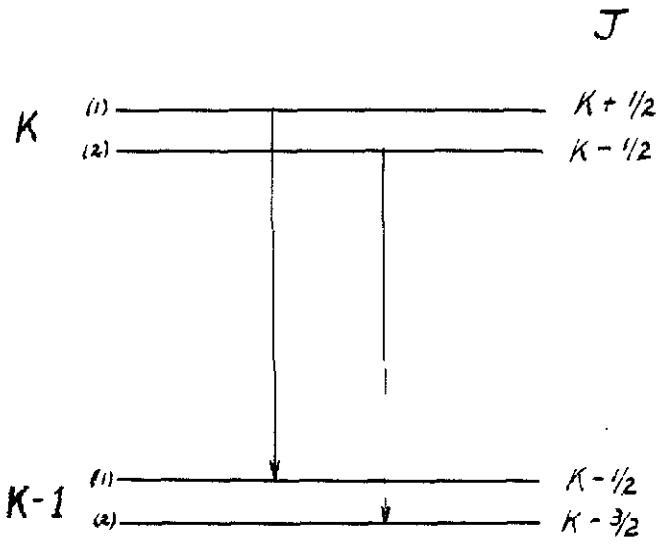

Fig. A. Pure rotation transition in a $^2\Sigma$ state

If N is the total number of molecules in an enclosure in thermal equilibrium the intensities of the two components of the $K \rightarrow K - 1$ transitions are (in emission):

$$I_1 = Q \cdot N \cdot 2(K+1) e^{-\frac{BK(K+1)hc}{kT}} A_K^{rot\,(1)}$$

and

$$I_2 = Q \cdot N \cdot 2K e^{-\frac{BK(K+1)hc}{kT}} A_K^{rot\,(2)} ,$$

Q being another constant. On the other hand, if the two components are lumped together, the intensity of the rotational line will be written

$$I = Q \cdot N \cdot 2(2K+1) e^{-\frac{BK(K+1)}{kT}} A_K^{rot} ,$$

Since $I = I_1 + I_2$, we obtain

$$A_K^{rot} = \frac{2(K+1)A_K^{rot\,(1)} + 2K A_K^{rot\,(2)}}{2(2K+1)}$$

or

$$A_K^{rot} = \frac{C}{2} \times \frac{K^4}{K + \frac{1}{2}} . \qquad (A4)$$

Hunaerts (1959b) has written

$$A_K^{rot\,(1)} = C_1 \times \frac{(K + \frac{1}{2})^4}{2(K+1)} , \qquad (A5)$$

$$A_K^{rot\,(2)} = C_2 \times \frac{(K - \frac{1}{2})^4}{2K} , \qquad (A6)$$

instead of equations A1 and A2. Equations A5 and A6 are incorrect because the wave number of the rotation transition has been expressed

in terms of J instead of K and because two different numerical values have been used for the same quantity C given by equation A3.

The lifetimes computed from equation A4 are given in table A1. The constant C has been evaluated on the basis of the value of the parameter R_1 given in chapter II. The numerical values given here for $\tau_{rot}(K)$ should not be considered as accurate, as they are based on the assumption that $\tau_{rot}(K_\ell) = \tau_{abs}(r)$. The third column in table A contains the heliocentric distance at which this relation is satisfied. It should be noted that $\tau_{abs}(r)$ includes the absorptions both in the violet and in the red system of CN.

Table A. Rotational lifetimes in the ground state of CN

K	τ_{rot}(K) (sec)	r (A. U.)
1	135000	
2	14000	
3	3900	
4	1600	
5	800	
6	460	
7	290	5.6
8	195	4.6
9	135	3.9
10	97	3.3
11	72	2.8
12	55	2.5
13	43	2.2
14	35	1.94
15	28	1.75
16	23	1.60
17	19	1.46
18	16	1.33
19	14	1.22
20	12	1.12
21	10	1.05
22	8.5	0.96
23	7.5	0.90
24	6.5	0.85
25	6.0	0.79
26	5.5	0.74
27	4.8	0.70
28	4.3	0.67
29	3.8	0.64
30	3.5	0.61

APPENDIX B

RELATIVE POPULATIONS OF THE ROTATIONAL LEVELS IN THE GROUND STATE OF CN IN COMETS AT VARIOUS HELIOCENTRIC DISTANCES

The following table gives the distribution of populations of the rotational level in the electronic ground state of CN calculated by means of the steady-state equations describing the fluorescence excited by the solar radiation at 20 different heliocentric distances ranging from 0.2 to 4.0 A.U. These distributions are correct in first approximation only, as they disregard the effects of Fraunhofer lines on individual rotational lines. Although they apply strictly to the $B\,^2\Sigma^+ - X\,^2\Sigma^+$ transition of CN, the results tabulated here can be used, with appropriate modifications concerning molecular characteristics, in other situations in order to obtain a rough idea of how the relative distributions vary with these molecular characteristics, and with heliocentric distance for a given molecule.

Table B. Relative populations of the rotation levels of the ground state of the CN radical in comets for various heliocentric distances (r in A. U.)

K	r = 0.2	0.3	0.4	0.5
0	0.0014	0.0018	0.0022	0.0027
	0.0043	0.0053	0.0067	0.0082
2	0.0071	0.0089	0.0111	0.0137
	0.0099	0.0124	0.0156	0.0191
4	0.0128	0.0160	0.0200	0.0245
	0.0156	0.0195	0.0244	0.0299
6	0.0184	0.0230	0.0288	0.0352
	0.0212	0.0264	0.0330	0.0402
8	0.0240	0.0298	0.0371	0.0450
	0.0267	0.0331	0.0410	0.0495
10	0.0295	0.0363	0.0447	0.0533
	0.0320	0.0393	0.0479	0.0566
12	0.0347	0.0421	0.0507	0.0589
	0.0369	0.0445	0.0529	0.0603
14	0.0394	0.0467	0.0544	0.0606
	0.0414	0.0484	0.0552	0.0598
16	0.0436	0.0498	0.0551	0.0577
	0.0450	0.0505	0.0542	0.0544
18	0.0469	0.0508	0.0524	0.0502
	0.0476	0.0504	0.0497	0.0451
20	0.0491	0.0494	0.0463	0.0394
	0.0489	0.0477	0.0423	0.0335
22	0.0501	0.0457	0.0378	0.0277
	0.0485	0.0428	0.0329	0.0221
24	0.0498	0.0400	0.0281	0.0171
	0.0462	0.0359	0.0233	0.0128
26	0.0486	0.0332	0.0191	0.0093
	0.0411	0.0273	0.0146	0.0064
28	0.0477	0.0275	0.0124	0.0046
	0.0316	0.0155	0.0060	0.0020

Table B Continued

K^r	0.6	0.7	0.8	0.9
0	0.0033	0.0038	0.0043	0.0048
	0.0098	0.0113	0.0129	0.0145
2	0.0163	0.0189	0.0215	0.0241
	0.0228	0.0264	0.0301	0.0337
4	0.0292	0.0339	0.0386	0.0432
	0.0355	0.0412	0.0468	0.0523
6	0.0417	0.0482	0.0546	0.0608
	0.0476	0.0547	0.0617	0.0683
8	0.0529	0.0605	0.0677	0.0744
	0.0577	0.0653	0.0723	0.0785
10	0.0616	0.0689	0.0752	0.0803
	0.0643	0.0708	0.0758	0.0793
12	0.0659	0.0710	0.0742	0.0756
	0.0659	0.0692	0.0701	0.0691
14	0.0644	0.0654	0.0640	0.0606
	0.0613	0.0599	0.0561	0.0507
16	0.0568	0.0530	0.0472	0.0404
	0.0511	0.0452	0.0379	0.0305
18	0.0446	0.0371	0.0291	0.0219
	0.0376	0.0292	0.0213	0.0149
20	0.0306	0.0220	0.0148	0.0095
	0.0241	0.0159	0.0098	0.0058
22	0.0182	0.0109	0.0062	0.0033
	0.0132	0.0072	0.0037	0.0018
24	0.0092	0.0045	0.0021	0.0009
	0.0062	0.0027	0.0011	0.0004
26	0.0040	0.0015	0.0006	0.0002
	0.0024	0.0008	0.0003	0.0001
28	0.0015	0.0004	0.0001	0.0000
	0.0006	0.0002	0.0000	0.0000

Table B Continued

K_r	1.0	1.1	1.2	1.4
0	0.0054	0.0059	0.0064	0.0074
	0.0161	0.0176	0.0192	0.0223
2	0.0267	0.0293	0.0319	0.0371
	0.0374	0.0410	0.0446	0.0517
4	0.0478	0.0523	0.0568	0.0657
	0.0577	0.0631	0.0683	0.0785
6	0.0668	0.0727	0.0784	0.0892
	0.0747	0.0807	0.0863	0.0965
8	0.0805	0.0861	0.0912	0.0994
	0.0839	0.0885	0.0922	0.0971
10	0.0843	0.0872	0.0889	0.0894
	0.0814	0.0821	0.0815	0.0773
12	0.0753	0.0735	0.0706	0.0624
	0.0664	0.0625	0.0577	0.0468
14	0.0558	0.0502	0.0442	0.0326
	0.0444	0.0379	0.0317	0.0210
16	0.0334	0.0269	0.0212	0.0125
	0.0237	0.0179	0.0132	0.0069
18	0.0159	0.0112	0.0077	0.0035
	0.0100	0.0065	0.0042	0.0017
20	0.0059	0.0036	0.0021	0.0007
	0.0033	0.0018	0.0010	0.0003
22	0.0017	0.0009	0.0004	0.0001
	0.0008	0.0004	0.0002	0.0000
24	0.0004	0.0002	0.0001	0.0000
	0.0002	0.0001	0.0000	0.0000
26	0.0001	0.0000	0.0000	0.0000
	0.0000	0.0000	0.0000	0.0000
28	0.0000	0.0000	0.0000	0.0000
	0.0000	0.0000	0.0000	0.0000

Table B. Continued

K_r	1.6	1.8	2.0	2.2
0	0.0084	0.0094	0.0105	0.0115
	0.0253	0.0284	0.0314	0.0344
2	0.0422	0.0472	0.0522	0.0572
	0.0587	0.0657	0.0725	0.0793
4	0.0744	0.0829	0.0912	0.0992
	0.0883	0.0976	0.1064	0.1147
6	0.0991	0.1080	0.1159	0.1229
	0.1052	0.1122	0.1176	0.1213
8	0.1053	0.1088	0.1101	0.1095
	0.0989	0.0979	0.0946	0.0896
10	0.0865	0.0811	0.0739	0.0660
	0.0702	0.0615	0.0524	0.0436
12	0.0525	0.0426	0.0335	0.0258
	0.0361	0.0268	0.0194	0.0138
14	0.0228	0.0154	0.0101	0.0066
	0.0132	0.0081	0.0048	0.0029
16	0.0070	0.0038	0.0021	0.0011
	0.0034	0.0017	0.0008	0.0004
18	0.0015	0.0007	0.0003	0.0001
	0.0006	0.0003	0.0001	0.0000
20	0.0002	0.0001	0.0000	0.0000
	0.0001	0.0000	0.0000	0.0000
22	0.0000	0.0000	0.0000	0.0000
	0.0000	0.0000	0.0000	0.0000
24	0.0000	0.0000	0.0000	0.0000
	0.0000	0.0000	0.0000	0.0000
26	0.0000	0.0000	0.0000	0.0000
	0.0000	0.0000	0.0000	0.0000
28	0.0000	0.0000	0.0000	0.0000
	0.0000	0.0000	0.0000	0.0000

Table B Continued

K_r	2.4	2.6	3.0	4.0
0	0.0124	0.0134	0.0154	0.0202
	0.0374	0.0404	0.0463	0.0608
2	0.0622	0.0671	0.0768	0.1006
	0.0860	0.0926	0.1056	0.1363
4	0.1071	0.1146	0.1290	0.1599
	0.1224	0.1296	0.1421	0.1624
6	0.1287	0.1336	0.1401	0.1403
	0.1236	0.1244	0.1222	0.1021
8	0.1072	0.1035	0.0933	0.0625
	0.0834	0.0764	0.0620	0.0324
10	0.0578	0.0499	0.0360	0.0144
	0.0357	0.0288	0.0183	0.0055
12	0.0196	0.0147	0.0082	0.0018
	0.0096	0.0067	0.0032	0.0005
14	0.0043	0.0027	0.0011	0.0001
	0.0017	0.0010	0.0004	0.0000
16	0.0006	0.0003	0.0001	0.0000
	0.0002	0.0001	0.0000	0.0000
18	0.0001	0.0000	0.0000	0.0000
	0.0000	0.0000	0.0000	0.0000
20	0.0000	0.0000	0.0000	0.0000
	0.0000	0.0000	0.0000	0.0000
22	0.0000	0.0000	0.0000	0.0000
	0.0000	0.0000	0.0000	0.0000
24	0.0000	0.0000	0.0000	0.0000
	0.0000	0.0000	0.0000	0.0000
26	0.0000	0.0000	0.0000	0.0000
	0.0000	0.0000	0.0000	0.0000
28	0.0000	0.0000	0.0000	0.0000
	0.0000	0.0000	0.0000	0.0000

Appendix C

a. Relative transition probabilities for pure vibration transitions in the ground state of CO^+

The relative transitions probabilities for pure vibration transitions $v_2 \rightarrow v_1$ can be derived by means of the wave functions corresponding to the so-called Morse potential used to describe the nuclear vibrations in the electronic ground state of a molecule (Morse, 1929):

$$R_v(r) = N_v e^{-z/2} z^{b/2} L^b_{K-v-1}(z) , \qquad (C1)$$

with

$$z = Ke^{-\alpha(r-r_e)} ,$$

$$K = \frac{\omega_e}{(\omega_e x_e)} ,$$

$$\alpha = 2\pi\left(\frac{2\mu c}{h}\right)^{1/2} (\omega_e x_e)^{1/2} ,$$

$$b = K - 2v - 1$$

$$N_v = \left(\frac{\alpha b(v)!}{\Gamma(K-v)}\right)^{1/2} e^{i\pi b} ,$$

and where the L^b_{K-v-1} are associated Laguerre polynomials. On the other hand, it can be verified that, in the region of r (internuclear distance) where the vibrational wave functions corresponding to the grojnd state of CO^+ are appreciably different from zero (i.e. in an interval of about 0.2 Å centered on $r = r_e$), the electronic dipole moment can be considered to be linear in r, on account of the similarity between the molecular characteristics of the ground states of

CO and CO^+:

$$\mu = 0.1 + \mu'\xi \quad \text{Debye,} \tag{C2}$$

where μ' is a constant and $\xi = \frac{r}{r_e} - 1$. Indeed, in the case of CO we have (Mulliken, 1934):

$$\mu = 0.11 + \mu'_{CO}\xi + \mu''_{CO}\xi^2 \quad \text{Debye} , \tag{C3}$$

and μ'_{CO}, μ''_{CO} are such that, in the interval $(-0.1, +0.1)$ of ξ ($r_e = 1.128$ Å), the ratio of the quadratic term to the linear term in equation C3 is always less than 0.004. Thus, it is a good approximation to write for the matrix element (v_2, v_1):

$$(v_2, v_1) \propto \int \psi^*_{v_2} \xi \psi_{v_1} \, d\xi ,$$

since the wave functions C1 form a complete set. Then, it can be shown that

$$(v_2, v_1) \propto N_{v_1} N_{v_2} G_{v_2 v_1} ,$$

with

$$G_{v_2 v_1} = \sum_{\sigma=0}^{v_1+v_2} (-1)^\sigma \frac{\Gamma(K-1-\sigma)}{\Gamma(K-1)} C(v_2, v_1, \sigma) g(K-1-\sigma) .$$

The expressions for $C(v_2, v_1, \sigma)$ and $g(K-1-\sigma)$ have been given in a paper by Fraser and Jarmain (1953). Actually, the numerical results that we need have been given by Rosenthal (1935). The vibrational transition rates required in chapter III are found to be very nearly in the ratios:

$$D_{10} : D_{21} : D_{32} = 1 : 2 : 3$$

On the other hand, the rates for transitions with $\Delta v = 2$ are of the order of or less than one percent of those for transitions with $\Delta v = 1$. It may be mentioned that the final solution of the computations of the fluorescence of CO^+ described in chapter III is rather insensitive to the precise values adopted for the relative $D_{v'', v''-1}$, the main factor which determines the $x_{v''}$-distribution being the parameter q, which is a measure of the absolute strengths of the pure vibration transitions as compared with those of the absorptions of solar light.

b. The f-value or oscillator strength of a molecular band system

By analogy with the atomic case we can write the relation between Einstein coefficient $A_{v'v''}$, oscillator strength $f_{v'v''}$, relative transition probability $p_{v'v''}$ and electronic transition moment $|R_e^{u\ell}|$:

$$f_{v'v''} = \frac{mc}{8\pi^2 e^2} \frac{g_u}{g_\ell} \lambda^2_{v'v''} A_{v'v''} \qquad (C4)$$

or

$$f_{v'v''} = \frac{8\pi^2 mc}{3e^2 h} \frac{1}{g_\ell} \frac{p_{v'v''}}{\lambda_{v'v''}} |R_\ell^{u\ell}|^2 , \qquad (C5)$$

u and ℓ designating the upper and lower electronic states respectively (note that $f_{v'v''}$ is an absorption f-value). Thus, we see that $f_{v'v''}$ may be appreciably different for different bands of a system owing to the presence of the factor $p_{v'v''}/\lambda_{v'v''}$ in equation C5. Since it would be convenient to have some means of characterizing the whole system by

a single parameter, we may define

$$f = \frac{\lambda_{v'v''}}{\bar{\lambda}} \frac{f_{v'v''}}{p_{v'v''}} , \qquad (C6)$$

where $\bar{\lambda}$ is, for instance, the wavelength of the strongest band of the system. If the $p_{v'v''}$'s are "improved relative transition probabilities," i.e. if they include the effect of variation of $|R_e^{u\ell}|$ with internuclear distance, the f-value defined by equation C6 will be completely independent of any particular band. An even more convenient quantity to consider is the product $(\bar{\lambda} f)$ itself, as this is rigorously proportional to $|R_e^{u\ell}|^2$, which is the essential factor determining the whole strength of the band system. This would facilitate the comparison of different systems among each other. With the above definition of f the Einstein coefficient of spontaneous emission and the rate of absorption of solar light become respectively:

$$A_{v'v''} = \frac{8\pi^2 e^2}{mc} \frac{g_\ell}{g_u} \frac{p_{v'v''}}{\lambda^3_{v'v''}} (\bar{\lambda} f) \qquad (C7)$$

and

$$C_{v'v''} = \frac{4\pi^2 e^2}{mc^3 h} (p\eta\lambda^2 F_\lambda)_{v'v''} W(\bar{\lambda} f) \qquad (C8)$$

For example, $(\bar{\lambda} f)$-values and absorption lifetimes at r = 1 A.U. are given in table C1 for transitions in cometary molecules. The necessary data have been found in papers by Bennett and Dalby (1959, 1960a, 1960b, 1962), Lyddane and Rogers (1941), and Carrington (1959). In the case of the $A\ ^2\Pi - X\ ^2\Sigma^+$ transition of CN the f-value has been determined by using the intensity ratio of the red (2, 0) band to the violet (0, 1) band

observed in Comet Mrkos (1957d) by Dufay and Swings (1958).

Table C1. $(\bar{\lambda} f)$-values and absorption lifetimes for molecular transitions observed in comets

Transition		$\bar{\lambda}$ (Å)	$(\bar{\lambda} f)$ *	τ_{abs} (sec)
CN	$B\ ^2\Sigma^+ - X\ ^2\Sigma^+$	3800	0.100	9
	$A\ ^2\Pi - X\ ^2\Sigma^+$	10930	0.010	
C_2	$A\ ^3\Pi_g - X\ ^3\Pi_u$	5165	0.130	4
CH	$A\ ^2\Delta - X\ ^2\Pi$	4300	0.021	37
NH	$A\ ^3\Pi_i - X\ ^3\Sigma^-$	3360	0.026	80
OH	$A\ ^2\Sigma^+ - X\ ^2\Pi_i$	3095	0.004	1000
CO^+	$A\ ^2\Pi - X\ ^2\Sigma^+$	4260	0.024	25
N_2^+	$B\ ^2\Sigma^+ - X\ ^2\Sigma^+$	3915	0.150	8

* $\bar{\lambda}$ is expressed in 10^3 Å.

The strength of a molecular system is sometimes determined by measuring the lifetimes of vibrational levels in the upper state against spontaneous emission. Then, some authors define an f-value by

$$(f) = \frac{mc}{8\pi^2 e^2} \frac{g_u}{g_\ell} \bar{\lambda}^2 \frac{1}{\tau} , \qquad (C9)$$

taking an average for τ. Although this is not incorrect, it may unfortunately lead to confusion and produce errors in some cases. For one writes, for instance:

$$A_{v'v''} = \frac{8\pi^2 e^2}{mc} \frac{g_\ell}{g_u} \frac{p_{v'v''}}{\lambda^2_{v'v''}} (f) \qquad (C10)$$

which is not exact, as can be easily seen*, or one merely quotes the f-value as computed from equation C9 without recalling its definition. Examples of such errors or omissions can be found in the literature. Therefore, before accepting the results of any determination of abundances, it would be advisable, as a rule to inquire about the validity of the f-value that has been used. For instance, the values derived for $A_{v'v''}$ from equation C10 with (f) = 0.002 for the principal bands of the CO^+ comet-tail system differ by a factor of about 3 from the correct value obtained from equation C7. When the Condon parabola is very narrow (as in the case of the CN violet system e.g.) (f) is nearly equal to f.

c. Rotational line strengths for the $A\ ^2\Pi - X\ ^2\Sigma^+$ transition of CO^+

Table C2 contains the rotational line strengths $S_{J'}$ for a transition $^2\Pi(a) \rightarrow {}^2\Sigma$ when the $^2\Pi$ is inverted. They are readily derivable from the formulae given by Mulliken (1931). The second part of table C2 gives the various values of J' corresponding to a given value of K (= K"). This correspondance has to be known for the evaluation of the sum occurring in equation 34 (chapter III).

*The relation between f and (f) is:

$$f = \frac{A_{v'v''_1}}{\sum_{v''} A_{v'v''}} \frac{1}{p_{v'v''_1}} \frac{\lambda^3_{v'v''_1}}{\bar{\lambda}^3} (f)$$

Table C2. Intensity relations in the $A\,^2\Pi - X\,^2\Sigma^+$ transition of CO^+ (low K)

	Branches	$S^{(2)}_{J'}$
	P_2, P_{21}	$(2J'+1)(2J'+3)/32(J'+1)$
$^2\Pi_{1/2} - {}^2\Sigma^+$	Q_2, Q_{21}	$(2J'+1)^3/32J'(J'+1)$
	R_2, R_{21}	$(4J'^2-1)/32J'$
		$S^{(1)}_{J'}$
	P_{12}, P_1	$(4J'^2-1)/32(J'+1)$
$^2\Pi_{3/2} - {}^2\Sigma^+$	Q_{12}, Q_1	$(4J'^2-1)(2J'+3)/32J'(J'+1)$
	R_{12}, R_1	$(2J'+1)(2J'+3)/32J'$

Correspondence between J' and K for the various branches

Branches	J'
P_{12}, P_2	$K - \frac{3}{2}$
P_1, P_{21} Q_{12}, Q_2	$K - \frac{1}{2}$
Q_1, Q_{21} R_{12}, R_2	$K + \frac{1}{2}$
R_1, R_{21}	$K + \frac{3}{2}$

REFERENCES

Alfvén, H. 1957, Tellus 9, 92.

Alfvén, H. 1960, Rev. Mod. Phys. 32, 710.

Allen, C. W. 1963, Astrophysical Quantities, 2nd ed. (London: The Athlone Press).

Arp, H. 1961, Ap. J. 133, 688.

Bennett, R. G., and Dalby, F. W. 1959, J. Chem. Phys. 31, 434.

Bennett, R. G., and Dalby, F. W. 1960a, J. Chem. Phys. 32, 1111.

Bennett, R. G., and Dalby, F. W. 1960b, J. Chem. Phys. 32, 1716.

Bennett, R. G., and Dalby, F. W. 1962, J. Chem. Phys. 36, 399.

Beyer, M. 1942, A. N. 272, 249.

Beyer, M. 1950, A. N. 275, 217.

Beyer, M. 1958, A. N. 284, 112.

Biermann, L. 1951, Zs. f. Ap. 29, 274.

Biermann, L., and Trefftz, E. 1960 Zs. f. Ap. 49, 111.

Biermann, L., and Trefftz, E. 1963, Zs. f. Ap. in press.

Biermann, L., and Lüst, R. 1963, The Moon, Meteorites and Comets, Ed. B. M. Middlehurst and G. P. Kuiper (Chicago: The University of Chicago Press), p. 618.

Bobrovnikoff, N. T. 1931, Publ. Lick Obs. 17, 305.

Carleton, N. P., and Lawrence, T. R. 1958, Phys. Rev. 109, 1159.

Carrington, T. 1959, J. Chem. Phys., 31, 1243.

Carrington, T. 1962, Ap. J. 135, 883.

Chamberlain, J. W. 1961, Physics of the Aurora and Airglow (New York: Academic Press), p. 571.

Coleman, P. J., Jr., Davis, L., Jr., Smith, E. J., Sonnett, C. P. 1962, Science, 138, 1099.

Ditchburn, R. W. and Öpik, U. 1962, Atomic and Molecular Processes, Ed. D. R. Bates (New York: Academic Press), p. 79.

Dossin, F., Fehrenbach, Ch., Haser, L., and Swings, P. 1961, Ann. d'Ap. 24, 519.

Dossin, F., and Rousseau, C. 1962, C. R. 255, 2373.

Dufay, J. 1938, C. R. 206, 1948.

Dufay, J., and Swings, P. 1958, Ann. d'Ap. 21, 260.

Eddington, A. S. 1910, M. N. 70, 442.

Fraser, P. A., Jarmain, W. R., and Nicholls, R. W. 1954, Ap. J. 119, 286.

Fraser, P. A., and Jarmain, W. R. 1953, Proc. Phys. Soc. London A 66, 1145

Fokker, A. D., Jr., 1953, La Physique des Comètes, 4th Liège Symposium, p. 241.

Gilbody, H. B., and Hasted, J. B. 1957, Proc. Roy. Soc. London A 238, 334.

Greenstein, J. L. 1958, Ap. J. 128, 106.

Greenstein, J. L. 1958, Encyclopedia of Physics, Vol. 50, 161.

Greenstein, J. L., and Arpigny, C. 1962, Ap. J. 135, 892.

Greenstein, J. L. 1962, Ap. J. 136, 688.

Grundzinska, S. 1960, Ann. d'Ap. 23, 797.

Harwit, M., and Hoyle, F. 1962, Ap. J. 135, 875.

Haser, L. 1957, Liège Inst. d'Ap., Reprint No. 394.

Hasted, J. B. 1952, Proc. Roy. Soc. London A 212, 235.

Herzberg, G. 1950, Spectra of Diatomic Molecules (New York: D. Van Nostrand Company, Inc.)

Houziaux, L. 1960, Ann. d'Ap., 23, 1025.

Hoyle, F., and Harwit, M. 1962, Ap. J. 135, 867.

Huebner, W. 1961, Rev. Mod. Phys. 33, 498.

Hunaerts, J. 1953, La Physique des Comètes, 4th Liège Symposium, p. 99.

Hunaerts, J. 1959a, Ann. d'Ap. 22, 790.

Hunaerts, J. 1959b, Ann. d'Ap. 22, 812.

Jarmain, W. R., Fraser, P. A., and Nicholls, R. W. 1953, Ap. J. 118, 228.

Johnson, F. S. 1961, Satellite Environment Handbook, Ed. F. S. Johnson (Stanford University Press).

Kopelman, R., and Klemperer, W. 1962, J. Chem. Phys., 36, 1693.

Levin, B. 1948, Soviet A. J. 25, 246.

Liller, W. 1960, Ap. J. 132, 867.

Lüst, R. 1962, Zs. f. Ap. 54, 67.

Lyddane, R. H., and Rogers, F. T. Jr., 1941, Phys. Rev. 60, 281.

Malaise, D. 1963, A. J. 68, 561.

Marochnik, L. S. 1962, Soviet A. J. 39, 678.

Massey, H. S. W. 1949, Rep. Prog. Phys. 12, 248.

Matheson, L. A. 1932, Phys. Rev. 40, 813.

McKellar, A. 1942, Rev. Mod. Phys. 14, 179.

McKellar, A. 1944, Ap. J. 99, 162.

McNally, D. 1963, The Observatory 83, 18.

Melbourne, W. G. 1959, Thesis, California Institute of Technology.

Mianes, P., Grundzinska, S., and Stawikowski, A. 1960, Ann. d'Ap. 23, 788.

Michard, R. 1950, B. A. N. 11, 227.

Miller, F. D. 1957, P. A. S. P. 69, 82.

Miller, F. D. 1961, Ap. J. 134, 1007.

Mitchell, A. C. G., and Zemansky, M. W. 1961, Resonance Radiation and Excited Atoms (Cambridge: The University Press), Chap. III.

Morse, P. M. 1929, Phys. Rev. 34, 57.

Mulliken, R. S. 1931, Rev. Mod. Phys. 3, 89.

Mulliken, R. S. 1934, J. Chem. Phys. 2, 400.

Mustel, E. R. 1958, Soviet A. J. 35, 351.

Mustel, E. R. 1960, Soviet A. J. 37, 396.

Nicholls, R. W. 1956, Proc. Phys. Soc. London A 69, 741.

O'Dell, C. R., and Osterbrock, D. E. 1962, Ap. J. 136, 559.

Rao, K. N. 1950, Ap. J. 11, 306.

Remy-Battiau, L. 1962, Ann. d'Ap. 25, 171.

Robinson, D. and Nicholls, R. W. 1960, Proc. Phys. Soc. London A 75, 817.

Rosen, B. 1953, La Physique des Comètes, 4th Liège Symposium, p. 317.

Roemer, E. 1962, P. A. S. P. 74, 351.

Schmidt, M., and van Woerden, H. 1956, Les Molécules dans les Astres, 7th Liège Symposium, p. 102.

Schwarzschild, K., and Kron, E. 1911, Ap. J. 34, 342.

Stawikowski, A., and Swings, P. 1960, Ann. d'Ap. 23, 585.

Stedeford, J. B. H., and Hasted, J. B. 1955, Proc. Roy. Soc. London A 227, 466.

Stumpff, P. 1959, Zs. f. Ap. 47, 225.

Swings, P. 1941, Lick Obs. Bull. 19, 131.

Swings, P., and Page, T. L. 1950, Ap. J. 111, 530.

Swings, P. 1956, Vistas in Astronomy, Ed. A. Beer (London: Pergamon Press), 2, 958.

Swings, P., and Haser, L. 1956, Atlas of Representative Cometary Spectra (Louvain: Ceuterick).

Swings, P., and Greenstein, J. L. 1958, C. R. 246, 511.

Swings, P. 1962, Ann. d'Ap. 25, 165.

Swings, P., and Fehrenbach, Ch. 1962, C. R. 255, 1826.

Van Biesbroek, G. 1962, Ap. J. 136, 1155.

Vorontsov-Velyaminov, B. A. 1960, Soviet A. J. 37, 709.

Weidemann, V. 1963, Zs. f. Ap. 57, 87.

Wurm, K. 1932, Zs. f. Ap. 5, 10.

Wurm, K. 1934, Zs. f. Ap. 8, 281.

Wurm, K. 1937, Zs. f. Ap. 15, 115.

Wurm, K. 1943, Mitt. Hamburger Sternwarte 8, no. 51.

Wurm, K. 1960, Le Spectre des Astres dans l'Ultraviolet Lointain. 10th Liège Symposium, p. 369.

Wurm, K. 1961, Zs. f. Ap. 52, 285.

Wurm, K. 1962, Icarus 1, 144.

Wurm, K. 1963, The Moon, Meteorites and Comets, Ed. B. M. Middlehurst and G. P. Kuiper (Chicago: The University of Chicago Press), p. 573.

Wurm, K. 1963a, Icarus 2, 29.

Zanstra, H. 1928, M. N. 89, 178.